Unveiling New Physics Hints through the Higgs Sector

Dissertation

zur

Erlangung der naturwissenschaftlichen Doktorwürde

(Dr. sc. nat.)

vorgelegt der

Mathematisch-naturwissenschaftlichen Fakultät

der

Universität Zürich

von

Andrea Pattori

aus

Italien

Promotionskommission

Prof. Dr. Gino Isidori

Prof. Dr. Ferruccio Feruglio

Prof. Dr. Thomas Gehrmann

Prof. Dr. Paride Paradisi

Zürich 2017

"The beginning is easy to recite for us,
The ending is nowhere in sight for us.
And though the answers may some day be nearer,
Things will get worse, before they get clearer."

Arthur Roberts,
Some People don't Know Where to Stop (1952).

Zusammenfassung

Um Physik jenseits des Standardmodells zu entdecken, muss man zwangsweise den Higgs Sektor besser verstehen. Nachdem die Gründe dafür rezensiert sind, diskutieren wir zwei zusammengehörige Ansätze: entweder man kann das phänomenologische Problem angehen, maximale Auskünfte aus Teilchenphysik Experimente zu herausziehen, oder die theoretische Untersuchung unternehmen, um die Kenntnis von dem Higgs Sektor zu verbessern.

Ersten Teil dieser Dissertation nehmen wir einen phänomenologische Standpunkt ein, und diskutieren das generelle Problem, infraroten Standard Modell Korrekturen in eine Modell-unabhängige Beschreibung von neuer Physik in Higgs Zerfälle und Produktion zu einfügen. Erstens analysieren wir infrarote elektromagnetische Korrekturen (Bremsstrahlung). Wir stellen einen kompakten Formalismus bereit, um allgemeingültig Fermionen Bremsstrahlung in führender logarithmischer Approximation zu beschreiben, danach erläutern wir ihn durch die $h \to 2e\,2\mu$ Fallstudie. Zweitens diskutieren wir doppelt-logarithmische Masse-Singularitäten, die sich aus dem elektroschwachen Sektor ergeben. Masse-Singularitäten sind für Higgs Produktionsprozesse bei hohen Energie wichtig, und wir stellen eine detaillierte Analyse dieser Beiträgen in neuer Physik Szenarien bereit. Wir beschränken hier unsere Diskussion auf die Higgsstrahlung Fallstudie.

Zweiten Teil der Dissertation nehmen wir einen zusammengehörigen Standpunkt ein und führen eine theoretische Studie der hoch-Energie Supersymmetrie durch. Wir nützen wichtige Merkmale der supersymmetrischen Theorien — wie die hoch eingeschränkt Struktur des supersymmetrischen Higgs Sektor, Eichkopplungen Vereinigung und Spontane elektroschwache Symmetriebrechung durch Strahlungskorrekturen — aus. Damit ziehen wir intrigante Schlussfolgerungen über die Durchführbarkeit von supersymmetrischen Theorien in der (m_h, m_t) Ebene.

Abstract

After reviewing the reasons to believe that the road to shed light to Beyond Standard Model physics pass through a better understanding of the Higgs sector, we outline two complementary approaches along this main line: either tackling the phenomenological challenge to extract as much information as possible from collider experiments, or undertaking a theoretical investigation of new physics scenarios in order to gain knowledge on possible explanations to the Higgs mysteries.

In the first part of the dissertation, we adopt a phenomenological approach and discuss the general problem of including infrared Standard-Model-like corrections in a model-independent new physics characterisation of Higgs decay and production processes. We deal first with infrared electromagnetic corrections (bremsstrahlung), providing a compact formalism to generally describe fermion bremsstrahlung in leading logarithmic approximation and then exemplifying its effectiveness through the $h \to 2e\,2\mu$ case study. Subsequently we switch to a discussion of double-logarithmic mass singularities stemming from the electroweak sector, which affects among the others also Higgs production processes in the high-energy regime. We provide here a detailed analysis of such mass singularities in generic new physics scenarios for the case study of Higgsstrahlung.

In the second part of the dissertation, we adopt a complementary approach and perform a theoretical study of high-scale supersymmetry. We exploit the highly constrained structure of the Higgs sector in such theories, together with other of their important features such as gauge coupling unification and radiative breaking of electroweak symmetry, to draw intriguing conclusions regarding the viability of such theories in the (m_h, m_t) plane.

Contents

Introduction

Nowadays, the most experimentally successful theory describing physics at its fundamental level is the Standard Model of Particle Physics. Despite its astonishing agreement with experimental data, it is widely believed that the Standard Model needs an ultraviolet completion, that is a theoretical improvement of the theory in order to more properly describe the behaviour of nature at higher energies (i.e. smaller distances).

Arguably, the most compelling reasons suggesting the existence of Beyond Standard Model physics come from the Higgs sector of the theory. The scalar potential of the Higgs boson is puzzling the physics community since decades and the innermost dynamic triggering the electroweak symmetry breakdown is still not properly understood. Furthermore, the very peculiar features displayed by Yukawa interactions, such as fermion masses hierarchies and Cabibbo–Kobayashi–Maskawa matrix structure, should just be seen as coincidences within the Standard Model, where no explanation of their origin is given. These issues have motivated an impressive theoretical effort, undertaken in the last four decades, to understand the hidden mechanisms behind the peculiarities of the Higgs sector and to unveil the right direction through the correct Standard Model ultraviolet completion.

In parallel, experimental physics has progressively pushed up the high-energy fronter, in order to eventually directly probe the Higgs sector in collider experiments, looking for revealing signatures of Beyond Standard Model physics. Despite the recent discovery of the Higgs boson [1, 2], its properties are still largely unknown. For this reason, an extensive program of precision measurements will be carried on at the Large Hadron Collided (LHC) facility for the decade to come.

Waiting for new, more precise data to be collected in the near future, one possibility to push further the investigation of Higgs sector is to adopt a pragmatic bottom-up approach to new physics. In particular, the important issue can be tackled of parametrising experimental data and characterising Higgs properties with high precision and least theoretical bias possible. Accomplishing such a task would provide experimentalists and theorists with a common and clear language to compare collider's results with phenomenological predictions, avoiding continuous recasting

of experimental analyses for different purposes as well as the hermeticity of some theoretical speculations.

A clear effort in the above direction has been made with the development of the so-called Higgs Pseudo Observables (hPO) framework [3, 4]. The basic idea of such program was to naturally extend the κ-framework adopted in the first run of LHC experiments [5–7], providing a general parametrisation, in terms of pseudo observables, of amplitudes for Higgs production and decay processes. To directly parametrise on-shell amplitudes, rather than computing them starting from explicit new physics Lagrangians (either effective or renormalisable), comes with several advantages. On the one hand, it discharge us from making several additional theoretical assumptions that are unavoidably connected with a Lagrangian approach. On the other hand, pseudo observables can be more transparently connected to raw data, allowing a clearer interpretations of experiments. Furthermore, pseudo observables allows for a systematic inclusion of higher-order corrections due to infrared physics (which is usually assumed to be Standard-Model-like), , leading to an accurate theoretical description of Higgs processes which recovers the best up-to-date Standard Model predictions in absence of new physics effects.

An important aspect of collider phenomenology is to properly take into account the kinematic distortion of decay and scattering processes due to radiative corrections. These includes the soft emission of photons and/or gluons, the so-called initial and final state radiation, as well as electroweak corrections in the high-energy regime, where W and Z bosons produce distortion of the same nature as the QED and QCD ones. Therefore, in order for the hPO framework to be a viable bridge between theory and experiments, a systematic and model-independent inclusion of radiative effects should be embedded in its language.

The first part of this dissertation will deal with the issue of including radiative corrections in the hPO description of Higgs decay and production processes [8]. As far as Higgs decays are concerned, only QED and QCD effects are relevant, since the Higgs mass sets an upper limit to the energy of the process too low to advocate for relevant distortions due to W and Z bosons. Being the Higgs decays involving coloured final states generally of less interest, we will further restrict our attention only to QED radiative effects.

The aspect of radiative corrections in electrodynamic is tightly constrained by crucial theorems developed in the 1960's [9–16]. Exploiting those results, we derive a simple but powerful formalism able to describe the kinematic distortion of processes' spectra due to soft and/or collinear photon emission by fermion currents. Such a tool is then exploited for a detailed differential analysis of the $h \to 4\ell$ decay in the hPO framework, to exemplify its application and emphasise the importance of QED radiative corrections. However, it is worth stressing that the developed formalism is by no mean limited to the hPO framework nor to Higgs processes and the same machinery has been also exploited in other contexts [17].

Higgs production processes call for additional concerns. A first issue is that coloured initial states are unavoidably involved, therefore QCD radiative corrections must be taken into account. However, in this dissertation we focus on a second, more subtle point. As already stressed, in the high-energy regime purely electroweak corrections due to W and Z bosons also generate distortion effects, but with a trouble-

some addition: a complicated interplay among different processes due to the $SU(2)_L$ rotation of initial and final state takes place as a consequence of soft W and Z rescattering.

Within the Standard Model, a detailed analyses of electroweak double- and single-logarithmic mass singularities have already been carried out in the literature [18–23], but a suitable extension to new physics scenario was missing. In this dissertation, we tackle the problem of a general discussion of double-logarithmic mass singularities in generic new physics scenarios, adopting an hPO perspective. Once again, analysis is performed and conclusions are drawn for a case study, namely Higgsstrahlung processes, but the developed methodology has wider validity and applications.

A completely different possibility is to pursue the investigation of the Higgs sector from a more model-building oriented top-down perspective. Rather than to assume the peculiarities of the Standard Model (and of the Higgs sector in particular) as inputs, as in bottom-up strategies, in top-down approaches the aim is to explain them, deriving their pattern from educated guesses on the structure of Beyond Standard Model physics.

Supersymmetric theories have long been considered the most appealing Standard Model ultraviolet completion. They are theoretically well-motivated, provide viable solutions to some long-standing problems of particle physics and are an essential ingredient of promising theoretical speculations such as supergravity and string theory. Despite the recent crisis of natural theories with TeV-scale supersymmetry, due to the negative results of direct searches at LHC, high-scale supersymmetric theories are still intriguing and with far-reaching consequences.

In this dissertation, we focus on the Minimal Supersymmetric Standard Model (MSSM) as a case study of supersymmetric theories. Disregarding naturalness considerations on the scale of supersymmetry breaking, the parameter space of the MSSM is explored to analyse its intriguing features, such as gauge coupling unification and successful prediction of the quartic Higgs coupling value.

Many studies in this direction have already been performed in the past (see e.g. [24–26]). Before the Higgs discovery, their main focus was to determine the Higgs mass viable region through a detailed investigation of the quartic Higgs coupling matching condition provided by supersymmetric theories. After the direct measurement of the Higgs mass, those studies continued with a different perspective: hopefully, an analysis of the landscape of possible quartic Higgs couplings could point out revealing peculiarities (or criticalities) of the physical value chosen by nature.

Here we present a significant conceptual improvement of such kind of investigations. A first important refinement regards the way the parameter space of MSSM is scanned. Differently from many previous works, a "natural" range for the spectrum of soft supersymmetry-breaking terms is suitably defined and imposed at its input scale (e.g. the scale of grand unification) rather than at low scales, where such spectrum can easily be broadened by running effects due to the renormalisation group flow. A second notable addition is the further scan over different top-quark masses since, as a matter of fact, it would be quite unreasonable to scan over the quartic Higgs coupling only. Indeed, the top Yukawa plays a major role in the supersymmetric matching condition for the quartic Higgs coupling, as well as in the renormalisation

group flow of many MSSM parameters. Furthermore, the physical value of top-quark mass chosen by nature is undeniably as peculiar and intriguing as the Higgs mass and an investigation of its possible criticalities is of equal interest.

Finally, another important novelty of our analysis is a systematic investigation of the so-called Radiative Electroweak Symmetry Breakdown (REWSB). Under suitable conditions, the theory can be seen to preserve the electroweak symmetry at its input scale, triggering its spontaneous breakdown at lower energies entirely through radiative effects driven by renormalisation group flow. This is an intriguing possibility which is included and studied within our scan of the parameter space of MSSM.

The dissertation is organised as follows. Chapter 1 discusses some general motivations to go beyond the Standard Model and to focus on the Higgs sector in particular. Chapter 2, 3 and 4 are dedicated to a bottom-up study of Higgs collider phenomenology. In chapter 2 we review the general hPO parametrisation first proposed in Ref. [3, 4]. In chapter 3 we investigate the distortion of Higgs decay spectra due to infrared QED effects (bremsstrahlung). In chapter 4 we extend the discussion to infrared distortion effects due to electroweak physics, which plays a role in Higgs production processes. Chapters 5 and 6 deal with our top-down analysis of supersymmetry. In chapter 5 we review supersymmetric theories in general, focusing then on the MSSM. In chapter 6, High-Scale Supersymmetry (and the MSSM in particular) is analysed from the perspective outlined above, with the attempt to shed light to an interesting criticality of the physical Higgs and top-quark masses.

Remarks on the Standard Model of Particle Physics

1.1 Why going beyond the Standard Model

The Standard Model of Particle Physics is a very successful theory. Its predictions, tested in the last three decades with increasingly high precision, are in excellent agreement with experimental data for a wide range of phenomena. The coronation of this success has been the recent discovery of the Higgs boson [1, 2], the missing piece of this theory that was still seeking for an experimental confirmation. Thus, if we do not take into account a few number of discrepancies between Standard Model and cosmological observations, and with the notable exception of evidence for neutrino masses (all to be briefly discussed in section 1.1.1), we are facing a rather astonishing absence of *new physics* signals.

Despite this lacking of experimental proofs, nowadays it is widely believed that the Standard Model is just an effective theory, i.e. the low energy approximation of a more fundamental theory. Therefore, if accepting that the Standard Model needs an ultraviolet completion, the most urgent question becomes which is the energy scale of such new physics. A great number of scenarios have been proposed so far to answer this compelling question, and a complete list of them is far beyond the scope of this dissertation. In this section, we will limit ourself to a general discussion of the energy scale at which such new physics might show up.

The need for a Beyond Standard Model theory becomes more pressing when the concept of *naturalness* is introduced. If adopted as a research instrument, this theoretical tool provides striking evidences that the Standard Model cannot be a definitive theory and, if pushed further, it could also give important hints on the energy scale where new physics should first occur.

1.1.1 Experimental evidence for new physics

As already mentioned, there are just a few experimental clues for Beyond Standard Model physics and most of them come from the comparison of Standard Model predictions with cosmological observations. Referring to the literature for a more complete discussion, we outline below the most intriguing of such discrepancies.

- *Dark matter.* Nowadays there is overwhelming evidence that the 84.5% of the total matter in the universe is constituted of dark matter [27], i.e. matter made of particles not included in the Standard Model and with largely unknown properties. Then the Standard Model obviously needs a completion to include one (or more) new particle(s) able to explain the very dark matter existence.

- *Baryon asymmetry.* Another well established cosmological observation is that there is exceedingly more matter than antimatter in the universe, an anomaly known as baryon asymmetry. Even though the Standard Model can in principle address such asymmetry, it spectacularly fails to quantitatively reproduce its amount [28]. This failure leads to a conflict between the Standard Model of particle physics and our present cosmological models. Maybe new interactions and mechanisms in the new physics sector could solve this problem.

- *Inflation.* The inflation mechanism was first proposed in the 1980's to solve some serious cosmological problems (such as the horizon and the flatness problems) [29]. In the last decades this theory has gained increasing credit and consideration, but the Standard Model is unable to explain in a satisfactory way the inflation era, resulting in a conflict between these two theories.

- *Neutrino masses and mixing.* Apart from the above cosmological arguments, the only known evidence for Beyond Standard Model physics are neutrino masses and oscillation. Within the Standard Model, neutrinos are massless particles. Instead, neutrinos are definitely massive particles, as shown by different experiments by now. In more recent years also the phenomenon of neutrino flavour oscillation has been studied and confirmed by experiments [30–33]. Both these observations require a mandatory modification of the Standard Model in order to accommodate such phenomena. There is not a unique way to do that and the solution to this problem can shed light to the new physics sector, as it will be briefly sketched later.

In summary, except for the neutrino masses and mixing, an unambiguous signal of new physics (such as an experimental deviation from the Standard Model predictions or an unexpected resonance at collider experiments) is still missing. Why is it so, despite the fact that an ultraviolet completion of the Standard Model should exist, is one of the most compelling questions in modern particle physics.

1.1.2   The energy scale of new physics

Independently from experimental observations, it can be theoretically argued that the Standard Model cannot be a theory valid up to arbitrarily high energies. The reason is a long-standing problem: the Standard Model does not include gravity interactions and, in fact, a consistent quantum theory of gravitation is still missing. Maybe this unification cannot be reached within the context of quantum field theories and a dramatic change of perspective might be needed, such as a string theory approach [34, 35]. Nevertheless, the energy scale at which quantum gravity effects eventually show up represents an ultimate ultraviolet cutoff for the Standard Model. In other words, even in the absence of any other kind of new physics, the Standard Model

needs at least the ultraviolet completion necessary to include gravity. Nowadays there is a broad agreement on putting such cutoff scale directly at the Planck scale, $\Lambda \sim m_P \simeq 10^{19}$ GeV, since no theoretical reasons can be found to lower this bound[1]. As mentioned, it is also believed that at those energies the quantum field theory approach eventually stops to be applicable and new techniques must be developed.

The above argument put an ultimate cutoff scale for the Standard Model at the Planck scale. However, there are some theoretical and experimental clues that new physics might exists at slightly lower energies, the so-called GUT scale, $m_G \sim 10^{14} \div 10^{16}$ GeV.

The first indication of physics at the GUT scale comes from the evolution of the three Standard Model gauge coupling under the renormalisation group flow. In the Standard Model they all merge at nearly the same value at energies $\sim 10^{14}$ GeV [36] and an even better situation occurs in the Minimal Supersymmetric Standard Model (MSSM), where they exactly merge at energies $\sim 10^{16}$ GeV [36], as it will be discussed in chapters 5 and 6. This gauge coupling unification is a genuine prediction of *Grand Unified Theories* (GUT), where the Standard Model gauge group is embedded in a simple group such as $SU(5)$ or $SO(10)$ [37,38].

A second theoretical clue comes from the see-saw mechanism, that tries to explain the small non-vanishing neutrino masses. It is well-known that there exist only one independent five-dimensional effective operator compatible with Standard Model symmetries [39], the Weinberg operator:

$$\mathcal{L}_5 = \frac{y}{\Lambda}(\tilde{\phi}^\dagger L)^T C (\tilde{\phi}^\dagger L) \; , \tag{1.1}$$

where $\tilde{\phi}$ is the charge conjugate of the Higgs doublet, L is the lepton left-handed doublet and C is the charge conjugation matrix. Here Λ represents the energy scale of the physics which originates this effective term and y is a dimensionless $\mathcal{O}(1)$ coupling constant[2]. After the electroweak symmetry breakdown, this term generates a mass for the left-handed neutrinos[3]:

$$m_{\nu_L} = \frac{y^2 v^2}{\Lambda} \; , \tag{1.2}$$

with $v = 176$ GeV the Higgs vacuum expectation value (v.e.v.). Now, if one tries to deduce the energy scale Λ by inverting this relation, one gets

$$\Lambda \simeq 3 \cdot 10^{14} \left(\frac{0.1 \; eV}{m_{\nu_L}} \right) y^2 \; \text{GeV} \; , \tag{1.3}$$

suggesting that, if the see-saw mechanism is the right answer to neutrino masses, the new physics behind it could be possibly found at the GUT scale.

The energy scales of new physics discussed so far (m_P and m_G) are very far from nowadays experimentally achievable energies (such as the TeV scale at LHC). This

---

[1]It can be said that the choice of this scale is a "natural" one, since the Planck mass is directly related to the Newton constant G_N: $m_P \equiv \sqrt{1/G_N}$. This concept of naturalness will be thoroughly discussed later.

[2]Again, this could be seen as a "natural" choice for the value of this parameter.

[3]The current upper cosmological bound for neutrino masses is $\sum_i m_{\nu_i} \lesssim 0.3$ eV [40]. Weaker bounds derive from laboratory experiments, for example $m_{\nu_e} \lesssim 2$ eV [41].

enormous energy gap would generate an high decoupling between the Standard Model and the new physics sector, which in turns could explain why experiments have not seen new physics signals yet. But then the interesting question becomes if this is the end of the story, i.e. if new physics appears only at very high energies, unreachable to nowadays collider experiments. Perhaps the answer is positive, but only if one completely ignores the naturalness problem. How this principle works and how it can be used to explore new physics scenarios is the topic of the next sections.

1.1.3   The naturalness problem

If accepted as a physical principle, the concept of *naturalness* can be used as a powerful theoretical tool that can put in crisis the Standard Model at much lower energy scales.

Following the formulation of naturalness by 't Hooft [42], a theory is natural if, for all its parameters p which are small with respect to their fundamental scale Λ, the limit $p \to 0$ corresponds to an enhancement of the symmetry of the system.

To understand the meaning of this definition, we take as an example the fermion masses m_f. Regularizing the theory through an ultraviolet cutoff Λ and computing the loop corrections δm_f to m_f, naively these corrections could be expected to be proportional to Λ. However, since the limit $m_f \to 0$ restores the fermion chiral symmetry, every contribution to δm_f should be proportional to m_f itself (in order to vanish in the $m_f \to 0$ limit). Then the dependence of δm_f through Λ can only be logarithmic, $\sim \log \Lambda$. This mechanism, that is a direct consequence of the fulfilment of the 't Hooft condition, protect the fermion masses from planckian corrections and makes a small value for the m_f/m_P ratio natural.

A complementary request to a natural theory is for all parameters that do not satisfy the 't Hooft condition to have an $\mathcal{O}(1)$ value with respect to their fundamental scale. Then, it can be said that a *naturalness problem* arises every time a theory exhibits a small parameter without furnishing any symmetry to protect its value.

We can turn this problem to a more quantitative form by introducing the notion of *fine tuning*. Once identified the unnatural small parameter p and its fundamental scale[4] Λ, one may define the amount f of fine tuning by:

$$f \equiv \frac{p}{\Lambda} \; . \tag{1.4}$$

The smaller f, the bigger the required fine tuning.

Generally, an high fine tuning would go against the belief that the observable properties of a physical theory are stable under small variations of its fundamental parameters. One talks about the naturalness of a theory to describe such behaviour.

Once formalised these concepts, it can be easily argued that the Standard Model is not a natural theory and a (sometimes huge) fine tuning is needed to explain the experimental values of several quantities. The most urgent questions arising from this principle and some attempts to solve them are:

---

[4] We have already argued that the natural scale for a parameter of mass dimension 1 is $\Lambda = m_P$. Thus, for $[p] = d$ in mass unit, we will have $\Lambda = (m_P)^d$ and $f \equiv p/(m_P)^d$. Note that the alternative choice $f \equiv (p^{1/d})/m_P$ would led to significantly different values for f.

- *Cosmological constant.* Cosmological observation are consistent with the existence of a cosmological constant. However its experimental value, $\Lambda_{cosmo} \sim 10^{-47}$ GeV^4 [27], is 123 order of magnitudes smaller than its natural theoretical value, $\Lambda_{cosmo} \sim m_P^4 \sim 10^{76}$ GeV^4. Until now this discrepancy has remained a true mystery to us.

- *Hierarchy problem.* The Standard Model Higgs sector includes one independent dimensionful parameter, equivalently the Higgs vacuum expectation value or the Higgs mass, of order $\sim 10^2$ GeV. Theoretically one would have expected a value of order $\sim m_P \sim 10^{19}$ GeV, leading to an astonishing fine tuning of 17 order of magnitude.

- *Charge quantisation.* The experiments suggest that the proton and electron charges are equal and opposite in sign: $|Q_e + Q_p| < 10^{-21}$ [41]. In the Standard Model this should be seen as a fine tuning ($f \simeq 10^{-21}$) since it does not provide any natural explanation for such coincidence. Theories of grand unification could be a possible solution, since they predict a quantisation of hypercharge [43].

- *Strong CP problem.* The dimension-four term $\int \mathrm{d}^4x\, \theta_{QCD}\, \epsilon^{\mu\nu\rho\sigma} G^a_{\mu\nu} G^a_{\rho\sigma}$, should in principle appear in the Standard Model Lagrangian, leading to a CP violation in the strong sector. However, its dimensionless coupling has an incredibly small upper bound, $\theta_{QCD} \lesssim 10^{-10}$ [41]. The Peccei–Quinn mechanism could explain this value, and in turn it also imply the existence of a new particle, the axion [44, 45].

- *Flavour puzzle.* The fermion mass spectrum ranges from ~ 170 GeV (top-quark mass) to $\sim 10^{-3}$ GeV (electron mass). Even though the smallness of the fermion masses cannot seen as a naturalness problem, such huge hierarchy in the mass spectrum (more that five orders of magnitude) is unnatural. Furthermore, also the Cabibbo–Kobayashi–Maskawa matrix, describing the flavour mixing between quark families, presents unexplained hierarchies.

According to the naturalness concept, all these problems require a Standard Model completion to accommodate them in a natural way. In particular, the hierarchy problem has dominated the phenomenological speculations of the last three decades, as it will be better discussed in the next section.

What itemised above are difficulties of the Standard Model, arising from the naturalness concept, that can be put in a numerical form (i.e. the fine tuning f can be quantitatively evaluated). However, other questions can be related to naturalness, once this principle is somehow extended to include more qualitative aspects. These new problems can be summarised with the following question: why the Standard Model is the way it is? In other words, is there any natural explanation for all the peculiar features of the Standard Model (such as particle content, particle quantum numbers, number of families, gauge groups)? After all, one verify an amazing cancellation of all gauge anomalies due to the particular choices of these Standard Model features. Can it be just a coincidence? Of course, according to personal taste, these

last issues can appear of philosophical nature and then with not much or no importance. But it is also completely licit to believe that a satisfactory physical theory should explain, or at least motivate, also these aspects.

1.2 The mysteries of the Higgs sector

Dissecting the Standard Model into its different pieces, there is little doubt that the Higgs sector is by far the least understood and the worst measured one.

In sharp contrast with the tightly constrained structure that the gauge sector must display, the Yukawa matrices appearing in the Higgs sector should be considered, within the Standard Model, just irreducible input parameters. Of the overall 18 independent parameters of the theory, 13 are needed just to describe Yukawa interactions. Despite the numerous efforts made in the literature since the 1970's, no clear theory to predict those parameters nor to explain their peculiar structure has so far emerged.

The very nature of the Higgs boson, even after its discovery, is still largely disputed. Its quantum numbers under the $SU(2)_L$ gauge group has been for long under debate, the contention between linear [39, 46–48] and non-linear [49–53] Standard Model effective field theory being just an example in that direction. Also its status of elementary particle is animatedly discussed, the possibility for the Higgs to be a composite particle being a thriving direction of research in present literature [54].

Most of all, however, what has puzzled particle physicist ever since the Standard Model formulation was the electroweak symmetry breakdown scale or, equivalently said, the Higgs mass scale. As already sketched in section 1.1.3, the dimensionful parameter appearing in the Higgs scalar potential is unnatural, in the sense that its mass scale is 17 order of magnitude smaller than what one would expect it to be, i.e. m_P. This is known in the literature as the hierarchy problem. Below, we will examine such issue from a different and more quantitative perspective.

1.2.1 Higgs mass corrections and the hierarchy problem

As already sketched, the core of the hierarchy problem is that the Higgs boson is unnaturally light. When discussing the naturalness concept, it has been argued that the fermions can have masses far below the Planck scale in a natural way, since chiral symmetry is restored in the massless fermions limit . In the case of the Higgs boson mass m_h, no such symmetry enhancement is found in the $m_h \to 0$ limit. This, in turn, implies that loop corrections δm_h^2 to m_h^2 are quadratically divergent, rather than logarithmically divergent as in the case of fermion masses, making unnatural a physical mass m_h far away from m_P, where is thought that quantum field theories find their ultimate ultraviolet cutoff.

To make this last point clearer we can use a simple $\lambda\phi^4$ theory, describing a single scalar boson ϕ. Indeed, introducing a cutoff scale Λ, the diagram given in Fig. 1.1 gives a contribution

$$\delta m^2 = \lambda_S \int^\Lambda \frac{\mathrm{d}k^4}{(2\pi)^4} \frac{1}{k^2} \sim \frac{\lambda_S}{16\pi^2} \int^\Lambda \mathrm{d}k^2 \sim \lambda_S \frac{\Lambda^2}{16\pi^2} \ , \tag{1.5}$$
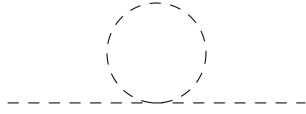
Figure 1.1: One-loop, quadratic divergent scalar mass correction in $\lambda\phi^4$ theory.
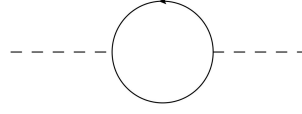
Figure 1.2: One-loop correction to Higgs squared mass m_h^2 due to a Dirac fermion.

where this turns out to be the correct result. Eq. (1.5) can be interpreted as the one-loop correction to the boson mass m^2; as anticipated, it presents a quadratic dependence on Λ.

Thus, in this theory, at one-loop level the physical mass of the boson is

$$m^2 = m_0^2 + \frac{\lambda_S}{16\pi^2}\Lambda^2 \ , \tag{1.6}$$

where m_0^2 is the bare mass, i.e. the parameter entering in the Lagrangian of the theory. We can now appreciate the problem arising from assuming the physical mass m far away from its fundamental scale Λ: even if we put a small value of the bare mass m_0 (that is a small value of the tree level boson mass), this hierarchy would be spoiled by one-loop corrections; if we insist to impose a small value of m at the one-loop order, we need an awkward fine tuning in order to gain a cancellation between the two contributions on the r.h.s. of Eq. (1.6).

In the Standard Model, the Higgs mass receives the most sizeable one-loop corrections from the top quark, through the diagram of Figure 1.2. For a generic fermion f with Yukawa coupling λ_f, such one-loop correction reads

$$\delta m_h^2 = -\frac{|\lambda_f|^2}{8\pi^2}\Lambda^2 \ , \tag{1.7}$$

which is again quadratically divergent. Regardless of the specific expression of one-loop corrections to m_h^2, the important point to stress is that such corrections are quadratically sensitive to the ultimate cutoff scale Λ. If we were to put such scale directly at m_P, the Standard Model would require a fine tuning

$$f \equiv \frac{m_h^2}{\delta m_h^2} \simeq \frac{m_h^2}{\Lambda^2} \sim 10^{-34} \ . \tag{1.8}$$

The intrinsic awkwardness of condition, Eq. (1.8), which looks extremely unlikely and lacks of an explanation whatsoever, is the essence of the hierarchy problem. A possible solution to eliminate (or at least reduce) such huge fine tuning could be to drastically lower the cutoff scale Λ, assuming that new physics first shows up at energies not far above the electroweak scale in order to stabilise the Higgs mass. This simple intuition has triggered and supported a formidable, four-decades-long and still ongoing theoretical effort toward the exploration of Beyond Standard Model theories just above the electroweak scale.

1.2.2 Two paradigms to investigate the Higgs sector

We have so far stressed the reasons why the Higgs sector should deserve particular attention and further dedicated studies. We have also underlined different aspects

which such investigation can focus on, such as the origin of Yukawa interactions or solutions to the hierarchy problem. Whatever the choice, two different (and actually complementary) strategies can be adopted.

A first methodology is the so-called *bottom-up* approach. In such a strategy, the available experimental data (the "bottom") are taken as first steps to build and analyse viable phenomenological models (i.e. to move "up"), in the hope of deriving some general conclusions which can further drive the theoretical investigation. Within such perspective, precise and diversified experimental data are of utmost importance to guide the subsequent phenomenological speculation and, to this extent, a formidable program of Higgs precision measurements will be performed at LHC in future years.

The opposite strategy that can be adopted is a *top-down* paradigm. Within top-down approaches, educated guesses on origin and aspect of new physics are the starting point for theoretical investigation on the structure of those theories. The ambitious aim of such an approach is to shed light to the Standard Model structure and parameters (i.e. to move "down"), starting from first principles (the "top").

In this dissertation, we will examine selected topics in Higgs physics, some of them originating from a bottom-up approach, others appearing from a top-down perspective.

Higgs Pseudo Observables

2.1 Why pseudo observables?

In physics, as in whole of science, the fundamental research is based on the comparison between experimental results and theoretical expectations. Sometimes a new phenomenon is observed before anyone has ever foreseen it and an innovative theoretical work is needed in order to explain it. Sometimes a theoretical insight anticipates, perhaps by decades, its experimental verification. However, the underlying dynamic can be always brought back to such (over)simplified pattern: a physical quantity A is experimentally measured and then compared with its theoretical prediction.

Needless to say, the quantity A should be a measurable quantity, in order for the above process to be meaningful. As trivial as this requirement might appear to a layman, every physicist knows its significance when it comes to quantum physics, where the definition of *physical observable* is highly non-trivial and of pivotal importance. The concept of *observable* in quantum field theory is definitely a sensible topic, whose discussion could easily occupy a whole dissertation on its own. For our present purposes, let us adopt a practical definition, perhaps a bit self-referential, considering an *observable* whatever quantity can be directly measured through an experiment.

Even with such a pragmatic point of view, the distinction between observable and non-observable quantities is not a completely settled issue. Indeed, in last few decades particle physics' experiments have reached unprecedented level of complexities, especially collider experiments. Particles colliders and their detectors are extremely convoluted machines, whose measurements and signals are processed at the hardware and software level even before being selected and stored for subsequent complicated analyses. In such a setting, an ambiguous gray zone clearly arises in our naive observable vs. non-observable distinction.

The physical quantities truly measured by a particle collider are the so-called *raw data*, which are e.g. the energy deposited in a calorimeter in a given event, or the signal registered by silicon trackers, and so on. In order to be useful in any way, those raw data should clearly be combined together. Such minimal recast of raw data results in what we will refer to as *realistic observables* (ROs), for example fiducial cross-sections or forward-backward asymmetries.

Of course one would like to deal with ROs, which suffers from the minimal amount of post-processing needed to convert raw data into useful physical quantities and for this reason are considered completely model independent. However, these qualities of ROs come with a high price both for experimentalists and theorists:

- From the experimental side, to combine different measurements of ROs (both among different experiments and within the same one) is an extremely complex task, given the large number of measurements with different cuts and the complicated structure of the experimental covariance matrices relating their errors.

- From the theoretical side, the prediction of ROs is a very convoluted exercise. Different physical phenomena undertake a complicated interplay which should be correctly described in order to produce a reliable prediction. Even owing such result and observing a discrepancy compared to the experimental RO, to disentangle the underlying physics and identify the origin of such disagreement is equally complicated.

These practical difficulties related to ROs motivate the need to go a step further in recasting experimental results. The aim of such extra processing should be:

- To put those results in a more practical format, which allows an easier combination among different measurements. At the same time, such additional analysis should avoid as far as possible any theoretical assumption.

- To allow a clear association of the measured quantities with theoretical objects. This would facilitate both the calculation of reliable phenomenological predictions and the theoretical interpretation of any anomalous result.

A drawback of such simplification of experimental results is the unavoidable introduction of some minimum theoretical bias. For this reason, the observables extracted in this way are commonly called *pseudo observables* (POs) meaning that, despite they are still technically measurable quantities (i.e. observables), an elaborated post-processing of the experimental data was needed to extract them. POs put themselves in the gray zone between observables and non-observables and they are often depicted as a bridge connecting these two categories. However, it should be stressed that POs are experimentally defined: they should be thought as measurable quantities to be compared with their theoretical predictions and not vice versa.

2.1.1   Theoretical strategy

The theoretical strategy to reduce a RO into POs typically goes through the description of the former in terms of some set of amplitudes. A specific analytical structure of those amplitudes is then assumed based on some motivated theoretical arguments. Such analytical decomposition will eventually depend upon a limited set of unknown parameters, called POs.

The connection between POs and ROs should be discussed in further detail. First of all, the underlying amplitudes deployed to describe the process under study will have a parametric dependence upon the POs, as well as upon a Standard Model complement ($\overline{\text{SM}}$), which are the additional input parameters needed and assumed to

be Standard-Model-like (typical examples are the Fermi constant G_F, or the gauge coupling constants). In formulas:

$$\mathcal{A}_{tot} = \sum_i \mathcal{A}_i(\text{PO}, \overline{\text{SM}}) \ . \tag{2.1}$$

Once the matrix element $\mathcal{A}_{tot}$ is computed, squared and integrated to obtain the cross section of the underlying hard process, one should take into account the soft QED and QCD corrections due to the *initial-* and *final-state radiation* (ISR, FSR). Only after the kinematic distortion of the process due to ISR and FSR is correctly taken into account, one is eventually able to closely relate ROs and POs.

To summarise, the relation between ROs and POs can be schematically represented as:

$$\text{RO} = \left[\left| \mathcal{A} \left(\text{PO} \oplus \overline{\text{SM}} \right) \right|^2 \otimes (\text{ISR} + \text{FSR}) \right] \otimes \begin{matrix} \text{experimental} \\ \text{setup (cuts, ...)} \end{matrix} \ . \tag{2.2}$$

The remaining of this chapter is devoted to a more thorough discussion of a sensible definition of POs, preliminarily in the context of Z, W decays and then in the context of Higgs processes. The complementary discussion regarding the ISR and FSR dressing of the matrix elements, needed to faithfully describe ROs in terms of POs, is left to chapters 3 and 4.

2.1.2 POs at LEP

The pseudo observable approach to collider measurements was first successfully deployed in the 1990's at LEP. One of the main goal of the LEP program was to precisely measure the properties of the Z boson [55–57]. The issue of effectively combining the results obtained by the four different LEP experiments (OPAL, ALEPH, DELPHI, L3) arose and the PO approach was chosen to overcome the difficulties related to this task [58,59]. A comprehensive summary of POs at LEP if far beyond the purposes of this dissertation. We will just focus our attention to a representative example of PO parametrisation, useful both to exemplify the PO paradigm and for our subsequent discussion.

As already well known in the 1990's, the effective interactions of the Z and W bosons to fermions could be modified by new physics effects. Partial decay widths and forward-backward asymmetries in $Z \to f\bar{f}$ and $W \to f_1\bar{f}_2$ decays were extremely interesting observables to this regard, since they are very sensitive to such $Zf\bar{f}$ and $Wf\bar{f}'$ coupling modifications. These possible new physics effects were taken into account by introducing appropriate POs to describe on-shell couplings of Z and W to fermions. In particular, one can parametrise the $V \to f\bar{f}'$ amplitude in terms of such POs as follows [58],

$$\mathcal{A}\left(Z \to f\bar{f}\right) = i\,\varepsilon_\mu^Z \sum_{f=f_L, f_R} g_Z^{ff}\ \bar{f}\gamma_\mu f \ ,$$

$$\mathcal{A}\left(W^+ \to f\bar{f}'\right) = i\,\varepsilon_\mu^W\, g_W^{ff'}\ \bar{f}_L\gamma_\mu f_L' \ , \tag{2.3}$$

where $\varepsilon_\mu^{Z,W}$ are the polarisation vectors of Z, W.

Eq. (2.3), once squared and dressed with ISR and FSR (as discussed in Eq. (2.2)), can be successfully used to express partial decay widths and forward-backward asymmetries of Z and W bosons in terms of their effective couplings with fermions, g_Z^{ff}, $g_W^{\ell\nu}$ and g_W^{ud}. These POs can be computed in any effective field theory (EFT) setting. Within the Standard Model and at tree level, one finds

$$g_Z^{ff,\,\text{SM}} = \frac{g}{c_W}\left(T_3^f - Q_f s_W^2\right)\ , \qquad g_W^{\ell\nu,\,\text{SM}} = \frac{g}{\sqrt{2}}\ , \qquad g_W^{ud,\,\text{SM}} = \frac{g}{\sqrt{2}}V_{ud}\ , \qquad (2.4)$$

where $s_W = \sin\theta_W$, $c_W = \cos\theta_W$ and V_{ud} denote the Cabibbo–Kobayashi–Maskawa (CKM) matrix elements. The LEP experiments measured these POs with an incredible precision, reaching in many cases the per mill level and no significant deviation from their Standard Model expectations was found [59].

2.1.3 POs in Higgs phenomenology

Let us now turn back the discussion to the LHC era and in particular to Higgs physics.

The phenomenology of processes involving one on-shell Higgs boson is a broad and incredibly rich source of informations about the structure of the electroweak sector and a great variety of such processes will be analysed by ATLAS and CMS collaborations in upcoming years [60]. It is therefore of utmost importance to agree on a framework to cast and combine those experimental results, in order to provide a common language both to experimentalists and theorists.

These premises are self-advocating a PO parametrisation of Higgs processes. Such decomposition is again advisable to be performed at the amplitude level, in order to own a direct link both to measurable cross-sections (i.e. ROs) as well as to easily computable quantities in perturbation theory. An immediate simplification is then provided by the narrow width of the Higgs particle, which allows the full factorisation of processes involving one on-shell Higgs into two parts: production and decay.

Once identified the objects to be parametrised with POs (i.e. Higgs production and decay amplitudes), we have to clearly identify the minimum theoretical bias needed to provide a coherent description of the processes under study, at the same time avoiding the proliferation of countless parameters that would frustrate any effort to constrain them.

Our key assumption, vindicated by current status of direct search experiments, is the absence of light new physics states interacting with the Higgs sector. In other words, new physics will be assumed heavier enough to justify an EFT point of view when analysing its contributions to Higgs processes. In fact, the EFT perspective will be used to systematically neglect new physics interaction terms with canonical dimension[1] $D > 6$.

It should be stressed that our deployment of EFT is limited to the power counting stated above, which in turn relies only on the general property that, in absence of light new physics, higher-dimensional operators suffer from a higher suppression. In particular, we will not rely at all on any detail about the realisation of such EFT and in fact we will not need to make any assumption regarding custodial symmetry

---

[1] The power counting will be based on the canonical dimensional analysis: bosons (h, Z, W) and derivatives (i.e. momenta) count as 1, fermions count as 3/2.

and $SU(2)_L$ properties of the Higgs boson. This is an important model independence that could not be achieved in effective Lagrangian descriptions of Higgs processes, which need a precise EFT basis (under definite hypotheses) in order to be predictive [39, 46–53].

To summarise, we want to characterise Higgs phenomenology through a comprehensive PO description of the amplitudes for Higgs decay and production processes, under the only theoretical assumption that no light new physics is involved. Such a program represents a neat improvement and a natural generalisation of the κ-framework so far adopted in LHC experiments [5].

The rest of this chapter is devoted to a review of the Higgs PO (hPO) parametrisation. After the early attempts proposed in Refs. [61, 62], a more general analysis of Higgs decay channels has been proposed in Ref. [3] and will be discussed in section 2.2. The generalisation of such parametrisation to Higgs production processes was first performed in Ref. [4] and will be reviewed in section 2.3.

2.2 POs in Higgs decay

In this section, we will discuss the parametrisation of Higgs decay amplitudes. The phenomenology of such decays in generic Beyond Standard Model contexts is extremely wide and, though possible in principle, we will not thoroughly explore it, in order to keep the presentation more concise. In particular, following the assumptions of Ref. [3],

  - we limit our attention to processes with at most four particles in the final state (besides soft QED and QCD radiation),

  - we assume an exact $U(1)_f$ symmetry acting on each of the light fermion species[2] and therefore no lepton flavour violating decay will be taken into account,

  - we neglect decays resulting from the effective coupling of the Higgs to gluons, such category being hardly accessible from the experimental point of view,

  - we do not consider contributions coming from effective dipole interactions of the Higgs field to light fermions and electroweak gauge bosons, being the interference of these contributions with the leading Standard Model amplitudes suppressed by the light fermion masses.

In addition, one should keep in mind that we will only consider new physics contributions coming from interaction terms with canonical dimension $D \leq 6$, as already discussed in section 2.1.3.

2.2.1 $h \to 4f$ decays

The $h \to 4f$ amplitudes are particularly interesting due to their rich kinematic structure. To analyse such structure with LHC data will allow both to study the effective

---

[2]In the case of left-handed fermions, such $U(1)_{f_L}$ symmetry is understood to act on the full $SU(2)_L$ doublet.

hZZ and hW^+W^- couplings (which cannot be probed on-shell) and to investigate possible new physics couplings of the Higgs with new massive states.

The purpose of our approach is to characterise as precisely as possible the three-point function

$$\mathcal{G}(J_\mu, J'_\nu, h) = \langle 0|\mathcal{T}\{J_\mu(x), J'_\nu(y), h(0)\}|0\rangle \qquad (2.5)$$

of an Higgs boson and two fermion currents, where all particles are on shell. As it will be discussed in the next section, this correlation function can be also probed in Higgs production processes, namely Higgs associated production ($pp \rightarrow h + Z, W$) and vector boson fusion ($pp \rightarrow pp + h$).

We want to take into account possible additional contributions to $\mathcal{G}(J_\mu, J'_\nu, h)$ from new physics interactions with dimension $D \leq 6$. Such problem is simplified by the fact that a local interaction $hJ_\mu J'_\nu g^{\mu\nu}$ has canonical dimension $D = 7$ and we can thus neglect it. As a result, the correlation function (2.5) is non-local at the electroweak scale, with at least one fermion pair generated by the propagation of one electroweak gauge boson. This crucial observation has two major consequences:

- Any $h \rightarrow 4f$ amplitude can be decomposed into a sum of neutral-current (NC) and charged-current (CC) contributions, according to the charge of the intermediate-state gauge boson(s) involved.

- The form factors involved in both NC and CC amplitudes can be Laurent-expanded around the physical poles produced by the propagation of the Standard Model gauge bosons (Z, W and γ).

These considerations can be symbolically represented by the following equation:

$$h \rightarrow 4f = \sum_{V^{(\prime)}=Z,A,W} \left[(h \rightarrow V^* f\bar{f} \rightarrow 4f) + (h \rightarrow f\bar{f} V'^* \rightarrow 4f) \right.$$
$$\left. + (h \rightarrow V^* V'^* \rightarrow 4f)\right], \qquad (2.6)$$

where the sum over $V^{(\prime)}$ accounts for NC and CC contributions (not both of them may always be present), while the different intermediate virtual states represent the different terms in the pole expansion of those contributions. In Eq. (2.6), an additional suitable sum to properly symmetrise the amplitude is also implicitly understood, as it will be discussed later.

Along the line of the above discussion, our PO description of correlation function (2.5) can be preformed in two steps. First, we define a comprehensive PO framework for the underlying NC and CC processes. Then, we explain how to describe realistic $h \rightarrow 4f$ decay amplitudes by means of such parametrisation. This discussion will be carried out here for leptonic channels, which are more interesting from the experimental point of view[3].

---

[3]The analysis of processes involving quarks is absolutely equivalent, with the only additional technical complication of the non-diagonal structure of the POs in flavour space (due to the CKM mixing), which would force us to keep track of numerous additional flavour indices.

In full generality, the tensor structure of the amplitude for both NC and CC processes can be decomposed as follows:

$$\mathcal{A}\left(h \to J(q_1)J'(q_2)\right)_{nc,cc} = i\,\frac{2m_V^2}{v}\,J_\mu\,J_\nu'^\dagger\,\mathcal{T}_{nc,cc}^{\mu\nu}(q_1,q_2)\,,$$

$$\mathcal{T}_{nc,cc}^{\mu\nu}(q_1,q_2) = F_L^{\ell\ell'}(q_1^2,q_2^2)_{nc,cc}\,g^{\mu\nu} + F_T^{\ell\ell'}(q_1^2,q_2^2)_{nc,cc}\,\frac{q_1\cdot q_2\,g^{\mu\nu} - q_2^\mu q_1^\nu}{m_V^2}$$

$$+ F_{\mathrm{CP}}^{\ell\ell'}(q_1^2,q_2^2)_{nc,cc}\,\frac{\varepsilon^{\mu\nu\alpha\beta}\,q_{1\,\alpha}\,q_{2\,\beta}}{m_V^2}\,,\tag{2.7}$$

where $J_\mu^{(\prime)} = \bar{\ell}^{(\prime)}\gamma_\mu\ell^{(\prime)}$ for NC and $J_\mu^{(\prime)} = \bar{\ell}_L^{(\prime)}\gamma_\mu\nu_L^{(\prime)}$ for CC ($\nu_L^{(\prime)}$ being the $SU(2)_L$ partner of $\ell_L^{(\prime)}$). Fermions are understood to be chiral. The m_V normalisation has been chosen for future convenience, being $m_V = m_Z, m_W$ for NC and CC, respectively.

The scalar form factors $F(q_1^2, q_2^2)$ of Eq. (2.7) can be now Laurent-expanded around the physical poles of the propagating Standard Model gauge bosons, accordingly to their charge and tensor properties. Each term of the expansion will then be controlled by a different PO.

For NC form factors, one gets

$$F_L^{\ell\ell'}(q_1^2,q_2^2) = \kappa_{ZZ}\frac{g_Z^{\ell\ell}\,g_Z^{\ell'\ell'}}{P_Z(q_1^2)P_Z(q_2^2)} + \frac{\epsilon_Z^{\ell\ell}}{m_Z^2}\frac{g_Z^{\ell'\ell'}}{P_Z(q_2^2)} + \frac{\epsilon_Z^{\ell'\ell'}}{m_Z^2}\frac{g_Z^{\ell\ell}}{P_Z(q_1^2)} + \Delta_L^{\mathrm{SM}}(q_1^2,q_2^2)\,,$$

$$F_T^{\ell\ell'}(q_1^2,q_2^2) = \epsilon_{ZZ}\frac{g_Z^{\ell\ell}\,g_Z^{\ell'\ell'}}{P_Z(q_1^2)P_Z(q_2^2)} + \epsilon_{Z\gamma}\left(\frac{eQ_\ell}{q_1^2}\frac{g_Z^{\ell'\ell'}}{P_Z(q_2^2)} + \frac{eQ_{\ell'}}{q_2^2}\frac{g_Z^{\ell\ell}}{P_Z(q_1^2)}\right)$$

$$+ \epsilon_{\gamma\gamma}\frac{e^2Q_\ell Q_{\ell'}}{q_1^2 q_2^2} + \Delta_T^{\mathrm{SM}}(q_1^2,q_2^2)\,,$$

$$F_{\mathrm{CP}}^{\ell\ell'}(q_1^2,q_2^2) = +\,\epsilon_{ZZ}^{\mathrm{CP}}\frac{g_Z^{\ell\ell}\,g_Z^{\ell'\ell'}}{P_Z(q_1^2)P_Z(q_2^2)} + \epsilon_{Z\gamma}^{\mathrm{CP}}\left(\frac{eQ_\ell}{q_1^2}\frac{g_Z^{\ell'\ell'}}{P_Z(q_2^2)} + \frac{eQ_{\ell'}}{q_2^2}\frac{g_Z^{\ell\ell}}{P_Z(q_1^2)}\right)$$

$$+ \epsilon_{\gamma\gamma}^{\mathrm{CP}}\frac{e^2Q_\ell Q_{\ell'}}{q_1^2 q_2^2}\,,\tag{2.8}$$

while for CC form factor one gets

$$F_L^{\ell\ell'}(q_1^2,q_2^2) = \kappa_{WW}\frac{g_W^{\ell\nu}\,(g_W^{\ell'\nu'})^*}{P_W(q_1^2)P_W(q_2^2)} + \frac{\epsilon_W^{\ell\nu}}{m_W^2}\frac{(g_W^{\ell'\nu'})^*}{P_W(q_2^2)} + \frac{(\epsilon_W^{\ell'\nu'})^*}{m_W^2}\frac{g_W^{\ell\ell}}{P_W(q_1^2)}\,,$$

$$F_T^{\ell\ell'}(q_1^2,q_2^2) = \epsilon_{WW}\frac{g_W^{\ell\nu}\,(g_W^{\ell'\nu'})^*}{P_W(q_1^2)P_W(q_2^2)}\,,$$

$$F_{\mathrm{CP}}^{\ell\ell'}(q_1^2,q_2^2) = \epsilon_{WW}^{\mathrm{CP}}\frac{g_W^{\ell\nu}\,(g_W^{\ell'\nu'})^*}{P_W(q_1^2)P_W(q_2^2)}\,,\tag{2.9}$$

In Eqs. (2.8) and (2.9), $g_{Z,W}^{\ell_1\ell_2}$ are the POs defined in Eq. (2.3), while $P_V(q^2) = q^2 - m_V^2 + i\,m_V\Gamma_V$.

Let us briefly summarise the full list of POs introduced to describe NC and CC $h \to JJ'$ processes:

- κ_{ZZ}, κ_{WW}, which parametrise the Standard-Model-like hZZ and hWW interactions. These are the only POs receiving a non-vanishing tree-level Standard Model contribution. Due to the chosen overall normalisation, we have

$$\kappa_{ZZ}^{\mathrm{SM,\,tree}} = \kappa_{WW}^{\mathrm{SM,\,tree}} = 1 \ . \tag{2.10}$$

- $\epsilon_{ZZ}^{\mathrm{(CP)}}, \epsilon_{Z\gamma}^{\mathrm{(CP)}}, \epsilon_{\gamma\gamma}^{\mathrm{(CP)}}, \epsilon_{WW}^{\mathrm{(CP)}}$, which parametrise the non-standard interactions of the Higgs with the Standard Model gauge bosons. These are real-valued, flavour-universal POs whose Standard Model tree-level prediction vanishes. Some of the CP-even POs receives small Standard Model contributions at next-to-leading order (NLO) [63, 64], which are nevertheless below the 1% level and practically unobservable [65].

- $\epsilon_Z^{\ell\ell}, \epsilon_W^{\ell\nu}$, which parametrise the contact interactions of the Higgs with a fermion current and a Standard Model gauge boson. These are flavour-dependent parameters. $\epsilon_Z^{\ell\ell}$ are real-valued, $\epsilon_W^{\ell\nu}$ are complex-valued.

- $\Delta_{L,T}^{\mathrm{SM}}(q_1^2, q_2^2)$. These functions encode non-local Standard Model contributions generated beyond tree level, which cannot be described in terms of $D \leq 6$ effective operators.

As promised, owing the parametrisation of the underlying NC and CC processes, we can now discuss the complete decomposition of a generic $h \to 4f$ amplitude. Once again, we will limit ourselves to (visible) leptonic decay channels, the generalisation to quark channels being notationally involved but conceptually straightforward.

The discussion is actually simpler than it might seems. In the case of $h \to 2\ell\, 2\ell'$, with $\ell \neq \ell'$, the full amplitude is determined by a single neutral current amplitude. For the case $h \to 2\ell\, 2\ell$, the proper symmetrisation of the underlying NC amplitude is needed:

$$\mathcal{A}\left(h \to \ell(p_1)\bar{\ell}(p_2)\ell(p_3)\bar{\ell}(p_4) \right) = \mathcal{A}\left(h \to J(p_1 + p_2)J'(p_3 + p_4) \right)_{nc}$$
$$+ \mathcal{A}\left(h \to J(p_1 + p_4)J'(p_3 + p_2) \right)_{nc} \ . \tag{2.11}$$

The $h \to \ell\bar{\nu}\,\bar{\ell}'\nu'$ decay, with $\ell \neq \ell'$ (and $\nu^{(\prime)}$ the $SU(2)_L$ partner of $\ell^{(\prime)}$), receives again contribution from a single (CC) amplitude. Finally, the $h \to \ell\bar{\ell}\nu\bar{\nu}$ channel results from the sum of a NC and CC process:

$$\mathcal{A}\left(h \to \ell(p_1)\bar{\ell}(p_2)\nu(p_3)\bar{\nu}(p_4) \right) = \mathcal{A}\left(h \to J(p_1 + p_2)J'(p_3 + p_4) \right)_{nc}$$
$$+ \mathcal{A}\left(h \to J(p_1 + p_4)J'(p_2 + p_3) \right)_{cc} \ . \tag{2.12}$$

On top of these prescriptions, one should of course remember to perform a sum over all possible fermion chiralities whenever the fermion polarisations are not experimentally accessible.

2.2.2 $h \to \gamma\gamma$ and $h \to f\bar{f}\gamma$

The formalism introduced to describe the $h \to 4f$ decay modes is automatically able to parametrise two additional interesting Higgs decay channels: $h \to \gamma\gamma$ and

$h \to f\bar{f}\gamma$. Indeed, it is evident from Eq. (2.6) that such two channels has been already considered (in the off-shell case) as part of the $h \to 4f$ decomposition.

Just by comparison with Eqs. (2.7) and (2.8), we can immediately write down:

$$\mathcal{A}\left(h \to \gamma(q,\varepsilon)\gamma(q',\varepsilon')\right) = i\frac{2}{v}\,\varepsilon'_\mu\varepsilon_\nu\left[\epsilon_{\gamma\gamma}(q\cdot q'\,g^{\mu\nu} - q^\mu q'^\nu) + \epsilon_{\gamma\gamma}^{\text{CP}}\,\varepsilon^{\mu\nu\alpha\beta}q_\alpha q'_\beta\right]\,, \quad (2.13)$$

$$\mathcal{A}\left(h \to J(p)\gamma(q,\varepsilon)\right) = i\frac{2}{v}\,J_\mu\varepsilon_\nu\left[F_T^{f\gamma}(p^2)(p\cdot q\,g^{\mu\nu} - p^\mu q^\nu) + F_{\text{CP}}^{f\gamma}(p^2)\,\varepsilon^{\mu\nu\alpha\beta}p_\alpha q_\beta\right]\,, \tag{2.14}$$

where $J_\mu = \bar{f}\gamma_\mu f$ and, in complete analogy with Eq. (2.8),

$$F_T^{f\gamma}(p^2) = \epsilon_{Z\gamma}\frac{g_Z^{ff}}{P_Z(p^2)} + \epsilon_{\gamma\gamma}\frac{eQ_f}{p^2} + \Delta_{T,f\gamma}^{\text{SM}}(p^2)\,,$$

$$F_{\text{CP}}^{f\gamma}(p^2) = \epsilon_{Z\gamma}^{\text{CP}}\frac{g_Z^{ff}}{P_Z(p^2)} + \epsilon_{\gamma\gamma}^{\text{CP}}\frac{eQ_f}{p^2}\,. \tag{2.15}$$

Once again, $\Delta_{T,f\gamma}^{\text{SM}}(p^2)$ encodes non-local Standard Model contribution arising at loop level.

2.2.3 Parameter counting and symmetry limits

We are now ready to identify the number of independent POs necessary to describe various sets of Higgs decay amplitudes, under the main assumption that only terms arising at $D \le 6$ in a generic EFT expansion are kept. We focus our attention on leptonic channels involving the first two generations, which are more interesting from the experimental point of view.

The neutral current processes $h \to 2e\,2\mu$, $h \to 4e$ and $h \to 4\mu$, together with the photon channels $h \to \gamma\gamma$ and $h \to \ell^+\ell^-\gamma$, can be described in terms of 11 real parameters,

$$\kappa_{ZZ}, \epsilon_{ZZ}^{(\text{CP})}, \epsilon_{Z\gamma}^{(\text{CP})}, \epsilon_{\gamma\gamma}^{(\text{CP})}, \epsilon_Z^{e_L e_L}, \epsilon_Z^{e_R e_R}, \epsilon_Z^{\mu_L \mu_L}, \epsilon_Z^{\mu_R \mu_R}\,, \tag{2.16}$$

of which only $\{\epsilon_{Z\gamma}^{(\text{CP})}, \epsilon_{\gamma\gamma}^{(\text{CP})}\}$ are necessary to describe $h \to \gamma\gamma, \ell^+\ell^-\gamma$. The charged-current process $h \to e^-\bar{\nu}_e e\mu^+\nu_\mu$ needs 7 further independent real parameters to be completely specified:

$$\kappa_{WW}, \epsilon_{WW}^{(\text{CP})}, \epsilon_W^{e_L\nu}, \epsilon_W^{\mu_L\nu}\,, \tag{2.17}$$

where $\epsilon_W^{e_L\nu_e}$ and $\epsilon_W^{\mu_L\nu_\mu}$ are complex. Finally, the mixed processes $h \to 2e\,2\nu$ and $h \to 2\mu\,2\nu$ can be described through the already introduced coefficients plus 2 further real parameters:

$$\epsilon_Z^{\nu_e\nu_e}, \epsilon_Z^{\nu_\mu\nu_\mu}\,. \tag{2.18}$$

Overall, we have introduced 20 real parameters. However, one could use symmetry arguments that allow to reduce such number of free parameters while remaining, at the same time, as model-independent as possible:

- One possibility is to assume flavour universality (i.e. enlarging the flavour symmetry to the full $U(3)^5$ flavour group). In our setup, this assumption affects the contact interaction coefficient, which becomes generation independent:

$$\epsilon_Z^{e_L e_L} = \epsilon_Z^{\mu_L \mu_L} \ , \quad \epsilon_Z^{e_R e_R} = \epsilon_Z^{\mu_R \mu_R} \ , \quad \epsilon_W^{e_L \nu} = \epsilon_W^{\mu_L \nu} \ , \quad \epsilon_Z^{\nu_e \nu_e} = \epsilon_Z^{\nu_\mu \nu_\mu} \ . \quad (2.19)$$

Since the last coefficients are complex in general, these are five relations which allow to reduce the number of parameters to 15. This assumption can be tested directly from data by comparing the extraction of the contact terms from $h \to 2e\,2\mu$, $h \to 4e$ and $h \to 4\mu$ modes.

- Another motivated assumption could be to take CP as a good approximate symmetry of the Beyond Standard Model sector and the Higgs as a CP-even state. This allows us to set to zero six independent (real) coefficients:

$$\epsilon_{ZZ}^{\mathrm{CP}} = \epsilon_{Z\gamma}^{\mathrm{CP}} = \epsilon_{\gamma\gamma}^{\mathrm{CP}} = \epsilon_{WW}^{\mathrm{CP}} = i\,\epsilon_W^{e_L \nu_e} = i\,\epsilon_W^{\mu_L \nu_\mu} = 0 \ . \quad (2.20)$$

Assuming at the same time flavour universality, the number of free real parameters reduces to 10.

- In numerous scenarios, the Beyond Standard Model sector is invariant under the custodial symmetry group $G = SU(2)_L \times SU(2)_R \times U(1)_X$, spontaneously broken to the diagonal $H = SU(2)_{L+R} \times U(1)_X$. Depending on the details regarding the implementation of such symmetry, non-trivial relations among different POs can be derived (see e.g. [3, 48, 66]).

2.2.4 differential distribution for $h \to 2e\,2\mu$

The study of differential decay distributions is of great importance and has gained attention in the literature [67–70]. CMS already performed a comprehensive study of $h \to 4\ell$ decays with present data, in the context of hVV anomalous couplings [71]. Such kind of analyses can be effectively exploited to extract the Higgs POs defined in section 2.2.2.

One can take as an example the $h \to 2e\,2\mu$ decay,

$$h \to e^-(p_1)e^+(p_2)\mu^-(p_3)\mu^+(p_4) \ , \quad (2.21)$$

which is a particularly clean channel. Calculating the modification of the total rate and keeping only terms linear in ϵ_X and $\delta\kappa_{ZZ} \equiv \kappa_{ZZ} - 1$, one finds [3]:

$$\frac{\Gamma(h \to 2e\,2\mu)}{\Gamma^{SM}(h \to 2e\,2\mu)} = 1 + 2\delta\kappa_{ZZ} - 2.5(\epsilon_Z^{e_R e_R} + \epsilon_Z^{\mu_R \mu_R}) + 2.9(\epsilon_Z^{e_L e_L} + \epsilon_Z^{\mu_L \mu_L})$$
$$+ 0.5\epsilon_{ZZ} - 0.9\epsilon_{Z\gamma} + 0.01\epsilon_{\gamma\gamma} \ . \quad (2.22)$$

Obviously, the measurement of the total rate is not enough to extract the POs and one should exploit the full kinematics of the process.

We then focus our attention to the double-differential decay distribution in each lepton pair's invariant mass, which is to say

$$\mathcal{F}_{\ell\ell}(q_1^2, q_2^2) = \frac{\mathrm{d}^2\Gamma(h \to 2e\,2\mu)}{\mathrm{d}q_1^2 \mathrm{d}q_2^2} \ , \quad (2.23)$$
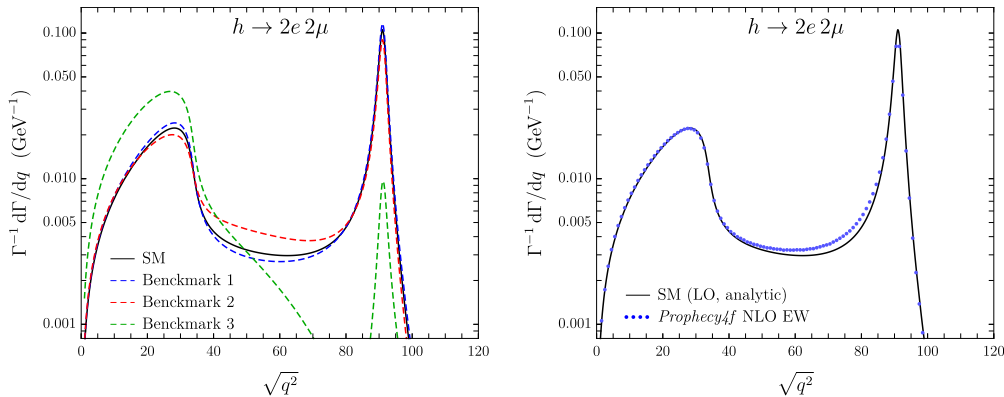
Figure 2.1: *Left*: Comparison of resulting dilepton spectrum $\mathcal{F}_\ell(\sqrt{q^2})$ between the Standard Model and three different new physics benchmarks (benchmark 1: $\kappa_{ZZ} = 1.3$, $\epsilon_Z^{e_R e_R} = \epsilon_Z^{\mu_R \mu_R} = -\epsilon_Z^{e_L e_L} = -\epsilon_Z^{\mu_L \mu_L} = 0.05$; benchmark 2: $\kappa_{ZZ} = 0$, $\epsilon_Z^{e_L e_L} = \epsilon_Z^{\mu_L \mu_L} = 0.26$; benchmark 3: $\kappa_{ZZ} = 0.3$, $\epsilon_Z^{e_L e_L} = -0.45$). *Right*: Comparison between LO Standard Model prediction for $\mathcal{F}_\ell(\sqrt{q^2})$ and NLO electroweak prediction through the Monte Carlo generator *Prophecy4f* [72].

where $q_1 = p_1 + p_2$ and $q_2 = p_3 + p_4$ (see Eq. (2.21)). Fully analytic expressions for $\mathcal{F}_{\ell\ell}(q_1^2, q_2^2)$ has been derived in Ref. [3]. For the purposes of this dissertation, it is only important to remark that:

- $\mathcal{F}_{\ell\ell}(q_1^2, q_2^2)$ is a second-order polynomial in the POs for each value of q_1^2 and q_2^2. This implies that, in principle, owing the experimental values of $\mathcal{F}_{\ell\ell}(q_1^2, q_2^2)$ for a sufficient number of bins would allow an exhaustive fit of the POs involved in the process.

- Given the kinematic of the process, one can derive

$$\sqrt{q_1^2} + \sqrt{q_2^2} \leq m_h \ , \tag{2.24}$$

which allows to define the single-differential decay width as

$$\mathcal{F}_\ell(q_1^2) = \int_0^{\zeta^2} dq_2^2 \, \mathcal{F}_{\ell\ell}(q_1^2, q_2^2) \ , \tag{2.25}$$

where $\zeta = m_h - \sqrt{q_1^2}$. In principle we could also define $\mathcal{F}_\ell(q_2^2)$ from the analogous integration over q_1^2. One should however notice that the two functions would differ only by terms suppressed by m_μ^2 / q_i^2, irrelevant for all practical purposes.

The single-differential width $\mathcal{F}_\ell(q_1^2)$ is as well a precious source of information and it can be used to disentangle new physics contributions from different POs. As an example, in Figure 2.1 we compare the Standard Model prediction for $\mathcal{F}_\ell(\sqrt{q^2})$ with three different new physics benchmarks, all predicting small deviations of the total decay width (according to Eq. (2.22)):
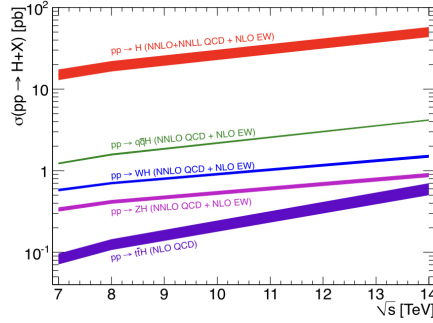
Figure 2.2: The Standard Model Higgs boson production cross sections as a function of the center of mass energy, $\sqrt{s}$, for pp collisions [74]. The theoretical uncertainties are indicated as a band.

- Benchmark 1 ($\kappa_{ZZ} = 1.3$, $\epsilon_Z^{e_R e_R} = \epsilon_Z^{\mu_R \mu_R} = -\epsilon_Z^{e_L e_L} = -\epsilon_Z^{\mu_L \mu_L} = 0.05$) represents a mild deviation of POs from their Standard Model values. As a result, the dilepton spectrum $\mathcal{F}_\ell(q_1^2)$ receives a moderate distortion (up to 15% in the central region).

- Benchmark 2 ($\kappa_{ZZ} = 0$, $\epsilon_Z^{e_L e_L} = \epsilon_Z^{\mu_L \mu_L} = 0.26$) represents a sizeable deviation from the Standard Model point. However, the PO configuration is such that deviations in the dilepton spectrum are not dramatic (up to 40% in the central region).

- Benchmark 3 ($\kappa_{ZZ} = 0.3$, $\epsilon_Z^{e_L e_L} = -0.45$) represents a scenario with a sizeable distortion of the Standard Model spectrum.

It should be clear at this point that the study of differential distributions in $h \to 2e\, 2\mu$ decay has a great potential in discovering and disentangling new physics effects. However, in order to reach the required level of precision, the issue of ISR and FSR introduced in section 2.1 (see Eq. (2.2)) should be addressed. The importance of including distortions due to ISR and FSR is shown in the right plot of Figure 2.1. The analytic prediction for $\mathcal{F}_\ell(\sqrt{q^2})$ within the Standard Model (at leading order, LO) is compared with the NLO electroweak results [73] obtained through the Monte Carlo generator *Prophecy4f* [72], which suitably takes ISR and FSR effects into account. Such distortions reaches the 20% of the leading-order value in the central $\sqrt{q^2}$ region, legitimising our need to include those effects in our discussion. In chapter 3 we will address such issues from an analytical perspective.

2.3 POs in Higgs production

The dominant Higgs production mechanism at LHC is by far gluon-gluon fusion ($gg \to h$), as can be appreciated in Fig. 2.2 [74]. Nevertheless the leading electroweak processes, namely vector-boson fusion (VBF, $f_1 f_2 \to h + f_3 f_4$) and associated Vh production ($f_1 f_2 \to h + W/Z$), are experimentally accessible and extremely interesting mechanisms, since they can provide complementary channels to characterise the Higgs boson properties.

In this section we want to extend the hPO framework, so far deployed for Higgs decays, to VBF and Vh production processes. The reason for such effort is twofold. On the one hand, electroweak production processes are closely connected to the $h \to 4f$ decays by crossing symmetry. As a result, the set of POs needed to describe the two class of processes is the same. The only important difference is that, while in the $h \to 4f$ case we were mainly interested in leptonic channels ($h \to 4\ell, h \to 2\ell 2\nu$), for Higgs production we should clearly focus our attention to quark currents (i.e. initial state partons and final state jets). On the other hand, studying production cross section allows us to explore different kinematic regimes compared to Higgs decays. By construction, the momentum transfer appearing in Higgs decay amplitudes is limited by the Higgs mass, while such limitation is not present in production amplitudes. This fact would also allows us to test the momentum expansion that is intrinsic in the PO decomposition, as well as in any effective field theory approach to physics beyond the Standard Model.

Despite the similarities at the fundamental level, the phenomenological description of VBF and Vh in terms of hPO is significantly more challenging compared to that of Higgs decays. On reason are QCD corrections, which play a non-negligible role in production processes [75–80]. Although technically challenging, this fact does not represent a conceptual problem for the PO approach: the leading QCD corrections factorise in VBF and Vh, similarly to the factorisation of QED corrections which will be discussed in the next chapter. Another reason is the non-trivial relation between kinematic variables at the basis of the PO decomposition (i.e. the momentum transfer of the partonic currents, q^2) and the kinematic variables accessible in pp collisions, especially in the VBF case.

In this dissertation we are only interested in the PO parametrisation of the relevant amplitudes, in order to subsequently discuss in chapter 4 the electroweak corrections due to their ISR and FSR dressing. The complications related to QCD soft radiation and collider accessibility of the kinematic variables has been mentioned here only for completeness and will not be discussed further.

2.3.1 VBF Higgs production

VBF is intimately related to $h \to 4f$ discussed in section 2.2.1 by crossing symmetry. In fact, both processes can be described by the same Green function $\mathcal{G}(J_\mu, J'_\nu, h)$ of Eq. (2.5),

$$\mathcal{G}(J_\mu, J'_\nu, h) = \langle 0 | \mathcal{T} \{ J_\mu(x), J'_\nu(y), h(0) \} | 0 \rangle \ .$$

As a consequence, the discussion of VBF can be made in close analogy to the discussion of section 2.2.1. In particular, we can again introduce the meaningful distinction between underlying NC and CC processes, perhaps both present and interfering with each other. We will first take care of parametrising such underlying processes, then discussing once again how to combine them to describe real processes.

Owing the distinction between NC and CC processes, the $q_i q_j \to q_k q_m h$ amplitude can be generally parametrised as follows:

$$\mathcal{A} \left(q_i(p_1) q_j(p_2) \to q_k(p_3) q_m(p_4) h(p_h) \right)_{nc,\,cc} = i \, \frac{2 m_V^2}{v} \left(\bar{q}_i(p_3) \gamma_\mu q_k(p_1) \right) \left(\bar{q}_m(p_4) \gamma_\mu q_j(p_2) \right)$$

$$\times \, \mathcal{T}_{nc,\,cc}^{\mu\nu}(q_1, q_2) \, ,$$

$$\mathcal{T}_{nc,\,cc}^{\mu\nu}(q_1, q_2) = F_L^{ijkm}(q_1^2, q_2^2)_{nc,\,cc}\, g^{\mu\nu} + F_T^{ijkm}(q_1^2, q_2^2)_{nc,\,cc}\, \frac{q_1 \cdot q_2 \, g^{\mu\nu} - q_2^\mu q_1^\nu}{m_V^2}$$

$$+ F_{\mathrm{CP}}^{ijkm}(q_1^2, q_2^2)_{nc,\,cc}\, \frac{\varepsilon^{\mu\nu\alpha\beta}\, q_{1\,\alpha}\, q_{2\,\beta}}{m_V^2} \, , \tag{2.26}$$

where $q_1 = p_1 - p_3$, $q_2 = p_2 - p_4$ and $m_V = m_{Z,W}$ depending whether the process is NC or CC.

As anticipated, the tensor structures $\mathcal{T}_{nc,\,cc}^{\mu\nu}(q_1, q_2)$ are in complete analogy with Eq. (2.7). In fact, also the form factors $F(q_1^2, q_2^2)$ are defined exactly as in Eqs. (2.8), (2.9), once the flavour indices are suitably generalised to consider the quark currents case. For example, $F_L^{ijkm}(q_1^2, q_2^2)_{nc}$ reads:

$$F_L^{ijkl}(q_1^2, q_2^2)_{nc,cc} = \kappa_{VV} \frac{g_V^{ik}\, g_V^{jm}}{P_V(q_1^2) P_V(q_2^2)} + \frac{\epsilon_V^{ik}}{m_V^2} \frac{g_V^{jm}}{P_V(q_2^2)} + \frac{\epsilon_V^{jm}}{m_V^2} \frac{g_V^{ik}}{P_V(q_1^2)} + \Delta_L^{\mathrm{SM}}(q_1^2, q_2^2) \, , \tag{2.27}$$

where $V = Z, W$ for NC and CC, respectively. The generalisation of the remaining form factors is straightforward and we refer to the original literature for their explicit expressions[4] [4].

Once parametrised the underlying NC and CC processes, one should again undertake a proper symmetrisation of the amplitude to describe real processes. For example, in $uu \to uu\,h$ two NC processes interfere, while in $ud \to ud\,h$ there is an interference between a NC and a CC process. A proper sum over all possible channels is thus to be performed, once again in complete analogy to the one discussed in Eqs. (2.11), (2.12).

We want to stress once more that the POs appearing in VBF parametrisation (Eq. (2.27) and similar) are the same that appear in Eqs. (2.8), (2.9). This is because they all belong to the same tensor and Laurent decomposition of the underlying Green function $\mathcal{G}(J_\mu, J'_\nu, h)$, which is the same for VBF and $h \to 4f$ decays. The only significant difference is that, while in Higgs decays the most interesting channels are the ones involving lepton currents ($h \to 4\ell, 2\ell2\nu$), VBF is clearly able to probe only quark currents. This fact gives decay and production channels complementary features when it comes to test the flavour-dependent POs (i.e. $\epsilon_V^{f_i f_j}$). Flavour-independent ones are instead typically best constrained using decay channels due to their higher cleanness.

2.3.2　Associated Vh production

At first sight the associated Vh production process, $q\bar{q} \to Vh$, cannot be described by the three-point Green function $\mathcal{G}(J_\mu, J'_\nu, h)$, used to parametrise both $h \to 4f$ and VBF, since we are now dealing with different external legs.

However, before rushing conclusions, one should have a closer look at the assumptions used to decompose $\mathcal{G}(J_\mu, J'_\nu, h)$. In particular it should be recalled that, as a

---

[4]We warn the reader that, in the original articles, form factors for the NC and CC case are called F and G respectively.

consequence of our EFT approach (i.e. neglecting interactions with canonical dimension $D > 6$), such correlation function is non-local and the propagation of at least one electroweak gauge boson should always be advocated in the decomposition. Through Eq. (2.6) one can see that, by imposing V^* to be on shell (and removing the second decay steps), the PO description of $h \to 4f$ can be straightforwardly exploited to describe $h \to Vff$, the latter being intimately related to Vh production by crossing symmetry.

The above argument eventually allows us to describe the amplitude for $f\bar{f} \to Vh$ with exactly the same formalism and the same POs used so far. Using a compact notation encoding both NC and CC processes, we then decompose the Vh production amplitude in a way that should be by now familiar to the reader:

$$
\mathcal{A}\left(f_1(p_1)\,\bar{f}_2(p_2) \to V(k)\,h(p_h)\right) = 2\,i\,\frac{m_V^2}{v}\,\bar{f}_2(p_2)\gamma_\nu f_1(p_1)\epsilon^*_{V\,\mu}(k)
$$
$$
\times \left[F_L^{f_1 f_2 V}(q^2)\,\eta^{\mu\nu} + F_T^{f_1 f_2 V}(q^2)\,\frac{q^\mu k^\nu - (q \cdot k)\eta^{\mu\nu}}{m_V^2} + F_{CP}^{f_1 f_2 V}(q^2)\frac{\epsilon^{\mu\nu\alpha\beta}q_\alpha k_\beta}{m_V^2} \right] ,
$$
$$
(2.28)
$$

where the form factors read

$$
F_L^{f_1 f_2 V}(q^2) = \kappa_{VV}\,\frac{g_V^{f_1 f_2}}{P_V(q^2)} + \frac{\epsilon_V^{f_1 f_2}}{m_V^2} + \Delta_L^{\mathrm{SM}}(q^2) ,
$$
$$
F_T^{f_1 f_2 V}(q^2) = \epsilon_{VV}\,\frac{g_V^{f_1 f_2}}{P_V(q^2)} + \delta_{VZ}\,\epsilon_{Z\gamma}\,\frac{e\,Q_{f_1}}{q^2} + \Delta_T^{\mathrm{SM}}(q^2) ,
$$
$$
F_{CP}^{f_1 f_2 V}(q^2) = \epsilon_{VV}^{\mathrm{CP}}\,\frac{g_V^{f_1 f_2}}{P_V(q^2)} - \delta_{VZ}\,\epsilon_{Z\gamma}^{\mathrm{CP}}\,\frac{e\,Q_{f_1}}{q^2} ,
$$
$$
(2.29)
$$

with $V = Z, W^\pm$. Here δ_{VZ} is a Kronecker delta, giving 1 for $V = Z$ and 0 otherwise.

Radiative corrections in Higgs decay

3.1 The issue of initial- and final-state radiation

In the previous chapter, we have analysed various Higgs processes, performing a parametrisation of their underlying Green functions. In fact, we were able to describe all processes of interest using only the correlation function

$$\mathcal{G}(J_\mu, J'_\nu, h) = \langle 0 | \mathcal{T}\big\{ J_\mu(x), J'_\nu(y), h(0) \big\} | 0 \rangle$$

introduced in Eq. (2.5).

Since we are working at the Green function level, it should be immediately clear that the PO framework is not a tree-level description which requires loop corrections and a renormalisation procedure, but is rather the parametrisation of a well-defined, non-perturbative object, $\mathcal{G}(J_\mu, J'_\nu, h)$. Nevertheless, we should care about another kind of next-to-leading order (NLO) corrections, namely the ones related to the issue of initial- and final-state radiation (ISR and FSR), already anticipated in section 2.1.

In order to understand the need of taking into account ISR and FSR, we should go back to the very concept of observable. A particular scattering or decay process should be considered an observable only if such process can be unambiguously distinguished, at least in principle, from the background. However, in the case of the extra emission of one (or more) undetectably soft photon(s) or gluon(s), such distinction is meaningless. In other words, processes with emission of massless boson(s) with energy lower than an experimental threshold[1] should be seen as processes equivalent[2] to the one where no soft radiation is emitted, therefore only the sum of all of them (non-radiative and soft-radiative) can be legitimately considered a well-defined observable.

The issue of soft radiation conceptually justify why we should always include ISR and FSR in our discussion, since they are necessary ingredients to relate realistic observables (ROs) to POs (the latter parametrising only the non-radiative process,

---

[1]Such threshold can be considered extremely small, but it is nevertheless always a finite experimental quantity.

[2]In other words, soft-radiative and non-radiative processes should be effectively considered as degenerate, since experimentally indistinguishable.

which is not a proper observable). In this chapter, we will concentrate ourselves to the discussion of QED corrections (i.e. soft photon emission), since we are eventually interested in discussing $h \to 4\ell$ processes. The corrections due to ISR and FSR will be from now on called simply *radiative corrections*[3].

Two important questions immediately arise from our present discussion:

- Though conceptually relevant, radiative corrections are in principle suppressed by the small fine structure constant, $\alpha/\pi \sim 10^{-3}$. Why should we care about corrections of this size?

- In principle, radiative corrections could completely change the structure of the non-radiative amplitude. Was our effort to parametrise non-radiative amplitudes worthless?

The remaining of this section is devoted to the discussion of these issues. As we will find out, radiative corrections are much bigger than the naive α/π estimate and, fortunately, they will not ruin the description of the non-radiative amplitude performed in chapter 2.

3.1.1   Infrared divergences and mass singularities

In discussing the degeneracy between non-radiative and soft-radiative processes, we have omitted one detail of crucial importance to understand the relevance of radiative corrections. Indeed, both non-radiative and soft-radiative processes, if individually computed, exhibit singularities known as infrared (IR) divergences.

IR divergences (also called soft divergences or soft singularities) are a well known issue that has plagued QED since its early days. Even after a careful renormalisation procedure is performed (i.e. ultraviolet divergences are removed), one-loop amplitudes involving a photon loop and charged external states display residual IR divergences which necessitate an additional regulator (i.e. an IR cutoff). The IR divergences issue was formally settled in the 1960's, when it was proven that those divergences systematically cancel at all order in perturbation theory when non-radiative amplitudes are combined with soft-radiative amplitudes to create proper observables [9–12].

There is a crucial difference between ultraviolet (UV) and IR divergences. The regulator of UV divergences is a completely non-physical parameter, therefore the final results display no dependence upon it whatsoever. On the contrary, once healed IR divergences one is left with a residual dependence upon the particular IR cutoff used to discern between soft (i.e. undetectable) and hard (i.e. detectable) photons. This is absolutely reasonable, since such parameter plays a crucial role in the definition of the observable itself.

Let us call such IR cutoff λ_γ for the time being, postponing the details regarding its possible definitions. It is important to notice that, at any finite order in perturbation theory, we expect our IR-safe observable to have a singularity for $\lambda_\gamma \to 0$. As a consequence, we are expecting our radiative corrections to benefit from a significant

---

[3]This nomenclature should not generate confusion. "Radiative corrections" won't refer to one-loop corrections coming from a renormalisation procedure, since from that point of view our parametrisation is non-perturbative.

enhancement whenever λ_γ is sufficiently small[4]. Such enhancement turns out to be logarithmic ($\propto \log \lambda_\gamma$) and in some circumstances can significantly compensate the α/π suppression, justifying our interest for radiative corrections.

We have seen that IR divergences lead to an enhancement of radiative corrections, whenever the IR cutoff λ_γ is sufficiently small (as in many experimental setups). There is another important class of divergences (and related enhancements) that should be discussed, which will play an important role also in chapter 4: mass singularities.

Let us consider QED with a massless charged fermion. Computing the transition probability involving one of such massless fermions f in the initial or final state, one would still face singularities even after recovering the IR divergences discussed so far [11]. The reason is that, in this case, there are additional degenerate processes to be included. Indeed, In such a theory the two states $|f(p)\rangle$ and $|f(p')\gamma(p-p')\rangle$ can be both on-shell as long as p' and $p-p'$ are collinear. These additional states, corresponding to collinear emission(s) of an arbitrarily hard photon(s), are experimentally indistinguishable from the single particle state $|f(p)\rangle$ and should be included in the computation in order to recover a finite result.

These divergences arising in the fermion massless limit are called *mass singularities* or *collinear divergences*. In the Standard Model there aren't such massless charged particles. Nevertheless, we should care about mass singularities for two reasons.

- In inclusive observables, i.e. processes involving photon radiation of arbitrarily hardness, no such mass singularities are expected. But as soon as exclusive observables are considered, i.e. processes where only undetectably soft photons are included (to recover IR divergences), we expect the presence of contribution formally divergent in the $m_f \to 0$ limit, for the same reason we were expecting singularities in the $\lambda_\gamma \to 0$ limit.

  We will refer to these contribution as mass singularities, since they are direct remnants of the collinear divergences that would be there if $m_f = 0$. Such mass singularities, once again logarithmic ($\propto \log m_f$), can be significant when dealing with light fermions and give enhanced contributions to radiative correction. They are thus not only conceptually but also numerically important.

- Whenever an explicit computation is performed neglecting fermion masses (as it will be the case later on), one should take care of recovering mass singularities that emerge as a direct consequence of such approximation. In particular, one should define the IR cutoff λ_γ in such a way to regulate also those singularities (or introduce a second suitable cutoff).

3.1.2 Factorisation of radiative corrections

We have understood that radiative corrections, despite the perturbative α/π suppression, can benefit from significant enhancement due to IR divergences and mass singularities, usually both present:

$$\log \lambda_\gamma \,, \qquad \log m_f \,, \qquad \log \lambda_\gamma \log m_f \,. \qquad (3.1)$$

---

[4]Such singularity for $\lambda_\gamma \to 0$ vanishes when a resummation at all order is performed [12]. However, such considerations are relevant only when $(\alpha/\pi) \log \lambda_\gamma \gtrsim 1$.

The last term correspond to a double logarithmic enhancement (both collinear and soft divergent) which is known in literature as *Sudakov double logarithm* [81].

We should now discuss the aspect of those radiative corrections. Our main concern is to make sure that such corrections can be effectively included in our description of the non-radiative amplitude performed in chapter 2. Fortunately, this will be the case. Here we will just summarise the main results concerning radiative corrections which we need for our subsequent discussion. A detailed proof of such results is beyond the purposes of this dissertations and we refer to the literature for further details [9–16].

Let us call $d\Gamma^{nr}$ a specific non-radiative process differential transition probability, $d\Gamma^{soft\text{-}rad}(\lambda_\gamma)$ the one for the soft-radiative process (i.e. undetectable photon), and $d\Gamma^{hard\text{-}rad}(\lambda_\gamma)$ the one for the hard-radiative process (i.e. detectable photon). The two latter widths clearly display a dependence upon the IR threshold λ_γ which define a detectable photon. One should notice that only the sum $d\Gamma^{nr} + d\Gamma^{soft\text{-}rad}(\lambda_\gamma)$ is IR-safe, as discussed in section 3.1.1.

The first crucial result, that can be shown to hold up to non-logarithmic-enhanced non-factorisable corrections, is:

$$d\Gamma^{nr} + d\Gamma^{soft\text{-}rad}(\lambda_\gamma) = d\Gamma^{nr\prime} \cdot \omega_{\mathrm{v}}(\lambda_\gamma) \ , \tag{3.2}$$

$$d\Gamma^{hard\text{-}rad}(\lambda_\gamma) = d\Gamma^{nr\prime} \cdot \omega_{\mathrm{r}}(\lambda_\gamma, \{x_i\}) \ , \tag{3.3}$$

where $d\Gamma^{nr\prime}$ is IR-safe[5] and $\{x_i\}$ is a set of differential variables introduced to fully characterise the radiative process[6]. All (IR-safe) radiative corrections, including logarithmic singularities (see Eq. (3.1)), are now encoded in the so-called *flux* or *radiator function*

$$\omega(\lambda_\gamma, \{x_i\}) = \omega_{\mathrm{v}}(\lambda_\gamma)\, \Pi_i\, \delta(1 - x_i) + \omega_{\mathrm{r}}(\lambda_\gamma, \{x_i\}) \ , \tag{3.4}$$

which allows us to write:

$$\left[d\Gamma^{nr} + d\Gamma^{soft\text{-}rad} + d\Gamma^{hard\text{-}rad} \right] (\lambda_\gamma, \{x_i\}) = d\Gamma^{nr\prime} \cdot \omega(\lambda_\gamma, \{x_i\}) \ . \tag{3.5}$$

In Eq. (3.4), $\omega_{\mathrm{v}}(\lambda_\gamma)$ encodes the virtual corrections, which are actually the IR-safe sum of virtual corrections (in Γ^{nr}) and real corrections for undetectably soft photon emissions (in $\Gamma^{soft\text{-}rad}$). Instead, $\omega_{\mathrm{r}}(\lambda_\gamma, \{x_i\})$ encodes the real corrections associated to the emission of a detectable photon (i.e. associated to $\Gamma^{hard\text{-}rad}$).

The implications of Eq. (3.5) are pivotal. Such factorisation legitimises our analysis and decomposition of non-radiative amplitudes performed in chapter 2, since radiative corrections can them be taken into account by dressing non-radiative amplitudes with suitable radiator functions ω. This also eventually justify the description of ISR and FSR given in Eq. (2.2), where such factorisation was assumed without further explanations.

The second important result that can be shown is:

$$\int_{\mathrm{inclusive}} dx_i\, \omega(\lambda_\gamma, \{x_i\}) = 1 + \mathcal{O}\left(\alpha/\pi\right) \ , \tag{3.6}$$

---

[5]As a consequence of the Low theorem [13–16], $d\Gamma^{nr\prime}$ has the analytical structure of $d\Gamma^{nr}$ once healed from IR divergences.

[6]We will conventionally set $x_i \in [0, 1]$, the non-radiative limit being $x_i = 1 \ \forall i$.

where the integration over all differential variables is meant to recover the fully inclusive observable, i.e. with arbitrary hard photon(s) emission. As long as we can neglect non-enhanced $\mathcal{O}\left(\alpha/\pi\right)$ contributions, Eq. (3.6) gives us an extremely useful normalisation condition for the radiator function. Indeed, let us assume the explicit computation of ω_r to be much simpler than the evaluation of ω_v (as it will be the case). Once obtained ω_r, we can easily derive ω_v from Eqs. (3.4), (3.6):

$$\omega_v(\lambda_\gamma) = 1 - \int_{\text{inclusive}} dx_i \, \omega_r(\lambda_\gamma, \{x_i\}) \;. \tag{3.7}$$

This relation will be extensively used in the following sections.

3.2 Radiator function of a fermion current

In this section we will address the very specific problem of identifying the expression of radiator function $\omega(\lambda_\gamma, \{x_i\})$, introduced in Eq. (3.4), in the case of radiation from a fermion neutral current,

$$J_\mu(q) = \bar{f}(p_1)\gamma_\mu f(p_2) \;, \qquad p_1 + p_2 = q \;, \tag{3.8}$$

where the fermion f is understood to be chiral.

For the sake of the argument, let us consider the decay of a neutral particle[7] X into a neutral current J_μ and other particles Y, $X \to Y J_\mu$. We want to suitably describe the radiative dressing of such decay,

$$X \to Y J_\mu^* \to Y J_\mu \gamma \;, \tag{3.9}$$

where the photon is emitted from the fermion current[8]. We already know that we can describe the inclusive process $X \to Y J_\mu(+\gamma)$ in terms of the non-radiative width and a radiator function,

$$d\Gamma(X \to Y J_\mu(+\gamma)) = d\Gamma(X \to Y J_\mu) \cdot \omega(\lambda_\gamma, \{x_i\}) \;. \tag{3.10}$$

Our aim is now to explicitly compute $\omega(\lambda_\gamma, \{x_i\})$.

The discussion can in principle be carried out to consider an arbitrary number of photon emissions. However, one should notice that every extra photon brings an additional α/π suppression factor. For this reason, we will limit ourselves to a single photon emission, systematically neglecting any $\mathcal{O}\left(\alpha^2/\pi^2\right)$ term. We will also neglect those $\mathcal{O}\left(\alpha/\pi\right)$ terms which do not benefit from any logarithmic enhancement[9].

3.2.1 Non-interference with other radiative processes

As specified above, we are interested in the radiator function parametrising the emission of a photon from a neutral current final state. However, there are generally other radiative amplitudes that contribute to $X \to Y J_\mu \gamma$ and those amplitudes interfere in principle with each other. In our case, the three different radiative amplitudes are

$$\mathcal{A}_1(X \to Y + J_\mu\gamma) \qquad \mathcal{A}_2(X \to Y\gamma + J_\mu) \qquad \mathcal{A}_3(X \to Y J_\mu\gamma)$$
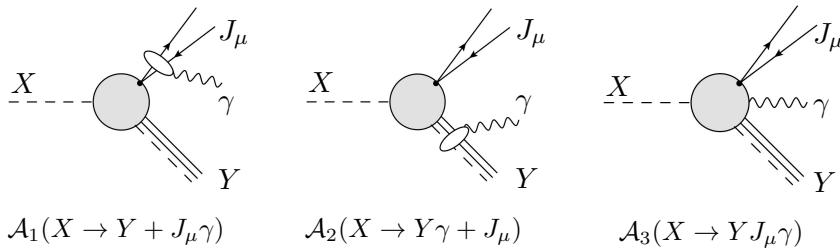
Figure 3.1: The three class of diagrams contributing to $X \to Y J_\mu\gamma$. Photon emission from the J_μ leg ($\mathcal{A}_1$) is the one we are interested in. As explained below, $\mathcal{A}_1$ does not interfere neither with $\mathcal{A}_2$ nor with $\mathcal{A}_3$.

depicted in Figure 3.1: photon emission from J_μ ($\mathcal{A}_1$), photon emission from Y ($\mathcal{A}_2$), photon emission from the hard process itself ($\mathcal{A}_3$).

Clearly, from a purely quantum-mechanical point of view, defining a photon emission from the J_μ leg makes sense if and only if $\mathcal{A}_1$ does not interfere with $\mathcal{A}_2$ and $\mathcal{A}_3$. Indeed, only in the absence of interference we can consistently compute a decay width corresponding only to the radiative process (3.9). Fortunately, this can be generally proven to be the case.

The explicit proof that the photon emission from a neutral current J_μ does not interfere, in Leading Logarithmic Approximation (LLA), with other amplitudes with same final state is rather technical and is postponed to appendix A.1[10]. The qualitative argument behind such property can be summarised as follows. Since J_μ is a neutral current, it can be considered a globally chargeless final state which cannot electromagnetically interact with its surroundings. This neutrality avoids any kind of interference with other amplitudes, though in principle we should have expected it.

Due to the non-interference of process (3.9) with other photon emission processes, we are allowed to carry on the discussion focusing only on the former. Other possible photon emission channels can then be taken into account in an additive fashion. Eventually, the complete radiator function can be defined as the sum of all radiators from all non-interfering channels contributing to radiative corrections.

Once settled this subtle issue, for the rest of the discussion we will refer to $X \to Y J_\mu\gamma$ only as process (3.9), being allowed for our purposes to neglect other (possible) radiative channels.

3.2.2 Formal definition of the radiator function $\omega^J(\lambda_\gamma, x)$

We want to derive a general expression for the radiator function ω of Eq. (3.10). In order to succeed, we should first of all properly define the radiator itself.

---

[7]The following discussion is nevertheless completely general and can be extended to decays of charged particles or scattering processes, as long as we have a neutral current J_μ in the final state.

[8]We will later show that this is as a matter of fact a meaningful definition.

[9]In other words, we will work in Leading Logarithmic Approximation (LLA).

[10]In appendix A.1 it will be proved that the interference term $\text{Re}(\mathcal{A}_1^* \mathcal{A}_{2,3})$ is always free from soft divergences. The issue of extending such result to single-logarithmic collinear singularities is more delicate and we will limit ourselves to some general remarks.

As a first step, let us properly define our decay widths by fixing their kinematic:

$$\Gamma_0 = \Gamma\Big(X(P_X) \to Y(\{b_i\})\, \ell^+(p_+)\, \ell^-(p_-)\Big) \, , \qquad (3.11)$$

$$\Gamma_{rad} = \Gamma\Big(X(P_X) \to Y(\{b_i\})\, \ell^+(p'_+)\, \ell^-(p'_-)\, \gamma(k)\Big) \, , \qquad (3.12)$$

where $p_+ + p_- = q_0$, $p'_+ + p'_- = q$, $q + k = q_0$ and $P_X = q_0 + \sum_i\{b_i\}$. Here $\{b_i\}$ collectively denotes the momenta of all particles in the Y final state (there will be no need to further specify such state).

Writing down explicitly the integrations over the phase space, we can recast Γ_0, Γ_{rad} as:

$$\Gamma_0 = \frac{(2\pi)^4}{2M_X} \int d\Phi(P_X; \{b_i\}, p_+, p_-)\, |\mathcal{M}_0|^2 \, , \qquad (3.13)$$

$$\Gamma_{rad} = \frac{(2\pi)^4}{2M_X} \int d\Phi(P_X; \{b_i\}, p_+, p_-, k)\, |\mathcal{M}_{rad}|^2 \, , \qquad (3.14)$$

where $d\Phi(P; p_1, \ldots, p_n)$ is the phase space for a particle P decaying into n particles with momenta p_i ($i = 1, \ldots, n$), following the notation of Ref. [41][11]. Such phase space can be split using an auxiliary kinematic variable q [41]:

$$d\Phi(P; p_1, \ldots, p_n) = d\Phi(P; p_1, \ldots, p_j, q)\, d\Phi(q; p_{j+1}, \ldots, p_n)\, (2\pi)^3 dq^2 \, , \qquad (3.15)$$

where clearly $q = \sum_{i=j+1}^n p_i$. Exploiting Eq. (3.15), we can conveniently recast Eqs. (3.13), (3.14) as follows:

$$\Gamma_0 = \frac{(2\pi)^7}{2M_X} \int d\Phi_Y(P_X; \{b_i\}, q_0)\, d\Phi_\ell(q_0; p_+, p_-)\, dq_0^2\, |\mathcal{M}_0|^2 \, , \qquad (3.16)$$

$$\Gamma_{rad} = \frac{(2\pi)^{10}}{2M_X} \int d\Phi_Y(P_X; \{b_i\}, q_0)\, d\Phi_\gamma(q_0; q, k)\, d\Phi_\ell(q; p_+, p_-)\, dq_0^2\, dq^2\, |\mathcal{M}_{rad}|^2 \, , \qquad (3.17)$$

where q and q_0 have been already defined after Eq. (3.12). For future reference, let us write down explicitly the phase space for the two-body decay (in the rest frame of the decaying particle):

$$d\Phi(P; p_1, p_2) = \frac{1}{8(2\pi)^6} \frac{\lambda(P^2, p_1^2, p_2^2)}{P^2}\, d\Omega_p \, , \qquad (3.18)$$

where $\lambda(x, y, z)^2 = x^2 + y^2 + z^2 - 2xy - 2xz - 2yz$, while Ω_p is the solid angle describing the $\vec{p}_1$ 3-momentum (clearly, $\vec{p}_1 = -\vec{p}_2$ in P rest frame).

Introducing the new variable $x = q^2/q_0^2$, we can now formally define the piece of radiator corresponding to real emission from a neutral current J_μ (see Eq. (3.3)) as:

$$\frac{d\Gamma_{rad}}{dx} = \Gamma_0 \cdot \omega_r^J(\lambda_\gamma, x) \, . \qquad (3.19)$$

---

[11]See section 47. Kinematics.

Assuming no other contributions to real emission, we can then exploit Eq. (3.7) to find $\omega_{\mathrm{v}}^J(\lambda_\gamma)$ and thus the full radiator (Eq. (3.4)):

$$
\omega_{\mathrm{v}}^J(\lambda_\gamma) = 1 - \int \mathrm{d}x \, \omega_{\mathrm{r}}^J(\lambda_\gamma, x) \ ,
$$
$$
\omega^J(\lambda_\gamma, x) = \omega_{\mathrm{v}}^J(\lambda_\gamma)\delta(1 - x) + \omega_{\mathrm{r}}^J(\lambda_\gamma, x) \ . \tag{3.20}
$$

In order to avoid future confusion, from now on the 'J' superscript will denote the radiator function in the specific case of a single J_μ current.

3.2.3   Master formula for $\omega_{\mathrm{r}}^J(\lambda_\gamma, x)$

Owing a proper definition of $\omega^J(\lambda_\gamma, x)$, Eqs. (3.19) and (3.20), we can now derive a master formula for its general expression.

The first, crucial observation is that we are allowed to differentiate Eq. (3.19) with respects to the kinematic variables which are not necessary for the factorisation of radiative corrections. In particular, the integration over $\mathrm{d}\Phi_\gamma$ is the only one needed to ensure the existence of a factorisable radiator function. By differentiation of Eq. (3.19) we get:

$$
\frac{\mathrm{d}}{\mathrm{d}x}\left(\frac{\mathrm{d}^2\Gamma_{rad}}{\mathrm{d}\Phi_Y \, \mathrm{d}q_0^2}\right) = \left(\frac{\mathrm{d}^2\Gamma_0}{\mathrm{d}\Phi_Y \, \mathrm{d}q_0^2}\right) \cdot \omega_{\mathrm{r}}^J(\lambda_\gamma, x) \ . \tag{3.21}
$$

Before plugging Eqs. (3.16), (3.17) into Eq. (3.21), we should first say something more about the matrix elements $\mathcal{M}_0$, $\mathcal{M}_{rad}$. Indeed, it can be easily shown that their generic expressions read

$$
\mathcal{M}_0 = Y_\mu \, J_0^\mu \ ,
$$
$$
\mathcal{M}_{rad} = Y_\mu \, J_{rad}^\mu \ , \tag{3.22}
$$

where Y_μ is common to both matrix elements, $J_0^\mu = \bar{\ell}(p_-)\gamma^\mu \ell(p_+)$, while J_{rad}^μ is given by the sum of the two Feynman diagrams of Figure 3.2. If we now compute the squared amplitudes $|\mathcal{M}|^2$, taking care of summing over final polarisation states, we get:

$$
|\mathcal{M}_0|^2 = Y_\mu^\dagger Y_\nu \, L_0^{\mu\nu} \ , \qquad\qquad L_0^{\mu\nu} = \sum_{\ell\,\mathrm{pol}} J_0^{\mu\,\dagger} J_0^\nu \ , \tag{3.23}
$$

$$
|\mathcal{M}_{rad}|^2 = Y_\mu^\dagger Y_\nu \, L_{rad}^{\mu\nu} \ , \qquad\qquad L_{rad}^{\mu\nu} = \sum_{\gamma\,\mathrm{pol}} \sum_{\ell\,\mathrm{pol}} J_{rad}^{\mu\,\dagger} J_{rad}^\nu \ , \tag{3.24}
$$

where "ℓ pol" and "γ pol" denote the sum over lepton and photon polarisations, respectively.

We can now derive a general expression for $\omega_{\mathrm{r}}^J(\lambda_\gamma, x)$. Deploying Eqs. (3.16), (3.17), (3.18), (3.23), (3.24) into definition (3.21), we get:

$$
(2\pi)^3 q_0^2 \, Y_\mu^\dagger Y_\nu \int \mathrm{d}\Phi_\gamma \, \beta \, \mathrm{d}\Omega_\ell \, L_{rad}^{\mu\nu} = \omega_{\mathrm{r}}^J(\lambda_\gamma, x) \, Y_\mu^\dagger Y_\nu \int \beta_0 \, \mathrm{d}\Omega_\ell \, L_0^{\mu\nu} \ , \tag{3.25}
$$
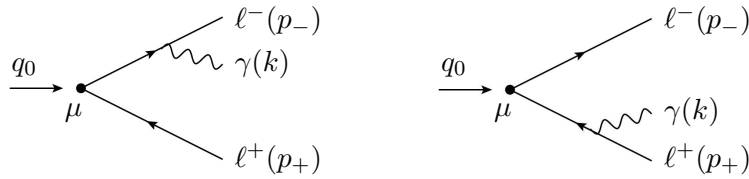
Figure 3.2: The two Feynman diagrams contributing to J^μ_{rad}, with $p_- + p_+ = q$, $k + q = q_0$.

where $\beta^2_{(0)} = 1 - 4m^2_\ell/q^2_{(0)}$ comes from the 2-body phase space of $\ell^\pm$. We can exploit our freedom to chose the angular frame to get rid of the unpleasant integration over $\mathrm{d}\Omega_\ell$. Furthermore, we claim that equation (3.25) still holds if we drop the $Y^\dagger_\mu Y_\nu$ terms on both sides[12]. If we now contract both sides with $g_{\mu\nu}$, we finally get

$$\omega^J_{\mathrm{r}}(\lambda_\gamma, x) = \frac{1}{32(2\pi)^3} \frac{\beta}{\beta_0} \frac{q^2_0}{q^2_0 + 2m^2_\ell} (1 - x) \int_{\mathrm{cut}(\lambda_\gamma)} \mathrm{d}\Omega_\gamma \, (-g_{\mu\nu} L^{\mu\nu}_{rad}) \,, \qquad (3.26)$$

where we have substituted $g_{\mu\nu} L^{\mu\nu}_0 = -4(q^2_0 + 2m^2_\ell)$. This is our master formula for $\omega^J_{\mathrm{r}}(\lambda_\gamma, x)$.

The integration over $\mathrm{d}\Omega_\gamma$ in Eq. (3.26) should be performed in the rest frame of q_0, where Ω_γ can be identified as the solid angle describing $\vec{k} = -\vec{q}$. Such integration clearly depends upon the details on the IR cutoff λ_γ. The integrand is instead universal and can be computed from Eq. (3.24) using the diagrams of Figure 3.2. Its expression reads:

$$-g_{\mu\nu} L^{\mu\nu}_{rad} = 64\pi\alpha \left(-1 + \frac{2}{1 - \beta^2 c^2_\theta} + \frac{4x(1 + x_\ell)}{(1-x)^2(1 - \beta^2 c^2_\theta)} - \frac{8x_\ell(1 + x_\ell)}{(1-x)^2(1 - \beta^2 c^2_\theta)^2} \right) \,, \tag{3.27}$$

where $x_\ell = 2m^2_\ell/q^2_0$, while c_θ is the polar angle of the Ω_γ coordinates: $\mathrm{d}\Omega_\gamma = \mathrm{d}\phi \, \mathrm{d}c_\theta$.

3.2.4 Explicit expressions for $\omega^J(\lambda_\gamma, x)$

Given definition (3.20) and master formula (3.26), we are ready to provide an explicit expression for $\omega^J(\lambda_\gamma, x)$. The only missing ingredient is a formal definition of the IR cutoff λ_γ, which influences the integration over $\mathrm{d}\Omega_\gamma$ in (3.26).

The IR cutoff should always be defined in order to emulate as accurately as possible the behaviour of the experiment itself. Such matching is always a very delicate issue. In our case, we will be interested in mimicking the ATLAS and CMS detectors. To achieve this result, we define a minimal invariant mass of a single lepton plus photon m_*. More precisely, we will consider the soft and/or collinear emission of a photon as undetectable if it satisfies the following condition:

$$|\ell(p_\pm + k)\rangle \rightarrow |\ell(p_\pm)\rangle \cdot |\gamma(k)\rangle \quad \text{undetectable if} \quad (p_\pm + k)^2 \leq m^2_* \,. \tag{3.28}$$

---

[12]A formal proof of this property would lead us too far from the purposes of our discussion. The idea is that if one could prove that Y_μ, which represents a whole family of 4-vectors, completely spans Lorentz space, the cancellation we claim would be a trivial result of complex linear algebra.

With such definition, one successfully emulates the limited resolution of the electromagnetic calorimeters of the two LHC detectors.

Condition (3.28) is very useful in the massless fermions limit, since it recovers both soft and collinear divergences. Indeed, taking $p_\pm^2 = m_\ell^2 = 0$, Eq. (3.28) reads

$$(p_\pm + k)^2 = \frac{1}{2} q_0^2 (1-x)(1 \pm c_\theta) \le m_*^2 \ . \tag{3.29}$$

From Eq. (3.29) one can easily realise that both soft ($x \to 1$) and/or collinear ($c_\theta \to \pm 1$) photons are systematically considered as undetectable, as it should be.

Condition (3.29) gives us an explicit definition of the region of integration over $d\Omega_\gamma$. By explicit evaluation of master formulas (3.20) and (3.26), one eventually gets

$$\omega^J(x_*, x) = \omega_{\rm r}(x_*, x) + \omega_{\rm v}(x_*, x)\delta(1-x) \ ,$$
$$\omega_{\rm r}^J(x_*, x) = \frac{\alpha}{\pi} \left(x - 1 + \frac{1+x^2}{1-x} \log\left(\frac{2(1-x) - x_*}{x_*} \right) \right) \theta(1 - x - x_*) \ ,$$
$$\omega_{\rm v}^J(x_*) = 1 - \frac{\alpha}{2\pi} \left(\frac{5}{2} - \frac{\pi^2}{3} + 3\log\frac{x_*}{2} + 2\log^2\frac{x_*}{2} \right) \ , \tag{3.30}$$

where $x_* = 2m_*^2/q_0^2$. It is interesting to notice that the Heaviside step function[13] θ in the $\omega_{\rm r}^J$ expression is an automatic result of the integration in dc_θ due to Eq. (3.29). Indeed, for $x > 1 - x_*$, the two conditions (3.29) cannot be simultaneously satisfied whatsoever and the region of integration vanishes. It is worth to remember that, in the case of multiple radiative channels, one should first add all the different real contributions $\omega_{\rm r}^J$ together and then compute the single virtual correction $\omega_{\rm v}^J$ through Eq. (3.20).

As a final addendum to this section, it is worth noting that Eq. (3.28) is not the only possible definition of an IR cutoff. In fact, such choice is unsuitable whenever it is favourable to retain the lepton mass dependence, for kinematic or other reasons. In that case, one might be also interested in a full photon acceptance. Inclusively integrating over Ω_γ, one gets:

$$\tilde{\omega}_{\rm r}^J(x_\ell, x) = -\frac{\alpha}{\pi} \frac{(1 + x^2 + 2xx_\ell)\beta - 2(1 + x^2 - 2x_\ell(1 - x + x_\ell))\,\text{arctanh}(\beta)}{(1-x)(1+x_\ell)\sqrt{1 - 2x_\ell}} \ . \tag{3.31}$$

Two final comments on radiator (3.31):

- Soft divergences are still to be recovered and indeed $\tilde{\omega}_{\rm r}^J(x_\ell, x)$ is divergent for $x \to 1$. A possibility is to add (this time by hand) an extra $\theta(1 - x - x_*)$ in Eq. (3.31), contextually defining a threshold x_* for undetectably soft photons.

- $\tilde{\omega}_{\rm r}^J(x_\ell, x)$ cannot be analytically integrated in dx. A good solution would be to analytically integrate only the logarithmic divergences of $\tilde{\omega}_{\rm r}^J(x_\ell, x)$, then numerically integrating the residual (non-singular) part. This was for example the strategy deployed in Ref. [17].

---

[13]This is the usual step function, defined as $\theta(x) = 1$ for $x > 0$, $\theta(x) = 0$ for $x < 0$.

3.3 Radiative corrections in $h \to 2e\,2\mu$

Once examined to some extent the general issue of radiative corrections from fermion currents, we will now focus our discussion to a specific Higgs decay, $h \to 2e\,2\mu$ [8]. We have already explained in chapter 2 the relevance of such process. In addition, we have argued in section 2.2.4 that the inclusion of radiative corrections, i.e. the spectrum distortion due to ISR and FSR, is of utmost importance in order to disentangle genuine new physics effects from NLO Standard Model effects. Once developed the necessary tools in section 3.2, we are now ready to quantitatively discuss how to include radiative corrections in the generic PO description of $h \to 2e\,2\mu$.

We will again limit our computations at NLO (i.e. at the $\mathcal{O}\left(\alpha/\pi\right)$ level) and at LLA (i.e. neglecting finite α/π contributions). Furthermore, we will work in the massless lepton limit, lepton masses being negligible in the kinematic regimes we are interested in.

3.3.1 Differential description of $h \to 2e\,2\mu(+\gamma)$

As a first step, we need to extend the formalism introduced in section 2.2.4 in order to describe the inclusive $h \to 2e\,2\mu(+\gamma)$ process, where an extra detectable γ can be either emitted or not[14]. As IR cutoff we will use the minimal lepton plus photon invariant mass m_* discussed in section 3.2.4, Eq. (3.28).

Let us call $\sqrt{q_{01,02}^2}$ and $\sqrt{q_{1,2}^2}$ the invariant masses of the two lepton currents (e^+e^- and $\mu^+\mu^-$) before and after bremsstrahlung, respectively. We further define

$$x_i = \frac{q_i^2}{q_{0i}^2} \ , \qquad x_{*i} = \frac{2m_*^2}{q_{0i}^2} \ , \qquad i = 1, 2 \ , \tag{3.32}$$

where $\sqrt{x_i}$ parametrises the fraction of invariant mass retained by the i-th lepton pair after bremsstrahlung (for $x_i = 1$, no detectable photon has been emitted). Our final goal is to determine the differential distribution

$$\mathcal{F}_{\ell\ell\gamma}(q_{01}^2, q_{02}^2, x_1, x_2) = \frac{\mathrm{d}^4\Gamma\left(h \to 2e\,2\mu(+\gamma)\right)}{\mathrm{d}q_{01}^2 \mathrm{d}q_{02}^2 \mathrm{d}x_1 \mathrm{d}x_2} \ , \tag{3.33}$$

which fully encode all information about the radiative distortion of the $h \to 2e\,2\mu$ decay.

As a result of factorisation of radiative corrections discussed in section 3.1, we are able to express the radiative spectrum $\mathcal{F}_{\ell\ell\gamma}$ in terms of the non-radiative $\mathcal{F}_{\ell\ell}^{nr}$ spectrum and a suitable radiator function ω. In formulas:

$$\mathcal{F}_{\ell\ell\gamma}(q_{01}^2, q_{02}^2, x_1, x_2) = \mathcal{F}_{\ell\ell}^{nr}(q_{01}^2, q_{02}^2) \cdot \omega_{tot}(x_{*1}, x_{*2}, x_1, x_2) \ , \tag{3.34}$$

where $\mathcal{F}_{\ell\ell}^{nr}$ has been first defined in Eq. (2.23),

$$\mathcal{F}_{\ell\ell}^{nr}(q_{01}^2, q_{02}^2) = \frac{\mathrm{d}^2\Gamma(h \to 2e\,2\mu)}{\mathrm{d}q_{01}^2 \mathrm{d}q_{02}^2} \ . \tag{3.35}$$

---

[14]It is important to require the extra emitted photon to be detectable. Indeed, as discussed, an indefinite number of undetectable photons is always emitted, this being the ultimate reason for IR divergences.
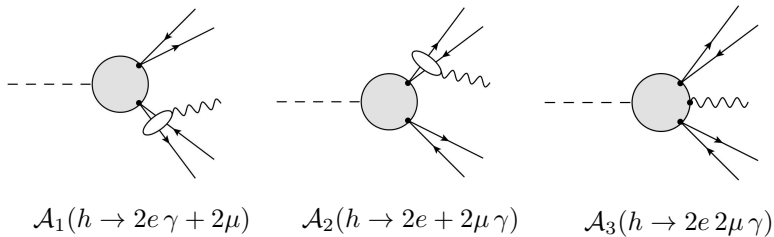
$$\mathcal{A}_1(h \to 2e\,\gamma + 2\mu) \qquad \mathcal{A}_2(h \to 2e + 2\mu\,\gamma) \qquad \mathcal{A}_3(h \to 2e\,2\mu\,\gamma)$$

Figure 3.3: The three possible bremsstrahlung channels in $h \to 4\ell\,\gamma$. $\mathcal{A}_{1,2}$ correspond to a photon emission from one of the two lepton currents. $\mathcal{A}_3$ corresponds to a photon emission from the hard process itself and is thus related to the Green function $\langle 0|\mathcal{T}\{J_\mu(x), J'_\nu(y), \gamma(z), h(0)\}|0\rangle$. Such correlation function can be proven to be IR-safe [10].

3.3.2   The radiator function ω_{tot}

We now want to deploy the discussion of previous sections to find and explicit expression for $\omega_{tot}(x_{*1}, x_{*2}, x_1, x_2)$. First of all, let us follow the usual strategy and introduce the distinction between virtual and real part of the radiator,

$$\omega_{tot}(x_{*1}, x_{*2}, x_1, x_2) = \omega_{\mathrm{v}}(x_{*1}, x_{*2})\,\delta(1 - x_1)\,\delta(1 - x_2) + \omega_{\mathrm{r}}(x_{*1}, x_{*2}, x_1, x_2)\ . \quad (3.36)$$

We will explicitly evaluate ω_{r}, thus obtaining ω_{v} through Eq. (3.7).

   In order to determine $\omega_{\mathrm{r}}(x_{*1}, x_{*2}, x_1, x_2)$, we should identify all the different radiative channels contributing to $h \to 2e\,2\mu\,\gamma$. These are summarised in Figure 3.3: the photon can be emitted either by one of the fermion currents ($\mathcal{A}_1$, $\mathcal{A}_2$) or by the hard process itself ($\mathcal{A}_3$). We have already argued in section 3.2.1 that $\mathcal{A}_1$ and $\mathcal{A}_2$ do not interfere with each other and with $\mathcal{A}_3$. Furthermore, $\mathcal{A}_3$ can be proven to be IR-safe [10], thus it does not contribute at all to ω_{r}.

   Following the above observations, we can conclude that ω_{r} is simply the sum of the two radiators describing real photon emission by the two fermion neutral currents:

$$\omega_{\mathrm{r}}(x_{*1}, x_{*2}, x_1, x_2) = \omega_{\mathrm{r}}^J(x_{*1}, x_1)\,\delta(1 - x_2) + \omega_{\mathrm{r}}^J(x_{*2}, x_2)\,\delta(1 - x_1)\ , \qquad (3.37)$$

where $\omega_{\mathrm{r}}^J(x_*, x)$ is given in Eq. (3.30). The Dirac δ functions are needed to ensure that we are describing the photon itself as a single quantum[15]. We can now explicitly compute $\omega_{\mathrm{v}}(x_{*1}, x_{*2})$ through Eq. (3.7),

$$\omega_{\mathrm{v}}(x_{*1}, x_{*2}) = 1 - \int_0^1 \mathrm{d}x_1 \int_0^1 \mathrm{d}x_2\, \omega_{\mathrm{r}}(x_{*1}, x_{*2}, x_1, x_2)$$
$$= \omega_{\mathrm{v}}^J(x_{*1}) + \omega_{\mathrm{v}}^J(x_{*2}) - 1\ , \qquad (3.38)$$

where $\omega_{\mathrm{v}}^J(x_*)$ is again given in Eq. (3.30).

   To summarise, the full radiator function for $h \to 2e\,2\mu\,\gamma$ reads:

$$\omega_{tot}(x_{*1}, x_{*2}, x_1, x_2) = \left(\omega_{\mathrm{v}}^J(x_{*1}) + \omega_{\mathrm{v}}^J(x_{*2}) - 1\right)\delta(1 - x_1)\,\delta(1 - x_2)$$
$$+ \omega_{\mathrm{r}}^J(x_{*1}, x_1)\,\delta(1 - x_2) + \omega_{\mathrm{r}}^J(x_{*2}, x_2)\,\delta(1 - x_1)\ . \qquad (3.39)$$

---

[15]If $x_1 \neq 1$ we should impose $x_2 = 1$ and vice versa. Otherwise, $x_{1,2} \neq 1$ would imply that the (single) emitted photon carries energy drained from both fermion currents, a scenario which is clearly forbidden (in absence of interference).

3.3.3 ISR and FSR dressing of the non-radiative spectrum

Eqs. (3.34) and (3.39) give us an explicit definition of $\mathcal{F}_{\ell\ell\gamma}(q_{01}^2, q_{02}^2, x_1, x_2)$, which fully characterise the radiative process $h \to 2e\,2\mu\,\gamma$, Eq. (3.33). We can now go back to the original purpose of our discussion, namely the ISR and FSR dressing of the non-radiative process $h \to 2e\,2\mu$ within the general PO framework.

In ATLAS and CMS analyses, the $h \to 2e\,2\mu$ spectrum is reconstructed without an effort to trace back possible photon(s) emission [71]. In order to mimic such experimental measure we should integrate, for each $\{\sqrt{q_1^2}, \sqrt{q_2^2}\}$ bin, over all possible pre-bremsstrahlung $\{\sqrt{q_{01}^2}, \sqrt{q_{02}^2}\}$ bins from which the event can migrate through a suitable photon emission. In formulas, the above prescription for the radiative dressing of the $\mathcal{F}_{\ell\ell}$ spectrum reads:

$$\mathcal{F}_{\ell\ell}^{rad}(q_1^2, q_2^2) = \iint_{\mathcal{D}(q_{01}, q_{02})} \mathrm{d}q_{01}^2 \mathrm{d}q_{02}^2 \, \mathcal{F}_{\ell\ell\gamma}\left(q_{01}^2, q_{02}^2, \frac{q_1^2}{q_{01}^2}, \frac{q_2^2}{q_{02}^2}\right) , \qquad (3.40)$$

where the integration domain is defined as

$$\mathcal{D}(q_{01}^2, q_{02}^2) = \left\{ (q_{01}^2, q_{02}^2) \mid q_{0i}^2 \geq q_i^2 \ \wedge \ \sqrt{q_{01}^2} + \sqrt{q_{02}^2} \leq m_h \right\} , \qquad (3.41)$$

according to Eq. (2.24). Making integration (3.40) explicit and changing the variables from q_i^2 to $\sqrt{q_i^2}$, one finds:

$$\mathcal{F}_{\ell\ell}^{rad}\left(\sqrt{q_1^2}, \sqrt{q_2^2}\right) = \int_{\sqrt{q_1^2}}^{m_h - \sqrt{q_2}} \mathrm{d}\sqrt{q_{01}^2} \int_{\sqrt{q_2^2}}^{m_h - \sqrt{q_{01}^2}} \mathrm{d}\sqrt{q_{02}^2} \cdot \frac{4\sqrt{q_1^2}\sqrt{q_2^2}}{q_{01}^2 q_{02}^2}$$
$$\times \mathcal{F}_{\ell\ell}^{nr}(\sqrt{q_{01}^2}, \sqrt{q_{02}^2}) \cdot \omega_{tot}(x_{*1}, x_{*2}, x_1, x_2) , \qquad (3.42)$$

with $x_i = q_i^2/q_{0i}^2$ and $x_{*i} = 2m_*^2/q_{0i}^2$.

As already seen in section 2.2.4, the single-differential distribution $\mathcal{F}_\ell\left(q^2\right)$ is another interesting observable. Indeed, such one-dimensional function is more effective to exemplify our analysis and to appreciate the impact of radiative corrections. Following Eq. (2.25), we can define the non-radiative single-differential distribution $\mathcal{F}_\ell^{nr}\left(\sqrt{q_0^2}\right)$ as

$$\mathcal{F}_\ell^{nr}(\sqrt{q_{01}^2}) = \int_0^{m_h - \sqrt{q_{01}^2}} \mathrm{d}\sqrt{q_{02}^2} \, \mathcal{F}_{\ell\ell}^{nr}(\sqrt{q_{01}^2}, \sqrt{q_{02}^2}) . \qquad (3.43)$$

Plugging Eq. (3.42) into Eq. (3.43) and performing a smart recast of the integration, it is indeed possible to show that

$$\mathcal{F}_\ell^{rad}\left(\sqrt{q_1^2}\right) = \int_{\sqrt{q_1^2}}^{m_h} \mathrm{d}\sqrt{q_{01}^2} \, \frac{2\sqrt{q_1^2}}{q_{01}^2} \cdot \mathcal{F}_\ell^{nr}\left(\sqrt{q_{01}^2}\right) \omega^J(x_{*1}, x_1) , \qquad (3.44)$$

where $\omega^J(x_{*1}, x_1)$ is the radiator function for a single fermion current, defined in Eq. (3.30). Eq. (3.44) gives us a general formula able to "dress" with radiative corrections a generic non-radiative dilepton spectrum (i.e. whether or not new physics is involved in the decay).
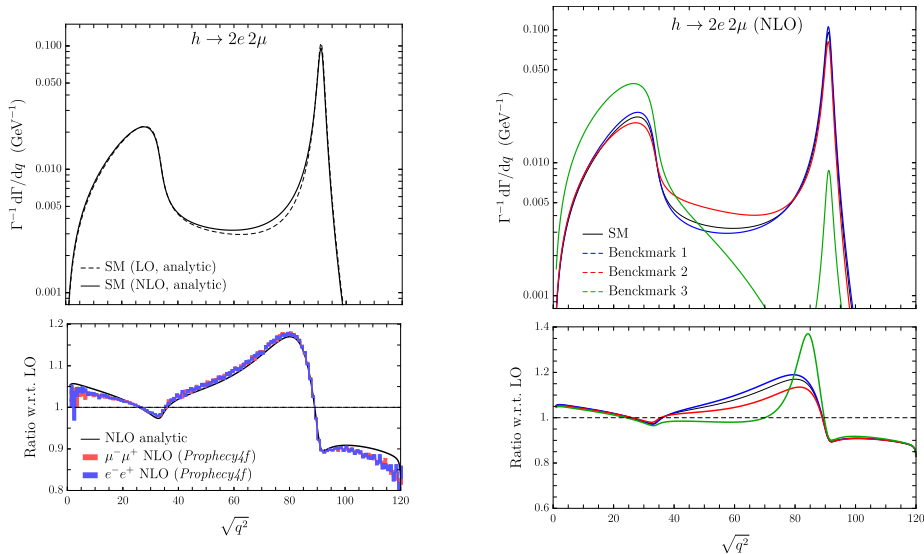
Figure 3.4: Different predictions for the dilepton decay spectrum $\mathcal{F}_\ell(\sqrt{q^2})$. *Left*: Comparison, within the Standard Model, between LO analytical result (dashed black), NLO analytical result through convolution (3.44) (solid black, $m_* = 1$ GeV) and NLO numerical result obtained through the Monte Carlo generator *Prophecy4f* [72]. *Right*: Comparison of NLO results (obtained through convolution (3.44), $m_* = 1$ GeV) between the Standard Model and the three benchmarks discussed in section 2.2.4 (see text for details).

A first test of Eq. (3.44) would be to compare its predictions with the full NLO corrections, available for the Standard Model case and already discussed in Figure 2.1. Such a comparison is presented in Figure 3.4 (left plot), in the case of $m_* = 1$ GeV. One can immediately appreciate how convolution (3.44) provides an excellent approximation (within 1% accuracy) to the spectrum obtained with full NLO electroweak corrections[16].

Having demonstrated the validity of our description of ISR and FSR by means of Eq. (3.44), we are in position to apply the method in the presence of arbitrary new physics contributions to $h \to 2e\,2\mu$ decay, parametrisable in the PO framework introduced in section 2.2.1. As an illustrative example, we consider the impact of the leading QED corrections for the three benchmark new physics scenarios (compared with the Standard Model) introduced in section 2.2.4 (Figure 2.1, left plot). Such comparison is proposed in Figure 3.4 (right plot).

- Benchmark 1 ($\kappa_{ZZ} = 1.3$, $\epsilon_Z^{e_R e_R} = \epsilon_Z^{\mu_R \mu_R} = -\epsilon_Z^{e_L e_L} = -\epsilon_Z^{\mu_L \mu_L} = 0.05$), blue line. Here the deviation at LO from the Standard Model spectrum is small. As a consequence, small deformations in the spectrum are obtained (upper panel) and the relative QED corrections are Standard-Model-like (lower panel). In this regime, the leading QED corrections could be reasonably estimated from the

---
[16]The $\sim 2\%$ deviations at the borders of the phase space are expected due the breakdown of the approximation $\sqrt{q_0^2} \gg m_*$, implicitly assumed in the analytic evaluation of radiation function. We will briefly return on this issue in chapter 4.

Standard Model result (via an appropriate NLO/LO re-weighting).

- Benchmark 2 ($\kappa_{ZZ} = 0$, $\epsilon_Z^{e_L e_L} = \epsilon_Z^{\mu_L \mu_L} = 0.26$), red line. Here the deviation from the Standard Model point is sizeable. However, the PO configuration is such that the deviations from the Standard Model in the spectrum are small. This implies that the relative impact of QED corrections is still Standard-Model-like.

- Benchmark 3 ($\kappa_{ZZ} = 0.3$, $\epsilon_Z^{e_L e_L} = -0.45$), green line. In this example we observe a sizeable distortion of the dilepton shape (upper panel). As a consequence, the relative impact of the QED corrections is quite different from the Standard Model case. A description of radiative corrections by NLO/LO re-weighting of the Standard Model result would not provide a good approximation and the full formalism of Eq. (3.44) is needed.

Our final conclusions regarding the $h \to 2e\,2\mu$ decay may not appear particularly impressive, since only under extreme configurations of PO values the naive estimate of radiative corrections through NLO/LO re-weighting of the Standard Model is not a viable option. Nevertheless, one should keep in mind some broader take-home messages that arise from the discussion in this chapter:

- Though implemented in the PO framework, our description of radiative corrections in $h \to 2e\,2\mu$ is not restricted to such formalism and it can be applied to "dress" arbitrary NP descriptions of such decay, even within different frameworks or explicit models. It would be perhaps too precipitate to conclude that a scenario is unlikely, just because it appears exotic in the PO parameter space. Furthermore, our formalism is undoubtedly an improvement of the very naive NLO/LO Standard-Model-like re-weighting.

- It should also be appreciated that convolution (3.44), from the computational point of view, is incredibly more efficient than a Monte Carlo simulation with *Prophecy4f*. The full NLO results shown in Figure 3.4 (left plot) has been obtained by generating 200 million events through *Prophecy4f* [72], definitely a non-negligible computational task. On the contrary, Eq. (3.44) can be easily implemented and run in few minutes on any laptop.

- As a final remark, it should be appreciated that our whole $h \to 2e\,2\mu$ discussion can be seen as an introductory example of how to use results of section 3.2 to build up a reliable radiator for a generic collider process which involves neutral current(s) in the final state. In other words, one can use our discussion to perform accurate NLO phenomenological studies (within and beyond the Standard Model) without relying on lengthy (and perhaps not yet available) full NLO results.

Electroweak corrections in Higgs production

In chapter 3 we have addressed the problem of QED radiative corrections. In this chapter, we will address the related issue of radiative corrections within the full electroweak theory, thus considering the additional contributions coming from the W and Z bosons.

The great difference between QED and electroweak theory is of course that the latter undergoes a spontaneous symmetry breakdown. This profound difference will force us to adopt another strategy to evaluate electroweak radiative corrections. After a very brief general introduction (section 4.1), we will immediately turn our attention to the very specific case of associated Vh production, introduced in section 2.3.2. We will first develop a general strategy within the Standard Model (section 4.2). The next step will be to extend our arguments to the hPO framework, which will lead us to our final results and considerations (section 4.3).

4.1 Electroweak mass singularities

At a first sight, it might appear a bit obscure why one should care about radiative corrections of a broken gauge symmetry, where bosons acquire masses and thus everything is IR-safe. In order to understand for what reason and to what extent one can talk about W and Z radiative corrections, we will exploit a close analogy with QED. Once understood the nature of electroweak IR corrections, we will turn our attention to the specific case of associated Vh production.

4.1.1 The nature of electroweak mass singularities

As extensively discussed in chapter 3, electromagnetic radiative corrections are not only conceptually but also numerically important, since they benefit from logarithmic enhancements. Those enhancements, in turns, were due to the existence of two different IR-singular phenomena:

- Soft photon emissions. Since photons are massless, 4-momentum conservation does not forbid the radiation of infinitesimally soft real photons. The transition probability of soft-bremsstrahlung processes turns out to be logarithmically

divergent, $\sim \log E_\gamma$, thus leading to an enhancement of properly defined IR-safe observable.

- Collinear photon emission. An IR divergence of completely different mathematical origin is triggered whenever a massless fermion emits a collinear photon. Though no charged massless fermions exist in the Standard Model, contributions formally divergent for $m_f \to 0$ are expected and those divergences are again logarithmic, $\sim \log m_f$. Such contributions are often called mass singularities.

The above arguments need to be further discussed for the purposes of the present chapter. Clearly, on can genuinely talk about a numerical enhancement only if soft and/or collinear logarithms, $\log E_\gamma$, $\log m_f$, are actually bigger than $\mathcal{O}(1)$. Of course, such a mathematical requirement can be formalised only for logarithms of dimensionless quantities. If we normalise E_γ, m_f by the overall energy scale of the process, E_{tot}, we can then write:

$$\log \frac{E_\gamma^2}{E_{tot}^2} \gg 1 \; , \qquad \qquad \log \frac{m_f^2}{E_{tot}^2} \gg 1 \; , \qquad \qquad (4.1)$$

where we take by convention the ratio of squared energies.

Condition (4.1) gives us a better defined requirement to determine whether or not one can consider the logarithmic enhancement of radiative corrections as numerically relevant. For example, in chapter 3 the relevant energy scale of the process $J_\mu(q_0) \to J_\mu(q)\,\gamma(k)$ was $\sqrt{q_0^2}$. Therefore, the logarithmic enhancement is expected to fade away whenever $m_*^2 \approx q_0^2$: this is indeed the reason why our predictions were less accurate at the borders of phase space, as commented in section 3.3.3, footnote 16.

Of course, the identification of the process scale E_{tot} is of crucial importance for the whole argument. More relevant, a given process can have different energy scales involved and this might complicate the discussion. We will comment on this point later on, but first we should turn our attention to the importance of electroweak radiative corrections.

From the above discussion it should be clear that, in order to experience logarithmic enhancement of radiative corrections, a "true" IR divergence (such as the one associated to soft photons) is not necessary. Indeed, a "would-be" IR divergence (such as the mass singularities associated to collinear photons) is enough to experience such enhancement, as soon as the energy scale E_{tot} of the process is sufficiently larger than the physical IR cutoff of such divergence.

The intuitive concept of "would-be" IR divergence gives us a bridge to understand the meaning of radiative corrections (which are an IR physics phenomenon) due to W and Z bosons (which are massive bosons, i.e. IR safe objects). The argument is as follows. In the $v \to 0$ limit[1] (i.e. massless W, Z limit), one would see IR soft and/or collinear divergences due to the emission of electroweak bosons. Triggering the electroweak symmetry breakdown, those contributions are still present, but they have clearly turned into "would-be" IR divergence, i.e. terms which are singular in the $m_V \to 0$ limit ($V = W, Z$). For these reasons, such contributions are often called

---

[1]Here and in the following, v will denote the Higgs vacuum expectation value (v.e.v.).

electroweak mass singularities and their appearance is known since many years (see, for instance, [18–22]).

It should not be surprising that electroweak mass singularities are (once again) logarithmic and they look like

$$\log \frac{m_V^2}{E_{tot}^2} \ , \qquad \log^2 \frac{m_V^2}{E_{tot}^2} \ , \tag{4.2}$$

where the second term corresponds to a soft and collinear mass singularity (i.e. is a Sudakov double logarithm).

The aspect of electroweak mass singularities immediately explains why we have not considered them while discussing radiative corrections in Higgs decays. Indeed, in such processes, we clearly have $E_{tot} \leq m_h$, thus preventing any enhancement of the logarithms in Eq. (4.2). However, the discussion is rather different for electroweak Higgs production processes. In such case, E_{tot} is not limited by the Higgs mass but rather by the energy of the underlying parton collision, which can reach the TeV scale at LHC.

These are the reasons why we should care about W and Z mass singularities when discussing electroweak Higgs production processes. Unfortunately, despite the analogy with QED exploited to understand the nature of such singularities, very little can be recovered of the general results discussed in chapter 3 to address this new issue. On the one hand, the non-abelian structure of the electroweak theory invalidate many useful results which hold for QED, including the very existence of a factorisable radiator function. Such results should be re-derived from scratch. On the other hand, the fact that W and Z are massive nullifies our strategy of deriving the virtual corrections from the computation of real emissions. The very concept of "undetectably soft W, Z" does not hold and we should find another way to evaluate the mass singularities, through loop computations.

From time to time, we will briefly comment on the general solutions of these issues during our discussion. However, the focus of this chapter will be to address these problems in the very specific case of associated Vh production. For this reason, we now turn our attention to such process, clearly stating the goals we want to achieve and the hypotheses under which our results will be obtained.

4.1.2 Electroweak mass singularities in associated Vh production

Our final aim is to identify the leading electroweak radiative corrections to Vh production processes:

$$\mathcal{A}\left(f_1(p_1)\,\bar{f}_2(p_2) \to V(k)\,h(p_h)\right) \ , \tag{4.3}$$

within the framework where amplitudes (4.3) are parametrised using the Higgs POs, see section 2.3.2. Given the electroweak loop suppression, $g/4\pi \sim 10^{-3}$, and the conceptual difficulty of the task, we will focus only on double-logarithmic (DL) mass singularities (Sudakov double logarithms), since they benefit the largest enhancement.

In our loop computation of DL contributions we restrict ourselves to the kinematic region where all external momenta are on shell, whereas all Mandelstam invariants

are assumed to be much larger than m_V:

$$S \sim T \sim U \sim E_{tot}^2 \gg m_V^2 \; , \tag{4.4}$$

where $S = (p_1 + p_2)^2$, $T = (p_1 + k)^2$, $U = (p_1 + p_h)^2$. On the one hand, assumption (4.4) legitimises the largeness of DL contributions which, according to Eq. (4.2), can be expressed as

$$\log^2 \left(\frac{S}{m_V^2} \right) \; , \qquad \log^2 \left(\frac{T}{m_V^2} \right) \; , \qquad \log^2 \left(\frac{U}{m_V^2} \right) \; . \tag{4.5}$$

On the other hand, such kinematic regime will provide us with an effective expansion parameter, $v/E_{tot} \ll 1$. In principle, it would be nice to keep the discussion at the lowest order, namely $\mathcal{O}\left((v/E_{tot})^0\right)$. Unfortunately, this is not possible for the process under study, $q\bar{q} \to Vh$ ($V = W, Z$), since already the tree-level matrix element (within the Standard Model) is of order[2] $\mathcal{O}\left(v/E_{tot}\right)$.

These premises allows us to clearly state the approximations which we will rely on to compute the DL mass singularities in Vh production:

- We will neglect fermion masses and Yukawa interactions. The only exception to this assumption would have been the top quark, which is however of no concern for our present purposes.

- We will also neglect CKM-suppressed contributions. In other words, we will consider the W–fermion interactions as diagonal. The extension of our results to relax such assumption would not be difficult but notationally quite involved, thus we will not explicitly discuss it in the following.

- According to Eq. (4.4), we will perform a perturbative expansion using as expansion parameter $v/E_{tot} \ll 1$. In particular, we will stop ourselves at the first order, neglecting terms of order $\mathcal{O}\left(v^2/E_{tot}^2\right)$ or higher.

A couple of subtleties related to the v/E_{tot} power counting should be immediately pointed out. The first one regards longitudinal polarisation of vector bosons (ϵ_L^μ), which have a dangerous behaviour,

$$\epsilon_L^\mu(k) = \frac{k^\mu}{m_V} + \mathcal{O}\left(\frac{m_V}{k^0}\right) \sim (v/E_{tot})^{-1} \; . \tag{4.6}$$

This is particularly annoying, since it can potentially ruin the power counting we want to deploy. Indeed an $\mathcal{O}\left(v^2/E_{tot}^2\right)$ amplitude, negligible according to the assumptions above, can experience an enhancement as soon as a longitudinal gauge boson is involve, thus becoming relevant. The possible solutions are:

- To work at the v^2/E_{tot}^2 order while computing all amplitudes, subsequently taking into account possible E_{tot}/v enhancements when dealing with longitudinal polarisations.

---

[2]This is not completely true since, as it will be discussed later, longitudinal polarisations are healed from such suppression.

- To exploit the Goldstone Boson Equivalence Theorem (GBET) [82,83] to relate amplitudes involving external longitudinal gauge bosons to amplitudes involving external would-be Goldstone bosons, therefore getting rid of longitudinal polarisations and their annoying enhanced behaviour.

In the next section, the first strategy will be adopted to reach our final results. We will later on deploy the second strategy to obtain a nice consistency check of our computations, in section 4.2.4.

A second subtlety related to our v/E_{tot} power counting concerns the pieces of amplitudes featuring a boson pole, i.e. proportionals to $1/(q^2 - m_V^2)$. The PO parametrisation distinguishes in principle between poles at different masses (see for example the distinction between $\epsilon_{ZZ}^{(\mathrm{CP})}$ and $\epsilon_{Z\gamma}^{(\mathrm{CP})}$, Eq. (2.29)). However, one should notice that

$$\frac{1}{q^2 - m_{V_1}^2} = \frac{1}{q^2 - m_{V_2}^2} + \mathcal{O}\left(\frac{m_{V_i}^2}{q^2}\right) \ , \tag{4.7}$$

which implies, since $q^2 \sim E_{tot}^2$, that we will not be able to distinguish between poles at different masses, given our approximations. In our results, poles at different masses will all appear simply as a $1/q^2 = 1/S$ pole.

4.2 Computation within the Standard Model

As a first step toward a general description of DL mass singularities in the PO framework, we will perform a detailed computation of such contributions within the Standard Model, for a generic Vh production process.

As argued in the previous section, the differences between QED and electroweak theory force us to rely on completely different theoretical results and methodologies. A very useful discussion is given in Ref. [23], where the issue of factorisation of electroweak mass singularities (both single and double logarithms) is addressed in very general terms. Unfortunately, Ref. [23] limits its discussion to the zero order, $\mathcal{O}\left((v^2/E_{tot})^0\right)$, and thus it could be applied to Vh production only for longitudinal final state gauge bosons.

The aim of this section is a complete identification of DL mass singularities in Vh production both for longitudinal and transverse final state gauge bosons. We are thus forced to push one step further the discussion in Ref. [23] in order to extend it to next-to-leading order in the v/E_{tot} expansion. As already discussed, we will make no distinction between boson's polarisations, subsequently taking into account potential enhancement of $\mathcal{O}\left(v^2/E_{tot}^2\right)$ terms due to Eq. (4.6). On the contrary, Ref. [23] exploits the GBET to deal with longitudinal polarisations. In this way, our treatment of longitudinal polarisations will be complementary to the one in [23] and we will be able to perform a non-trivial cross check between the two results. This will be performed in section 4.2.4.

Despite the different handling of longitudinal polarisations, the computation of DL mass singularities performed in this section will follow closely the argument given in Ref. [23]. Such argument can be sketched as follows:

1. Adopting a diagrammatic point of view, all relevant topologies contributing to mass singularities are identified.

2. Exploiting the common structure of all diagrams involved, a general master formula to extract the mass singularities is derived.

3. General prescriptions to perform the sum over all possible Feynman diagrams involved are given.

The genuinely original contribution of this section is the extension of such discussion to the next-to-leading order in the v/E_{tot} expansion, an issue completely overlooked in Ref. [23]. Our focus will be on the process we are interested in, Vh production. However, it is worth to stress that the following discussion could be also seen as a first step toward a general next-to-leading order description of DL mass singularities.

4.2.1   Notation and conventions

Though we will try to limit the technicalities to their minimal amount, the following discussion of DL mass singularities will be rather involved. For this reason, we introduce here a moderate amount of notation and conventions, in order to make the subsequent analysis more fluent.

As anticipated above, we will perform the computations in a diagrammatic fashion. In particular, we will work in the 't Hooft–Feynman gauge. We will symbolically call φ a generic particle, f ($\bar{f}$) the fermions (antifermions), V the gauge bosons (A, Z, $W^{\pm}$), ϕ the would-be Goldstone bosons (ϕ_Z, $\phi^{\pm}$) while $\Phi = \phi, h$ will denote all scalars. Throughout the discussion, (anti)fermions f ($\bar{f}$) should always be understood to be chiral fermions (meaning that the two fermion chiralities should be considered as different fermions).

As a convention, we will consider amplitudes where all external particles and momenta are incoming. The matrix element for such processes will be called

$$\mathcal{A}\left(\varphi_1\,\varphi_2\,\varphi_3\,\varphi_4 \to 0\right) = \mathcal{M}^{\varphi_1\varphi_2\varphi_3\varphi_4}\ . \tag{4.8}$$

Whenever those matrix elements should be understood to be at tree level (i.e. Born level), we will add a '0' subscript, $\mathcal{M}_0^{\cdots\varphi_i\cdots}$. The corresponding amplitudes for physical $2 \to 2$ scattering processes can be easily obtained from $\mathcal{M}^{\cdots\varphi_i\cdots}$ by crossing symmetry.

Here follows the list of all tree-level scattering processes that will be needed in our discussion:

$$\mathcal{A}\left(f_1(p_1)\,\bar{f}_2(p_2) \to \bar{V}(-k)\,h(-p_h)\right) = \mathcal{M}_0^{f_1\bar{f}_2 Vh} = \mathcal{G}_{0\,\mu}^{f_1\bar{f}_2 Vh}\,\epsilon_V^\mu(k)\ ,$$

$$\mathcal{A}\left(f_1(p_1)\,\bar{f}_2(p_2) \to \bar{\phi}(-k)\,h(-p_h)\right) = \mathcal{M}_0^{f_1\bar{f}_2\phi h}\ ,$$

$$\mathcal{A}\left(f_1(p_1)\,\bar{f}_2(p_2) \to \bar{\phi}_1(-k_1)\,\bar{\phi}_2(-k_2)\right) = \mathcal{M}_0^{f_1\bar{f}_2\phi_1\phi_2}\ ,$$

$$\mathcal{A}\left(f_1(p_1)\,\bar{f}_2(p_2) \to \bar{V}(-k_1)\,\bar{\phi}(-k_2)\right) = \mathcal{M}_0^{f_1\bar{f}_2 V\phi} = \mathcal{G}_{0\,\mu}^{f_1\bar{f}_2 V\phi}\,\epsilon_V^\mu(k_1)\ ,$$

$$\mathcal{A}\left(f_1(p_1)\,\bar{f}_2(p_2) \to \bar{V}_1(-k_1)\,\bar{V}_2(-k_2)\right) = \mathcal{M}_0^{f_1\bar{f}_2 V_1 V_2} = \mathcal{G}_{0\,\mu_1\mu_2}^{f_1\bar{f}_2 V_1 V_2}\,\epsilon_{V_1}^{\mu_1}(k_1)\,\epsilon_{V_2}^{\mu_2}(k_2)\ .$$

$$\tag{4.9}$$

For future convenience, in amplitudes involving one (or more) vector gauge boson(s) we have also explicitly decomposed $\mathcal{M}_0$ in amputated Green function $\mathcal{G}_{0\,(\mu\nu)}$ and boson's polarisation ϵ_V^μ. It is worth to immediately point out that processes $\mathcal{M}_0^{f_1\bar{f}_2 Vh}$ and $\mathcal{M}_0^{f_1\bar{f}_2 V\phi}$ are order $\mathcal{O}\left(v/E_{tot}\right)$, while processes $\mathcal{M}_0^{f_1\bar{f}_2\phi h}$, $\mathcal{M}_0^{f_1\bar{f}_2\phi_1\phi_2}$, and $\mathcal{M}_0^{f_1\bar{f}_2 V_1 V_2}$ are order $\mathcal{O}\left((v/E_{tot})^0\right)$.

As it will become clear in the following, when building one-loop diagrams leading to DL contributions the relevant interactions are the trilinear Standard Model vertices. For our purposes, we can divide them in three groups accordingly to the behaviour of their Feynman rules:

1. VVV, $V\Phi\Phi$, $Vf\bar{f}$ Feynman rules do not feature a v and can be considered $\mathcal{O}\left((v/E_{tot})^0\right)$. We will call these vertices "unsuppressed". The couplings corresponding to these gauge vertices will be parametrised by the matrices $ieI_{\varphi_1\varphi_2}^V$.

2. $VV\Phi$, $\Phi\Phi\Phi$ Feynman rules, on the contrary, features a v and can thus be considered $\mathcal{O}\left(v/E_{tot}\right)$. We will call these vertices "suppressed". The couplings corresponding to these vertices will be parametrised by the matrices $ie^2 v\Upsilon_{\varphi_1\varphi_2}^\Phi$.

3. $\Phi f\bar{f}$ Feynman rules are proportional to Yukawa couplings and are thus negligible.

A detailed discussion of the $I_{\varphi_1\varphi_2}^V$ and $\Upsilon_{\varphi_1\varphi_2}^\Phi$ matrices used to parametrise the Standard Model vertices, together with their explicit formulas, can be found in appendix B.1.

4.2.2 Loop diagrams producing DL mass singularities

As a first step, we have to determine all classes of Feynman diagrams that potentially give rise to DL mass singularities. To this end we can exploit the detailed discussion in Ref. [23]. We can summarise the main outcomes of such discussion as follows:

i. DL mass singularities arise from the subset of loop diagrams where a virtual particle is exchanged between two on-shell external particles [10].

ii. Further, DL mass singularities originates from specific regions of momenta integration (so called *leading regions*), where the exchanged virtual particle momentum q^μ becomes soft and collinear to one of the external momenta [10].

iii. To evaluate such DL contributions, one can make use of the eikonal approximation, which consists of setting the soft momentum $q^\mu \to 0$ everywhere but in the propagators. In this way the loop integral assumes the form of a scalar three-point function (usually called C_0) from which the relevant DL mass singularities can be easily extracted.

Result *i* provide us with a comprehensive list of all loop diagrams possibly leading to DL contributions. In fact, we just need to dress the tree-level amplitude $\mathcal{M}_0^{f_1\bar{f}_2 Vh}$ (see Figure 4.1) with all possible soft-particle exchanges between external legs allowed by the Feynman rules of the theory.
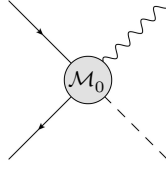
Figure 4.1: Diagrammatic representation of tree-level Vh production amplitude, $\mathcal{M}_0^{f_1 \bar{f}_2 V h}$.

$$(a) \qquad\qquad (b) \qquad\qquad (c) \qquad\qquad (d)$$
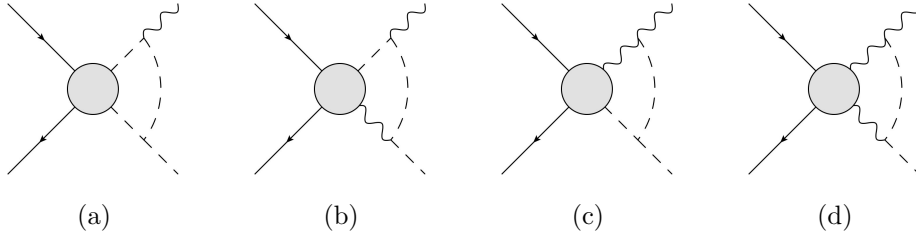
Figure 4.2: The four possibilities of a soft scalar exchange between V and h external legs. In eikonal approximation diagrams (a) and (b) vanish, while diagrams (c) and (d) turn out to be $\mathcal{O}\left(v^3/E_{tot}^3\right)$ and thus negligible.

We can actually further shrink the subset of relevant diagrams by exploiting our v/E_{tot} expansion, with the help of results *ii* and *iii*. Indeed, evaluating the v/E_{tot} order of each diagram for $q^\mu \to 0$ (eikonal approximation), we can consistently drop all diagrams which are $\mathcal{O}\left(v^3/E_{tot}^3\right)$ or more[3]. Such analysis leads us to very interesting and useful results.

- A soft fermion exchange can always be neglected, since the numerator of the fermion propagator simply vanishes in eikonal approximation (once neglected fermion masses).

- A soft scalar exchange from a fermion leg is negligible, since Yukawa-suppressed. On the other hand, a soft scalar exchange between V and h legs is always $\mathcal{O}\left(v^3/E_{tot}^3\right)$ or worse, thus should not be considered as well.

  We can prove the latter statement by explicit evaluation of the v/E_{tot} order of all possible soft scalar exchanges between V and h, represented in Fig. 4.2. Diagrams 4.2.a and 4.2.b vanish in eikonal approximation, given $\epsilon_V(k) \cdot k = 0$. Diagram 4.2.c is clearly $\mathcal{O}\left(v^3/E_{tot}^3\right)$, since $\mathcal{M}_0^{f\bar{f}Vh} \sim \mathcal{O}\left(v/E_{tot}\right)$ and the two vertices $VV\phi$, $\phi\phi\phi$ are both $\mathcal{O}\left(v/E_{tot}\right)$ as well. Diagram 4.2.d can be proven to be $\mathcal{O}\left(v^3/E_{tot}^3\right)$, once evaluated in eikonal approximation and once used the Slavnov–Taylor identity $\mathcal{G}_{0\,\mu\nu}^{f_1 \bar{f}_2 V_1 V_2}\, p_{V_2}^\nu = M_{V_2}\, \mathcal{G}_{0\,\mu}^{f_1 \bar{f}_2 V_1 \phi_2} \sim \mathcal{O}\left(v^2/E_{tot}^2\right)$.

- A soft vector gauge boson (V) exchange is the only possibility which leads to relevant contributions, i.e. $\mathcal{O}\left(v/E_{tot}\right)$.

---

[3]One should recall that, even though we are interested in $\mathcal{O}\left(v/E_{tot}\right)$ results, we are forced at this point to retain $\mathcal{O}\left(v^2/E_{tot}^2\right)$ contributions, since longitudinal V polarisations can enhance those pieces to the relevant $\mathcal{O}\left(v/E_{tot}\right)$ order.

Therefore, for our purposes, loop diagrams with a soft V exchange are the only ones that should be considered further. In fact, it was already proved in Ref. [23] that a soft V exchange is the only one leading to $\mathcal{O}\left((v/E_{tot})^0\right)$ DL mass singularities, independently on the process under study. We managed here to extend this conclusion to $\mathcal{O}\left(v^2/E_{tot}^2\right)$, in the specific case of Vh production[4].

The possible soft V exchanges which dress the Born process, Figure 4.1, can be categorised using two different criteria. The first criterion regards the v/E_{tot} order of the hard process $\mathcal{M}_0$:

A. Processes which involve $\mathcal{O}\left(v/E_{tot}\right)$ hard scatterings (i.e. $\mathcal{M}_0^{f\bar{f}V\Phi}$). The soft V exchange then involves unsuppressed vertices (i.e. VVV, $V\phi\phi$ or $Vf\bar{f}$).

B. Processes which involve $\mathcal{O}\left((v/E_{tot})^0\right)$ hard scatterings (i.e. $\mathcal{M}_0^{f\bar{f}VV}$ or $\mathcal{M}_0^{f\bar{f}\Phi\Phi}$). The soft V exchange will then involve a suppressed $VV\phi$ vertex.

The second criterion concerns the topology of the soft V exchange:

I. Soft V exchange between the two fermions.

II. Soft V exchange between a fermion and the gauge boson.

III. Soft V exchange between a fermion and the Higgs.

IV. Soft V exchange between the gauge boson and the Higgs.

For diagrams of type I and II, the hard process is a Vh production process, $\mathcal{M}_0^{f\bar{f}Vh}$ or $\mathcal{M}_0^{f\bar{f}\phi h}$. For diagrams of type III and IV, the hard process is an electroweak scattering process (not involving the Higgs[5]), $\mathcal{M}_0^{f\bar{f}VV}$, $\mathcal{M}_0^{f\bar{f}V\phi}$ or $\mathcal{M}_0^{f\bar{f}\phi\phi}$.

Table 4.1 summarises all possible diagrams with a V exchange, ordered according to the two criteria above. The diagrams in the first column (type-A diagrams) could have been predicted by the analysis of Ref. [23] and, in fact, for their evaluation one can almost straightforwardly rely on the discussion therein (except for a subtlety related to the VVV vertex, to be discussed in the following). On the contrary, diagrams in the second column (type-B diagrams) are a novelty, since they display a suppressed $VV\Phi$ vertex. Therefore, their evaluation will require a non-trivial improvement of the arguments in Ref. [23].

We will now proceed with the evaluation of the 12 classes of diagrams of Table 4.1. One should keep in mind that each class can produce more than one Feynman diagram, once the particles running in the loop are specified. In particular, a sum over all possible soft V bosons $(A, Z, W^{\pm})$ is always understood.

---

[4]An interesting question might be whether this conclusion can be generalised to other processes. However, it seems that the possibility of a soft-Φ exchange between V and Φ legs cannot be a priori excluded without relying on explicit details regarding the hard process involved.

[5]As we will discussion in section 4.3, there is one small exception to this consideration involving type-IVB diagrams.

	A	B
I		$\emptyset$
II	1: 2:	1: 2:
III	1: 2:	1: 2:
IV		1: 2:

Table 4.1: Summary of possible soft V exchanges to be considered to account for DL contributions. In the A column are diagrams with a hard process $\mathcal{M}_0 \sim \mathcal{O}\left(v/E_{tot}\right)$ and unsuppressed soft V scattering, while in the B column are diagrams with an $\mathcal{O}\left((v^2/E_{tot}^2\right)$ hard process $\mathcal{M}_0$ and a soft V scattering involving a $VV\Phi$ vertex (which is $\mathcal{O}\left(v/E_{tot}\right)$ according to our power counting).

4.2.3 Master formula for DL mass singularities

We will evaluate loop diagrams of Table 4.1 by computing their amplitude in a generalised fashion and exploiting results *ii* and *iii* stated in section 4.2.2. As a first step, simplified expressions for the soft V exchange vertices can be found within the eikonal approximation. Such expressions for each possible vertex are summarised below:

$$\frac{f_1 \quad f_2}{V_s^\mu} \left(\mathcal{M}_0\right) = -2\,p_i^\mu\,\frac{eI_{f_2f_1}^{V_s}}{D_i}\mathcal{M}_0 \;, \qquad \frac{V_1 \quad V_2}{V_s^\mu}\left(\mathcal{G}_0^\rho\right) = \frac{eI_{V_2V_1}^{V_s}}{D_i}\left(\epsilon_{V_1}^\mu p_i^\rho - 2\,p_i^\mu\epsilon_{V_1}^\rho\right)\mathcal{G}_{0\,\rho} \;,$$

$$\frac{\bar{f}_1 \quad \bar{f}_2}{V_s^\mu}\left(\mathcal{M}_0\right) = -2\,p_i^\mu\,\frac{eI_{\bar{f}_2\bar{f}_1}^{V_s}}{D_i}\mathcal{M}_0 \;, \qquad \frac{h \quad V_2}{V_s^\mu}\left(\mathcal{G}_0^\rho\right) = \frac{e^2\,v\,\Upsilon_{V_2V_s}^h}{D_i}\mathcal{G}_0^\mu \;,$$

$$\frac{h \quad \phi}{V_s^\mu}\left(\mathcal{M}_0\right) = -2\,p_i^\mu\,\frac{eI_{\phi h}^{V_s}}{D_i}\mathcal{M}_0 \;, \qquad \frac{V_1 \quad \phi_2}{V_s^\mu}\left(\mathcal{M}_0\right) = \frac{e^2\,v\,\Upsilon_{\bar{V}_1V_s}^{\phi_2}}{D_i}\epsilon_{V_1}^\mu\,\mathcal{M}_0 \;. \qquad (4.10)$$

In all above expressions, a shorthand notation for the trilinear vertices (involving I^V and Υ^Φ matrices) has been used. We refer to appendix B.1 for the explanation of such notation. By convention, the soft boson V_s^μ and the external leg have been considered incoming, while the internal leg is oriented from the soft vertex to the hard process. The external leg has incoming momentum p_i^α, while D_i is the internal particle propagator's denominator (in Feynman gauge).

Once again, it is worth to compare our results with Ref. [23]. For $Vf\bar{f}$ and $V\phi h$ vertices we recover the same expressions as in [23] (as it should be, since they are

Figure 4.3: Generalised loop diagram involving a V_s exchange between external particles φ_i and φ_j (whose incoming momenta are $p_{i,j}$).

unsuppressed vertices). The expression for the VVV vertex instead displays an extra term: indeed, the piece proportional to p_i^ρ was dropped in [23] since it could be argued that

$$\mathcal{G}_{0\,\rho} \sim \mathcal{O}\left((v/E_{tot})^0\right) \qquad \Rightarrow \qquad p_i^\rho\,\mathcal{G}_{0\,\rho} \sim \mathcal{O}\left(v/E_{tot}\right) \tag{4.11}$$

due to the Slavnov–Taylor identities. However, since the left hand side of implication (4.11) no longer holds in our setup, we are forced to keep also such extra term, which indeed turns out to give non-negligible contributions. Finally, the expressions for the $VV\Phi$ vertices finds no correspondence in [23], since those vertices are $\mathcal{O}\left(v/E_{tot}\right)$ and only a genuine next-to-leading order analysis in v/E_{tot} needs to retain them.

With an abuse of notation, we now introduce the following expression to summarise all vertices in Eq. (4.10):

$$\vcenter{\hbox{}} \;=\; \frac{1}{D_i} R_i^\mu \mathcal{M}_0 \;, \tag{4.12}$$

where the substitution $R_i^\mu \mathcal{M}_0 \to R_i^{\mu\rho}\mathcal{G}_{0\,\rho}$ should be understood to take place whenever needed[6].

We are now able to extract the DL mass singularities from loop diagrams of Table 4.1 through a generalised computation. The generalised representation of the loop diagram to be evaluated is represented in Figure 4.3. With the (ab)use of Eq. (4.12), we can derive:

$$\vcenter{\hbox{}} \;=\; \frac{1}{(4\pi)^2}\,\eta_{\mu\nu} R_i^\mu\, R_j^\nu\, \mathcal{M}_0 \left[-i\,(4\pi)^2 \int \frac{\mathrm{d}^d q}{(2\pi)^d} \frac{1}{D_i D_j D_V} \right]$$

$$\;=\; \frac{1}{(4\pi)^2}\,\eta_{\mu\nu} R_i^\mu\, R_j^\nu\, \mathcal{M}_0 \cdot \frac{1}{4\,p_i\!\cdot\! p_j}\mathrm{DL}(2\,p_i\!\cdot\! p_j, V, \varphi_i, \varphi_j) \;. \tag{4.13}$$

To derive the second equality we have evaluated the DL mass singularities of the loop function in square brackets (which is a simple C_0 scalar loop function), along the line of Ref. [23]. To encode DL contributions, we have introduced the shorthand notation

$$\mathrm{DL}(\Sigma, V_s, \varphi_i, \varphi_j) = \log^2\left(\frac{\Sigma}{M_{V_s}^2}\right) - \frac{1}{2}\delta_{V_s A}\left(\log^2\left(\frac{m_{\varphi_1}^2}{\lambda^2}\right) + \log^2\left(\frac{m_{\varphi_2}^2}{\lambda^2}\right)\right) \;, \tag{4.14}$$

---

[6]The use of expression $R_i^\mu \mathcal{M}_0$ to replace $R_i^{\mu\rho}\mathcal{G}_{0\,\rho}$ is an improper identification and should be understood to be just a formal substitution to unify the notation.

where λ is a fictitious photon mass which regulates IR divergences.

Using master formula (4.13) and vertices expressions (4.10), we are now able to evaluate all class of diagrams of Table 4.1. One finds:

$$\text{(diagram)} = \frac{\alpha}{4\pi} I^{\bar{V}_s}_{f'_1 f_1} I^{V_s}_{\bar{f}'_2 \bar{f}_2} \cdot \mathrm{DL}(S, V_s, f_1, f_2) \cdot \mathcal{M}_0^{f'_1 \bar{f}'_2 \bar{V} h} ,$$

$$\text{(diagram)} = \frac{\alpha}{4\pi} I^{\bar{V}_s}_{f'_1 f_1} I^{V_s}_{\bar{V}' \bar{V}} \cdot \mathrm{DL}(T, V_s, f_1, V) \cdot \left(\mathcal{M}_0^{f'_1 \bar{f}_2 \bar{V}' h} + \frac{p_1 \cdot \epsilon_V}{T} k^\rho \mathcal{G}_{0\,\rho}^{f'_1 \bar{f}_2 \bar{V}' h} \right) ,$$

$$\text{(diagram)} = \frac{\alpha}{4\pi} I^{\bar{V}_s}_{\bar{f}'_2 \bar{f}_2} I^{V_s}_{\bar{V}' \bar{V}} \cdot \mathrm{DL}(U, V_s, f_2, V) \cdot \left(\mathcal{M}_0^{f_1 \bar{f}'_2 \bar{V}' h} + \frac{p_2 \cdot \epsilon_V}{U} k^\rho \mathcal{G}_{0\,\rho}^{f_1 \bar{f}'_2 \bar{V}' h} \right) ,$$

$$\text{(diagram)} = \frac{\alpha}{4\pi} I^{\bar{V}_s}_{\bar{f}'_2 \bar{f}_2} I^{V}_{\phi_{V_s} h} \cdot \mathrm{DL}(T, V_s, f_2, h) \cdot \mathcal{M}_0^{f_1 \bar{f}'_2 \bar{V} \phi_{V_s}} ,$$

$$\text{(diagram)} = \frac{\alpha}{4\pi} I^{\bar{V}_s}_{f'_1 f_1} I^{V}_{\phi_{V_s} h} \cdot \mathrm{DL}(U, V_s, f_1, h) \cdot \mathcal{M}_0^{f'_1 \bar{f}_2 \bar{V} \phi_{V_s}} ,$$

$$\text{(diagram)} = \frac{\alpha}{4\pi} I^{\bar{V}_s}_{\bar{V}' \bar{V}} I^{V_s}_{\phi_{V_s} h} \cdot \mathrm{DL}(S, V_s, V, h) \cdot \left(\mathcal{M}_0^{f_1 \bar{f}_2 \bar{V}' \phi_{V_s}} + \frac{p_h \cdot \epsilon_V}{S} k^\rho \mathcal{G}_{0\,\rho}^{f_1 \bar{f}_2 \bar{V}' \phi_{V_s}} \right) ,$$

$$\text{(diagram)} = -\frac{\alpha}{4\pi} e \, \Upsilon^{\phi'}_{VV_s} I^{\bar{V}_s}_{f'_1 f_1} \frac{v}{T} \cdot \mathrm{DL}(T, V_s, f_1, V) \cdot p_1 \cdot \epsilon_V \, \mathcal{M}_0^{f'_1 \bar{f}_2 \bar{\phi}' h} ,$$

$$\text{(diagram)} = -\frac{\alpha}{4\pi} e \, \Upsilon^{\phi'}_{VV_s} I^{\bar{V}_s}_{\bar{f}'_1 \bar{f}_1} \frac{v}{U} \cdot \mathrm{DL}(U, V_s, f_2, V) \cdot p_2 \cdot \epsilon_V \, \mathcal{M}_0^{f_1 \bar{f}'_2 \bar{\phi}' h} ,$$

$$\text{(diagram)} = \frac{\alpha}{4\pi} e \, \Upsilon^{h}_{V_s V_s} I^{\bar{V}_s}_{\bar{f}'_2 \bar{f}_2} \frac{v}{T} \cdot \mathrm{DL}(T, V_s, f_2, h) \cdot \epsilon_V^\mu \, p_2^\nu \, \mathcal{G}_{0\,\mu\nu}^{f_1 \bar{f}'_2 \bar{V} V_s} ,$$

$$\text{(diagram)} = \frac{\alpha}{4\pi} e \, \Upsilon^{h}_{V_s V_s} I^{\bar{V}_s}_{f'_1 f_1} \frac{v}{U} \cdot \mathrm{DL}(U, V_s, f_1, h) \cdot \epsilon_V^\mu \, p_1^\nu \, \mathcal{G}_{0\,\mu\nu}^{f'_1 \bar{f}_2 \bar{V} V_s} ,$$

$$\text{(diagram)} = \frac{\alpha}{4\pi} e \, \Upsilon^{h}_{V_s V_s} I^{\bar{V}_s}_{VV'} \frac{v}{S} \cdot \mathrm{DL}(S, V_s, V, h) \cdot \left(\epsilon_V^\mu \, k^\nu - \frac{1}{2} \epsilon_V^\nu \, k^\mu \right) \mathcal{G}_{0\,\mu\nu}^{f_1 \bar{f}_2 \bar{V}' V_s} ,$$

$$\text{(diagram)} = -\frac{\alpha}{4\pi} e \, \Upsilon^{\Phi'}_{VV_s} I^{V_s}_{\bar{\phi}'' h} \frac{v}{S} \cdot \mathrm{DL}(S, V_s, V, h) \cdot p_h \cdot \epsilon_V \mathcal{M}_0^{f_1 \bar{f}_2 \bar{\Phi}' \phi''} . \tag{4.15}$$

Conventions for particle names are specified in Fig. 4.4 for each diagram class. All particles and momenta are understood to be incoming. The final connection to the physical $2 \to 2$ scattering process is eventually given by crossing symmetry (see Eqs. (4.9)). The poles $1/S$, $1/T$, $1/U$ appearing in some of the expressions should be interpreted with the caveat expressed in Eq. (4.7): possible shifts of these poles by an amount of order v^2 have been neglected for consistency with the rest of the $\mathcal{O}(v/E_{tot})$ computation (e.g. a $1/S$ term could be a photon pole as well as a Z or W pole).

For the last time, let us discuss the new features of Eqs. (4.15) with respect to results in Ref. [23]. Referring to Table 4.1 for diagram's nomenclature, we can see that:

- Diagrams IA and IIIA have exactly the same expressions as in [23]. This is clear since for those diagrams we have obtained the same soft V vertices' expressions, Eqs. (4.10).
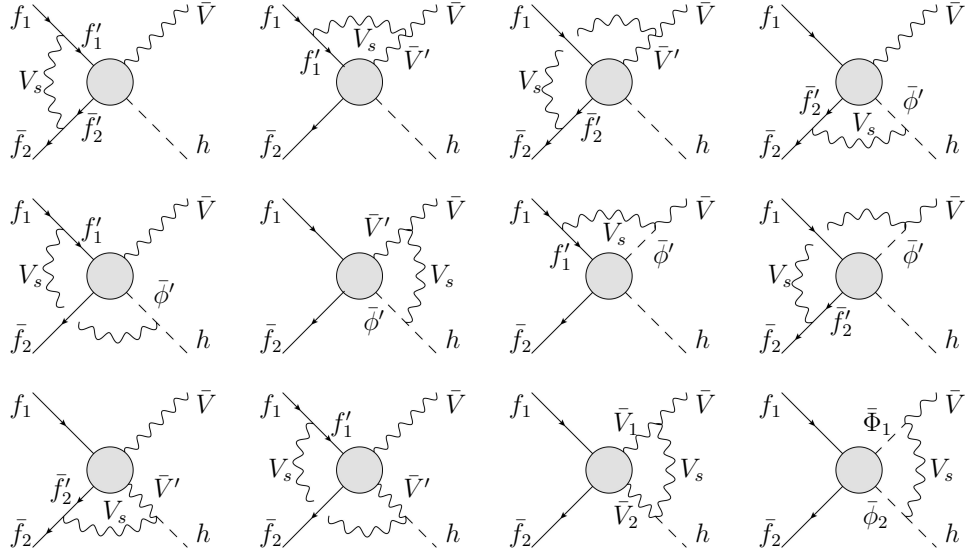
Figure 4.4: Convention for particle names used to derive results in Eqs. (4.15). All particles should be understood to be incoming. The direction of V_s is irrelevant, since a sum over all V_s possibilities $(A, Z, W^{\pm})$ is eventually performed.

- Results of diagrams IIA and IVA have two different pieces. The first one recovers the result in [23], while the second one has a different structure and stems from the additional $\propto p_i^{\rho}$ piece in VVV soft vertices discussed after Eqs. (4.10).

- Type-B diagrams has in general more complicated expressions. These results are new and needs a different cross check, since they all stems from $VV\Phi$ vertices which are neglected in Ref. [23].

Eqs. (4.15) were the last ingredient missing to allow the explicit computation of DL mass singularities in Vh production processes, within the Standard Model. Such computation can now be performed along this simple path:

1. To specify the process under study, i.e. its external legs.

2. To find all loop diagrams contributing to DL mass singularities, by taking diagrams of Table 4.1 and identifying for each of them all possible loop particle contents.

3. To compute the DL contributions from each loop diagram using Eqs. (4.15).

4. To sum all contributions together.

4.2.4 Cross checks of the Standard Model results

Our final expressions for $\mathcal{O}\left(v/E_{tot}\right)$ DL mass singularities in Vh production processes has been derived in Eqs. (4.15). A first check of our expressions has been already performed above, where we have compared results in Eqs. (4.15) with Ref. [23] whenever a correspondence was possible. Clearly, a more detailed and complete cross check

of our results would be preferable. In particular, it would be useful to compare our explicit results for the six possible Vh production processes ($\chi = L, R$),

$$u_\chi \bar{u}_\chi \to Zh \ , \qquad d_\chi \bar{d}_\chi \to Zh \ , \qquad u_L \bar{d}_L \to W^+ h \ , \qquad d_L \bar{u}_L \to W^- h \ , \qquad (4.16)$$

with a second independent computation of DL mass singularities.

A first possibility, already sketched in section 4.1.2, is to compare our full results with the one obtained through Ref. [23], for the case of longitudinal W or Z bosons in the final state. The strategy in [23] to evaluate those mass singularities is to exploit the GBET and then work with diagrams featuring ϕ external legs. Our strategy instead keeps V external legs and then applies Eq. (4.6) at the end of the computation. In the end, the two results should coincide up to $\mathcal{O}\left(v/E_{tot}\right)$ terms.

Such analytical comparison for longitudinal final state bosons has been performed for all six processes of Eq. (4.16). Remarkably, not only the $\mathcal{O}\left((v/E_{tot})^0\right)$ coincides, but one also finds out that no terms of order $\mathcal{O}\left(v/E_{tot}\right)$ appears. In other words, the first non-vanishing corrections to the $\mathcal{O}\left((v/E_{tot})^0\right)$ results for longitudinal polarisations turn out to be order $\mathcal{O}\left(v^2/E_{tot}^2\right)$. This result is particularly pleasant, since it relieves us from warring about $\mathcal{O}\left(v^2/E_{tot}^2\right)$ terms in expressions (4.15): those contributions are simply vanishing.

Despite the positive results obtained so far, a cross check of the genuine $\mathcal{O}\left(v/E_{tot}\right)$ contributions is still missing. Given the limited set of different processes to be analysed, Eq. (4.16), a brute-force evaluation of the Standard Model one-loop diagrams with an automated tool is a viable solution. This is indeed the strategy we deployed to perform a final check of our results.

More specifically, we used the *FeynArts* [84] and *FormCalc* [85] packages for *Mathematica* to analytically evaluate the one-loop results for processes (4.16), performing a Passarino–Veltman reduction [86] to express the final results in terms of scalar loop integral functions (A_0, B_0, C_0, D_0). We then retained only terms featuring a C_0 or D_0 scalar function, since these are the only ones that can produce Sudakov double logarithms (see for example [87]). Once extracted the DL mass singularities from C_0, D_0 using the eikonal approximation, we dropped all negligible terms according to our approximations (see section 4.1.2) to obtain an independent evaluation of the full $\mathcal{O}\left(v/E_{tot}\right)$ results.

Through this procedure we obtained a full match of DL mass singularities between our master formulas, Eqs. (4.15), and the brute-force computations, for all six processes of Eq. (4.16). It is worth stressing the highly non-trivial value of such cross check, since there is not even a one-to-one correspondence between the diagrams of Table 4.1 and the explicit Feynman diagrams entering the brute-force one-loop computations.

Type-IVB diagrams of Table 4.1, for example, corresponds to the sum of two loop diagrams: a triangle diagram in S-channel and a box diagram. Diagrammatically:

$$(4.17)$$

The same box diagram, on the other hand, contributes not only to that type-IVB diagram, but also to other diagrams of Table 4.1, according to which internal box line is considered soft. Diagrammatically:

$$\Rightarrow \qquad + \qquad + \qquad . \tag{4.18}$$

This intricate correspondence between the two computations was nevertheless unfolded and each line of Eqs. (4.15) has been cross-checked individually, in order to add robustness to our final result.

4.3 Discussion in the PO framework

The final purpose of this section is to apply the analysis of DL mass singularities performed in the previous section to the PO description of Vh production.

To this end, we will first discuss what should be improved in the arguments of section 4.2 in order to extend those results to the PO parametrisation. As a result, we will be able to carry out a general computation of DL corrections in the hPO framework. At that point we will manage to perform a phenomenological analysis of the interesting effects arising in Vh production due to electroweak radiative corrections.

4.3.1 Extension of computations in the PO framework

There are two important differences between Standard Model and PO framework that should be immediately stressed. On the one hand, the discussion within the Standard Model has been carried out in a perturbative fashion, analysing the one-loop radiative dressing of a tree-level (Born) amplitude. On the contrary, we would now like to discuss DL contributions in terms of radiative dressing of Green functions, since this is the language of the PO parametrisation. On the other hand, within the PO framework we should take into account new physics terms whose presence was a priori excluded in the Standard Model computation.

Before any quantitative analysis about how to extend our results to POs, we should first of all make sure that the two important differences outlined above do not introduce qualitative changes in the discussion of section 4.2. In other words, nothing guarantees that the whole argument of the previous section can still be deployed at all within the PO framework. Nevertheless, as a matter of fact, we will be able to fully recover the argument of section 4.2, with very few quantitative changes in our master formulas.

An crucial step toward a PO-oriented interpretation of results in section 4.2 is to observe that the whole argument still holds if the tree-level matrix elements $\mathcal{M}_0$ are substituted with non-perturbative correlations functions. This might appear at first sight an odd statement: the one-loop dressing of a Green function seems an inconsistent approach, a perturbative improvement of a non-perturbative object. However, one should keep in mind that such one-loop computation is not meant to derive UV

corrections to such Green function (which would be inconsistent), but only the radiative (i.e. IR) corrections which deform its analytical structure. Indeed, we are retaining from such loop computation only the mass singularities emerging in eikonal approximation.

The eikonal approximation itself gives us another way to explain the correctness of our claim. The result that DL mass singularities appear only in diagrams with exchange of a soft and collinear virtual particle between external legs still holds in the PO framework, since it relies only on the analytical structure of the loop computation involved [10]. From a diagrammatic perspective, we can summarise our argument as follows:

$$\lim_{q^\mu \to 0} \qquad q^\mu \quad = \qquad \times \qquad . \qquad (4.19)$$

In other words, we can effectively describe these classes of diagrams in eikonal approximation as the product of a hard process, which can as well be described through a non-perturbative Green function, and a soft re-scattering of a gauge boson.

As we will discuss in a moment, there is still work to be done in order to integrate the PO point of view (i.e. correlation functions) within the one-loop-fashioned computation of DL mass singularities exploited in section 4.2. For example, we should be careful at every step of the argument that new physics effects do not spoil results that were deployed within the Standard Model, identifying any quantitative modification of our formulas when switching to the PO description. However, Eq. (4.19) is already a major step forward, since it authorises us to deploy the same qualitative strategy of section 4.2 to evaluate electroweak radiative corrections in the PO framework.

Once verified that the structure of the argument of section 4.2 remain unchanged for the PO case, we should turn our attention to the quantitative aspects of the analysis. In particular, we would like to recover a result as master formulas (4.15). It turns out that the re-derivation of Eqs. (4.15) in our new setup requires different arguments depending on the hard process involved which, as already clear from Table 4.1, can be of three kinds: Vh production (i.e. $\mathcal{M}^{f\bar{f}Vh}$), "ϕh" production (i.e. $\mathcal{M}^{f\bar{f}\phi h}$), electroweak scatterings (which do not feature an h leg).

We first state our final results, i.e. the prescriptions to be adopted in order to extend the validity of master formulas (4.15) to the PO scenario. As anticipated, those prescriptions are different depending on the kind of hard process involved:

1. When the hard process is Vh production (diagrams IA, IIA), one should just substitute, in Eqs. (4.15), $\mathcal{M}_0^{f_1\bar{f}_2Vh}$ (or $\mathcal{G}_{0\,\rho}^{f_1\bar{f}_2Vh}$) with the corresponding PO parametrisation, Eq. (2.28).

2. When the hard process is "ϕh" production (diagrams IIB and, on special cases, IVB), one should again substitute $\mathcal{M}_0^{f_1\bar{f}_2\phi h}$ with the corresponding PO parametrisation. The PO parametrisation of the non-physical $f\bar{f} \to \phi_V h$ amplitude is given by the usual GBET,

$$\mathcal{M}^{f_1\bar{f}_2\phi_V h} = i^{(Q_V-1)} \frac{1}{m_V} p_{\phi_V}^\mu \, \mathcal{G}_\mu^{f_1\bar{f}_2Vh} \,, \qquad (4.20)$$

where $\mathcal{G}_\mu^{f_1 \bar{f}_2 Vh}$ is given by Eq. (2.28) once removed the polarisation vector ϵ_V^μ.

3. Whenever the soft V exchange involves an h leg (diagrams IIIA, IIIB, IVA, IVB), one should add an extra κ_{VV} factor for each h leg involved (where V is the exchanged soft boson). This rule applies to all diagrams whose hard process is an electroweak scattering process (in that case, exactly one extra κ_{VV} factor should be added), but not exclusively to them, as will be discussed below.

Each prescription above requires a dedicated discussion in order to prove it. The first prescription, regarding Vh hard processes, actually does not need further comments than Eq. (4.19). Once argued that the soft-dressing factorises from the hard process itself, we can fully recover the discussion of the former from section 4.2 (since Standard-Model-like) and then exploit the PO parametrisation to express the latter. This is basically what prescription 1 says.

The second prescription adds a further step, since in this case the GBET is needed in order to obtain an expression, within the PO framework, for the (non-physical) correlation functions involving would-be Goldstone bosons. One might be concerned about the applicability of the GBET in the unfamiliar PO scenario. However, it should be recalled that the proof of the GBET relies only on the Slavnov–Taylor identities of a spontaneously broken $SU(2)_L \times U(1)_Y \to U(1)_Q$ symmetry. Rephrasing this crucial observation, the GBET still holds in generic new physics scenarios, as long as the underlying gauge structure and spontaneous symmetry breaking pattern is kept. These are all conditions fulfilled by the PO framework, thus the deployment of the GBET, Eq. (4.20), is fully justified.

Though mathematically meaningful, one might still feel uncomfortable with the extension of PO parametrisation, born to describe physical correlation functions characterising Higgs processes, to a non-physical amplitude like $f\bar{f} \to \phi h$. However, one should not over-think Eq. (4.20). In the end, it is just an analytical continuation of the PO parametrisation needed to perform the computations, exactly as our loop formalism is just an analytical tool to extract the DL mass singularities we are interested in.

We are left with the discussion of the third prescription, whose formulation is rather simple but whose proof will need a bit more words to be fully unfolded. The initial observation is that, if an h leg is involved in the soft V exchange, the soft exchange itself should be seen as an Higgs process and thus should be described through the PO parametrisation. In other words, the PO framework should be used to evaluate both factors on the right-hand side of Eq. (4.19). The first two prescriptions were dealing with situations where the first factor (the hard process) was to be described using Higgs POs. The third prescription deals with situations where Higgs POs should be used to describe the soft V exchange. We will refer to the latter contingency as "soft PO".

A soft PO is a delicate issue, since it forces us to describe the soft V exchange as a whole. This in principle invalidates the entire analysis that through Eqs. (4.10) arrives at master formula (4.13). However, as we will now show, a formal treatment of soft PO turns out to be equivalent to the old Standard-Model-like discussion, the only difference being exactly prescription 3 stated above.

As an explicit example, we consider the loop diagram of Fig. 4.5, where a $V_s V_s h$
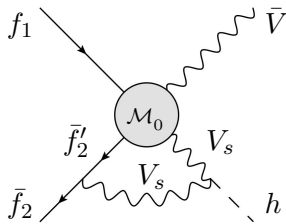
Figure 4.5: Example of loop diagram involving an h leg in the soft V exchange.
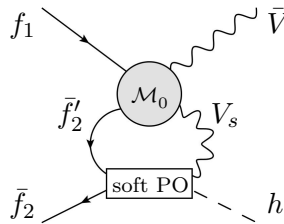
Figure 4.6: Loop diagram of Fig. 4.5, with the soft V_s exchange interpreted as a "soft PO".

soft vertex is involved. Using the soft PO point of view, the whole V_s re-scattering should be considered as a Vh production process (i.e. $f_1 f_2 \to V_s h$), taking place at a very soft invariant mass (according to the eikonal approximation $q^\mu \to 0$). This interpretation is depicted in Figure 4.6.

One should now perform the computation of DL mass singularities using the point of view of Figure 4.6, i.e. putting parametrisation (2.28) in the loop amplitude. The crucial observation is that, in eikonal approximation, only the F_L piece survives, and moreover only the κ_{VV} piece has the pole structure needed to develop Sudakov double logarithms[7]. At this point, one can immediately realise that parametrisation (2.28), in these limits, exactly recovers the Standard Model amplitude up the multiplicative factor κ_{VV} itself[8].

The above discussion, exemplified for the diagram of Figure 4.5, can be straightforwardly extended to all soft PO configurations. It is a completely general feature of the PO parametrisation that only the F_L part survives in eikonal approximation and that, considering that part, only the κ_{VV} piece has the pole structure needed to develop DL mass singularities. Since the κ_{VV} piece represent a multiplicative distortion of the Standard Model amplitude by construction, prescription 3 has been proven.

The above argument is completely general and set the issue of soft POs. It is worth to stress a couple of point which, if overlooked in the first place, might cause confusion later on.

- The example chosen to discuss soft POs, Figure 4.5, was a type IIIB diagram (see Table 4.1) and therefore featured a soft Vh production process. However, other classes of diagrams features different soft POs. Type IIIA diagrams features a soft ϕh production, whose discussion can be linked to the one above using the GBET. Type IVA and IVB diagrams feature a soft Higgs decay instead. The detailed discussion might differ a bit from soft Vh production, but it can be easily shown that prescription 3 still holds.

- A second subtlety is related to certain IVB diagrams. While filling out explicitly the virtual states, solutions as the one depicted in Figure 4.7 might appear. Situations of that kind simultaneously involves a Vh hard process and soft POs

---

[7]Indeed, as already discussed, we need at least three propagators to develop DL mass singularities. The additional $1/P_V(q^2)$ pole of the κ_{VV} piece of the parametrisation is therefore essential.

[8]This last feature should be of no surprise, since the κ_{VV} piece of the PO parametrisation was designed exactly to recover the Standard Model in the $\kappa_{VV} \to 1$ limit, see Eq. (2.10).
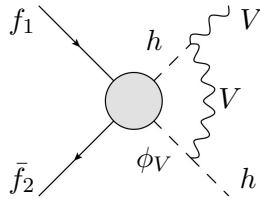
Figure 4.7: Possible loop diagram of type IVB featuring both a hard Vh process and soft POs (two soft Higgs decays, bringing an extra κ_{VV}^2 factor).

(two soft Higgs decays), thus both prescription 2 and 3 should be applied. What is particularly annoying of these diagrams is that their dependence upon POs is not linear and an extra κ_{VV}^2 factor arises.

The three prescriptions proven above are all we need to extent master formulas (4.15) to the PO framework. We are now able to compute and describe in full generality the DL mass singularities for every Vh production process. This will be the focus of next session.

4.3.2 Results in the PO framework

In this section, we want to qualitatively and quantitatively discuss the dressing of PO parametrisation with DL mass singularities. The first important thing to immediately point out is that, differently from QED, electroweak radiative corrections are not just a diagonal factor. On the contrary, they trigger a mixing between different POs. In other words, DL corrections will not be straightforwardly proportional to the "undressed" amplitude itself, but they will also depend upon POs from different amplitudes.

The fundamental reason for the PO mixing phenomenon is the non-abelian structure of the electroweak theory. By having a look at diagrams in Figure 4.4, it can be immediately realised that the hard process usually have different external legs than the original process to be dressed, since soft W or Z boson exchanges trigger a switch among $SU(2)_L$ partners.

Though conceptually simple, the PO mixing phenomenon complicates the quantitative discussion of electroweak radiative corrections considerably. Nevertheless, at a closer look such mixing is not completely anarchic and one can group the phenomenology of PO mixing in three categories:

- The bulk of DL corrections is a linear mixing between POs. However, two different POs mix linearly under a specific condition, namely only if they refer to the same tensor and pole structures. This can be understood since radiative corrections cannot have effects on those structures, which are amplitude's properties determined by UV physics. Performing such grouping, we get:

$$\{\kappa_{ZZ}, \kappa_{WW}\}\ ,\quad \{\epsilon_Z^{uu}, \epsilon_Z^{dd}, \epsilon_W^{ud}\}\ ,\quad \{\epsilon_{ZZ}, \epsilon_{Z\gamma}, \epsilon_{WW}\}\ ,\quad \{\epsilon_{ZZ}^{\text{CP}}, \epsilon_{Z\gamma}^{\text{CP}}, \epsilon_{WW}^{\text{CP}}\}\ . \quad (4.21)$$

- As discussed in section 4.3.1, some diagrams give rise to DL corrections which features an extra κ_{VV}^2 factor (see Figure 4.7 and relative discussion). Such non-linear effect does not affect CP-odd POs.

- Finally, we also observe DL corrections resulting in new kinematic and tensor structures. A first effect is the rise of extra contributions to Δ_T, which ceases both to be Standard-Model-like and to be a scalar function of q^2 only. A second effect is the appearance of an extra tensor structure in Eq. (2.28):

$$
\mathcal{A}\left(f_1\bar{f}_2 \to Vh\right) = 2i\,\frac{m_V^2}{v}\,\bar{f}_2\gamma_\nu f_1\,\epsilon_{V\mu}^*(k)\left[\cdots + \tilde{\Delta}_T\left(\frac{p_\Delta^\mu k^\nu - (p_\Delta \cdot k)\,\eta^{\mu\nu}}{m_V^2}\right)\right]\,,
\tag{4.22}
$$

where $p_\Delta^\mu = p_1^\mu - p_2^\mu$ (with momenta defined as in Eq. (2.28)). Both Δ_T and $\tilde{\Delta}_T$ are linear in the contact terms $\epsilon_V^{ff'}$ and feature $1/T$ and $1/U$ poles (but never $1/S$ poles). Indeed, these extra terms origin from diagrams type II and III, where the soft V is exchanged between an initial fermion and a final leg.

In the original hPO decomposition [3, 4], reviewed in chapter 2, the fermion current was considered as a whole, completely characterisable through its total momentum q^μ. This is why the additional tensor structure of Eq. (4.22) was not included, since such a structure arises only if the internal kinematic of the fermion current is resolved. Indeed, such a structure is generated radiatively from type II and III diagrams exactly because through these diagrams the two fermions interact non-symmetrically with the rest of the process[9] (the two asymmetries being the different momenta and, for charged currents, the different quantum numbers under $SU(2)_L$).

Once explained the different radiative effects we should characterise, we can switch to a quantitative description of them. In particular, given a generic PO ζ, we should specify both its linear mixing with the POs belonging to the same class and its possible non-linear correction. Calling $\delta^{\mathrm{DL}}\zeta$ the DL corrections to ζ, we can cast them as follows:

$$
\delta^{\mathrm{DL}}\kappa_{VV} = \frac{\alpha}{4\pi}\sum_{V'=Z,W}\Lambda_{VV'}^L\,\kappa_{V'V'} + \frac{\alpha}{4\pi}N_V^L\,\kappa_{VV}^3\,,
$$

$$
\delta^{\mathrm{DL}}\epsilon_{VV} = \frac{\alpha}{4\pi}\sum_{V'=Z,W}\Lambda_{VV'}^T\,\epsilon_{V'V'} + \frac{\alpha}{4\pi}\Lambda_{V\gamma}^T\,\epsilon_{Z\gamma} + \frac{\alpha}{4\pi}\kappa_{VV}^2\sum_{\{[f_1f_2]\}}N_{V,[f_1f_2]}^T\,\epsilon_V^{f_1f_2}\,,
$$

$$
\delta^{\mathrm{DL}}\epsilon_{VV}^{\mathrm{CP}} = \frac{\alpha}{4\pi}\sum_{V'=Z,W}\Lambda_{VV'}^{\mathrm{CP}}\,\epsilon_{V'V'}^{\mathrm{CP}} + \frac{\alpha}{4\pi}\Lambda_{V\gamma}^{\mathrm{CP}}\,\epsilon_{Z\gamma}^{\mathrm{CP}}\,,
$$

$$
\delta^{\mathrm{DL}}\epsilon_V^{f_1f_2} = \frac{\alpha}{4\pi}\sum_{\substack{V'=Z,W\\\{[f_1'f_2']\}}}\Lambda_{[f_1f_2],[f_1'f_2']}^f\,\epsilon_{V'}^{f_1'f_2'} + \frac{\alpha}{4\pi}\kappa_{VV}^2 N_V^f\epsilon_V^{f_1f_2}\,.
\tag{4.23}
$$

with $V = \{Z, W\}$. In the expressions above, matrices Λ encode the linear mixing between POs, while N encode the non-linear mixing proportional to κ_{VV}^2. It should be kept in mind that, according to Eq. (4.7) and relative discussion, it is meaningless to distinguish between $\epsilon_{ZZ}^{(\mathrm{CP})}$ and $\epsilon_{Z\gamma}^{(\mathrm{CP})}$ within our approximations. This is the reason

---

[9]For this reason, one would expect the form factor $\tilde{\Delta}_T$ to vanish under suitably defined symmetry limits. In particular, for neutral currents one should verify that $\lim_{U\to T}\tilde{\Delta}_T = 0$. This is indeed the case, see appendix B.2, Eq. (B.34).

why Eqs. (4.23) do not include $\delta^{\mathrm{DL}}\epsilon^{(\mathrm{CP})}_{Z\gamma}$: they has been simply added to $\delta^{\mathrm{DL}}\epsilon^{(\mathrm{CP})}_{ZZ}$, since only such sum is a well defined object at order $\mathcal{O}\left(v^2/E^2_{tot}\right)$.

Together with the explicit formulas for Λ and N, we also need to give the expressions for Δ_T and $\tilde{\Delta}_T$. All of this is done in Appendix B.2, since such expressions are quite lengthy and notationally involved and not at all interesting from the qualitative point of view.

A few final comments are in order.

- As for the discussion of chapter 3, the results of this chapter can be extended to generic descriptions of Beyond Standard Model physics in Vh production. Indeed, even if immersed in the PO language, our arguments are completely general and can be easily interpreted and deployed within different formalisms. Even if the intermediate step of the PO parametrisation is advisable for the reasons outlined in section 2.1, DL mass singularities can be also directly computed through our results in explicit new physics models.

- Results in section 4.2, i.e. the extension of the analysis of DL corrections in Ref. [23] at order $\mathcal{O}\left(v/E_{tot}\right)$ within or beyond the Standard Model, in principle can be applied to other processes, as long as the possibility of a soft ϕ exchange is shown to be negligible (see section 4.2.2, footnote 4).

  More important, the v/E_{tot} expansion itself should be proven to be a consistent expansion. In $2 \to 2$ scattering processes, requirement (4.4) is enough since the three Mandelstam variable completely characterise the kinematic. In turns, this allows to clearly define the kinematic regime where the v/E_{tot} expansion holds. However, in processes with more than 4 legs such as VBF, the issue is more subtle and it is in principle possible to have kinematic invariants that stays at low energy even if the overall process takes place at very high energies. Such latter behaviour is very dangerous, since it breaks the underlying power counting deployed in section 4.2, and it is the ultimate reason why we have not extended our discussion to VBF in this chapter.

- The issue of single logarithmic mass singularities has been completely overlooked in this chapter, albeit they are known to play a significant role in certain circumstances, for instance if the DL contributions undergo accidental cancellations [88]. The difficulty of extending the analysis of Ref. [23], which consider also single logarithms, to a more general framework is twofold. On the one hand, from the purely technical point of view, the extension to generic new physics scenarios of such discussion is more involved, since it more heavily deploys a series of Standard Model properties which should be re-derived or bypassed when switching to more general contexts. On the other hand, the very approach of deploying the point of view of Green functions, a necessary condition to apply the PO framework, is not guaranteed to work also for single logarithmic corrections.

Supersymmetry

In chapter 1 we outlined the reasons why the Higgs sector deserves particular attentions and further dedicated studies. In chapters 2 through 4 we adopted a bottom-up perspective, admitting our ignorance about possible new physics completions of the Standard Model and addressing the humbler but not less important problem of parametrising in a general as well as accurate manner collider Higgs phenomenology.

In this and the following chapter we will instead tackle the problem from an opposite perspective, adopting a top-down approach. On the one hand, top-down strategies are unavoidably less general and (several) initial assumptions are needed, sometimes with nothing but reasonable guesses to support them. However, on the other hand, they can lead to very interesting and definite conclusions that cannot be achieved within more conservative approaches.

5.1 Supersymmetric theories

In our top-down approach, we will focus our attention on a particular class of Standard Model extensions called supersymmetric theories. Historically, *supersymmetry* was developed in the early 1970's to circumvent some no-go theorems (and in particular the Coleman–Mandula theorem [89]) regarding the (im)possibility of combining spacetime and internal symmetries in any but a trivial way.

In a modern language, the basic idea of supersymmetric theories is to relate fermionic and bosonic states through a supersymmetry transformation. The operators $Q, Q^\dagger$ that generate such transformations must be anticommuting spinors, with

$$Q|\text{Boson}\rangle = |\text{Fermion}\rangle \,, \qquad Q|\text{Fermion}\rangle = |\text{Boson}\rangle \,. \tag{5.1}$$

Being Q and $Q^\dagger$ fermionic operators, they carry spin angular momentum 1/2, so it is clear that supersymmetry must be a spacetime symmetry. The possible forms for such symmetries in an interacting quantum field theory are highly restricted by the Haag–Łopuszański–Sohnius extension [90] of the Coleman–Mandula theorem. For realistic theories with chiral fermions (as in the Standard Model), this theorem implies that the generators Q and $Q^\dagger$ must satisfy an algebra of anticommutation and commutation

relations with schematic form

$$\{Q, Q^\dagger\} = P^\mu \ ,$$
$$\{Q, Q\} = \{Q^\dagger, Q^\dagger\} = 0 \ ,$$
$$[P^\mu, Q] = [P^\mu, Q^\dagger] = 0 \ ,$$
$$[T^a, Q] = [T^a, Q^\dagger] = 0 \ , \qquad\qquad\qquad (5.2)$$

where P^μ is the four-momentum generator of spacetime translations, while T^a are the generators of gauge transformations. Relations (5.2) define a supersymmetric algebra or *superalgebra*. It is worth noting that the introduction of anticommutation relations in the superalgebra is the extra ingredient allowing to bypass the Coleman–Mandula no-go theorem.

From the mathematical point of view, nothing would prevent us from introducing an "extended" supersymmetry, which means considering more than one distinct copy of supersymmetry generators $Q, Q^\dagger$. Though mathematically amusing, such theories are not phenomenologically viable in four dimensions and higher-dimensional field theories with suitable compactification of extra dimensions would be needed. The ordinary, non-extended, phenomenologically viable type of supersymmetric models are sometimes called $N = 1$ supersymmetry, with N referring to the numbers of distinct $Q, Q^\dagger$ generators.

5.1.1   Hierarchy problem and supersymmetry breaking

The single-particle states of a supersymmetric theory fall into irreducible representations of the superalgebra, called *supermultiplets*. Each supermultiplet contains both fermion and boson states, which are commonly known as *superpartners* of each other and are loosely related by relations (5.1). One should immediately point out that:

- Since the squared-mass operator $-P^2$ is an invariant of the superalgebra (it commutes with the operators Q, $Q^\dagger$, as well as with all spacetime operators), it follows immediately that particles inhabiting the same irreducible supermultiplet must have equal eigenvalues of $-P^2$, i.e. equal masses.

- Since operators Q, $Q^\dagger$ commute with all generators of internal (gauge) transformations, superpartners must belong to the same representation of the gauge group (meaning they must have same electric charge, weak isospin and color degrees of freedom).

- It can be also rigorously shown that each supermultiplet must contain an equal number of fermionic and bosonic degrees of freedom.

A far-reaching consequence of superpartners properties has made the fortune of supersymmetry in the past decades. As we have discussed in section 1.2, the Higgs squared mass receives quadratically divergent one-loop contributions, which are the essence of the hierarchy problem. Recalling Eqs. (1.5) and (1.7), for scalars and fermions such corrections take the form

$$\delta m_h^2\big|_{\text{scalar}} = \frac{\lambda_S}{16\pi^2}\Lambda^2 \ , \qquad\qquad \delta m_h^2\big|_{\text{fermion}} = -\frac{|\lambda_f|^2}{8\pi^2}\Lambda^2 \ , \qquad\qquad (5.3)$$

where λ_S, λ_f are the couplings of the Higgs with the particle circulating in the loop. If, as supersymmetry implies, there are two (real) scalar superpartners for each (Weyl) fermion, we would have $\sum \delta m_h^2 = 0$ as soon as

$$\lambda_S = |\lambda_f|^2 \ , \tag{5.4}$$

a condition which is in fact imposed by supersymmetry. In other words, the tightly constrained structure of supersymmetric theories forces the quadratically divergent Higgs squared mass corrections to vanish [91]: supersymmetry seems therefore to furnish a clear-cut solution to the hierarchy problem.

There is an easier way to justify the Higgs mass stability in supersymmetric theories. Owing to supersymmetry, the Higgs boson should have a fermionic superpartner (called Higgsino) which must have the same mass as the ordinary Higgs (for exact supersymmetry). However, the Higgsino mass is protected by the well-known chiral symmetry of fermions, therefore the hierarchy problem is solved without further requirements but supersymmetry itself. In other words supersymmetry, relating each scalar mass to a fermion mass, bounds the former through the UV-safe behaviour of the latter.

At this point we are forced to stress an aspect of supersymmetric theories which has been already excessively delayed. Indeed, it seems overwhelmingly clear that none of the Standard Model particles have superpartners of exactly the same mass (and quantum numbers), i.e. we do not observe in nature bosonic states with mass equal to any Standard Model fermion or vice versa. It is therefore an unavoidable conclusion that supersymmetry must be a broken symmetry in the vacuum state chosen by nature.

An important clue as to the nature of supersymmetry breaking can be obtained by returning to the motivation provided by the hierarchy problem. We have seen that supersymmetry forces us to introduce bosonic superpartners for each Standard Model fermion, which is just what is needed to enable a cancellation of the quadratically sensitive (Λ^2) loop corrections to the Higgs squared mass. This sort of cancellation also requires that the associated dimensionless couplings should be related (see Eq. (5.4)), as indeed occurs in unbroken supersymmetry[1]. Now, if broken supersymmetry is still to provide a solution to the hierarchy problem, then the relationships between dimensionless couplings that hold in an unbroken supersymmetric theory must be maintained. Otherwise, there would be quadratically divergent loop corrections to the Higgs scalar mass of the form

$$\delta m_h^2 = \frac{1}{8\pi^2} \left(\lambda_S - |\lambda_f|^2 \right) \Lambda^2 \ . \tag{5.5}$$

We are therefore led to consider "soft" supersymmetry breaking [92]. This means that the effective broken-supersymmetry Lagrangian can be written in the form

$$\mathcal{L} = \mathcal{L}_{\text{SUSY}} + \mathcal{L}_{\text{soft}} \ , \tag{5.6}$$

---

[1]In fact, unbroken supersymmetry guarantees that quadratic divergences in scalar squared masses must vanish to all orders in perturbation theory. This can be seen as a consequence of the degeneracy of scalar and fermion masses, as discussed above.

where $\mathcal{L}_{\text{SUSY}}$ preserves supersymmetry invariance, while $\mathcal{L}_{\text{soft}}$ violates it but contains only mass terms and coupling parameters with positive mass dimension.

Without further justification, soft supersymmetry breaking might seem a rather arbitrary condition. Fortunately, theoretical models for supersymmetry breaking do indeed yield effective Lagrangians satisfying the above requirements. If the largest mass scale associated with the soft terms is denoted m_{soft}, then the additional non-supersymmetric corrections to the Higgs scalar squared mass must vanish in the $m_{\text{soft}} \to 0$ limit, so by dimensional analysis they cannot be proportional to Λ^2. The corrections also cannot go like $\delta m_h^2 \sim m_{\text{soft}}\Lambda$, because in general loop momentum integrals cannot diverge linearly. So they must be of the form

$$\delta m_H^2 = m_{\text{soft}}^2 \left[\frac{\lambda}{16\pi^2} \ln(\Lambda/m_{\text{soft}}) + \ldots \right] \, . \tag{5.7}$$

Here λ is schematic for various dimensionless couplings, and dots stand both for finite terms and for higher loop corrections (which depend on Λ through powers of logarithms).

As it is clear from Eq. (5.7), is now the soft supersymmetry breaking scale m_{soft} that governs the quadratic divergences in loop corrections to Higgs mass. A possible line of thought, highly exploited in past decades, is to conclude that m_{soft} itself should be not much above the electroweak scale, in order to provide a neat solution to the hierarchy problem without excessive fine tuning. However, since m_{soft} determines also the mass splitting between know Standard Model particles and their superpartners, the problematic drawback of such reasoning is that superpartners masses cannot be too huge. In particular, the absence so far of any positive result from collider searches of superpartners [41] poses major challenges to the popular assumption that supersymmetry is broken not too far above the electroweak scale.

Instead of dealing with those intrinsic difficulties of "low-scale" supersymmetry, a different perspective can be adopted. Indeed, one can renounce the ambition to solve the hierarchy problem, which as a matter of fact was not among the original motivations of supersymmetric theories, focusing instead on other successful aspects of those theories, for example gauge coupling unification [93–96]. Under these premises, m_{soft} can be pushed as high as 10^6 GeV (or even higher, depending on which requirements are relaxed) [26], neutralising the tensions with collider searches and opening wide scenarios for viable and still successful supersymmetric theories.

We will come back to the above phenomenological issues in chapter 6. For the remaining of the present chapter, we will limit ourselves to a formal discussion of supersymmetric theories and no assumption on the m_{soft} scale will be needed whatsoever. In particular, we now move to a quantitative discussion of supersymmetric Lagrangians.

5.1.2 Supersymmetric Lagrangians

As already explained, particles of supersymmetric theories are grouped into supermultiplets, i.e. representations of the supersymmetric algebra. For the case of $N = 1$ renormalisable supersymmetric theories (without gravity), each superalgebra representation can be reduced to a combination of two irreducible supermultiplet's classes:

- *Chiral* (or *matter*) supermultiplet. It consists of a single spin-1/2 Weyl fermion and one complex scalar (both have two degrees of freedom on shell).

- *Vector* (or *gauge*) supermultiplet. It consists of a massless spin-1 boson (which should be a gauge boson for renormalisability) and a massless spin-1/2 Weyl fermion (called *gaugino*). They both have two degrees of freedom on shell.

An important observation is that a gaugino should transform as the adjoint representation of the gauge group (as its superpartner does). Since the adjoint representation is always real, the two gaugino helicities always have the same gauge transformation. In a spontaneously broken gauge theory, where gauginos acquire mass, the above property tells us that left- and right-handed gauginos' components should still have the same gauge transformation. Therefore, only chiral supermultiplets can account for chiral fermions whose left- and right-handed components have different quantum numbers (as in the Standard Model). It will be important to keep this in mind when building viable phenomenological supersymmetric models in the next section.

We now turn to the description of supersymmetric Lagrangians for chiral and vector supermultiplets. We will just state here without justification the main results which will be needed for our purpose, which is the introduction of the Minimal Supersymmetric Standard Model (MSSM) in the next section. In particular, no space will be given to the definition of supersymmetric transformations, nor to the explicit proof that those Lagrangians are actually supersymmetric. An extended and pedagogic discussion of those issues can be found e.g. in Ref. [97], which we refer to for all results stated in this section.

We start from the simplest example of supersymmetric Lagrangian. It involves a single chiral supermultiplet, whose scalar and fermion components will be called ϕ and ψ, respectively. The simplest Lagrangian involving just the two kinetic energy terms for ϕ and ψ,

$$\mathcal{L}_{\text{free}} = -\partial^\mu \phi^* \, \partial_\mu \phi + i \, \psi^\dagger \bar{\sigma}^\mu \partial_\mu \psi \; , \tag{5.8}$$

can be shown to be supersymmetric[2]. This is called the massless, non-interacting Wess–Zumino model [98, 99]. In Eq. (5.8) we have $\bar{\sigma}^\mu = (\mathbb{1}, -\sigma^i)$, where σ^i are the Pauli matrices.

The next step is to extend the discussion to many chiral supermultiplets and investigate the most general possible theory of masses and non-gauge interactions for those particles. The result can be proven to be the following:

$$\mathcal{L} = -\partial^\mu \phi^{*i} \partial_\mu \phi_i + i\psi^{\dagger i} \bar{\sigma}^\mu \partial_\mu \psi_i - \frac{1}{2} \left(W^{ij} \psi_i \psi_j + W^*_{ij} \psi^{\dagger i} \psi^{\dagger j} \right) - W^i W^*_i \; , \tag{5.9}$$

where indices i, j label the different chiral supermultiplets and a sum over those indices is understood. Interaction terms in Eq. (5.9) are encoded in W^{ij} and W^i, which are defined as

$$W^i = \frac{\delta W}{\delta \phi_i} \; , \qquad W^{ij} = \frac{\delta^2 W}{\delta \phi_i \delta \phi_j} \; , \tag{5.10}$$

---

[2]The issue of the auxiliary field F, needed to preserve supersymmetry off shell, will not be discussed here.

where W, called *superpotential*, is a polynomial in the scalar fields ϕ_i of third degree and mass dimension 3. Its general form reads:

$$W = L^i \phi_i + \frac{1}{2} M^{ij} \phi_i \phi_j + \frac{1}{6} y^{ijk} \phi_i \phi_j \phi_k \ , \tag{5.11}$$

where the L^i parameters are only allowed when ϕ_i is a gauge singlet. Since we will not be interested in such possibility, we will drop from now on the linear term in Eq. (5.11). Plugging Eqs. (5.10), (5.11) into Eq. (5.9), we find:

$$\mathcal{L}_{\text{chiral}} = -\partial^\mu \phi^{*i} \partial_\mu \phi_i + i\psi^{\dagger i} \bar{\sigma}^\mu \partial_\mu \psi_i - \frac{1}{2} \left(M^{ij} \psi_i \psi_j + y^{ijk} \phi_i \psi_i \psi_j + \text{h.c.} \right) - V(\phi, \phi^*) \ ,$$

$$V(\phi, \phi^*) = \frac{1}{2} M_{ik}^* M^{kj} \phi^{*i} \phi_j + \frac{1}{2} M^{in} y_{jkn}^* \phi_i \phi^{*j} \phi^{*k} + \frac{1}{8} y^{ijn} y_{kln}^* \phi_i \phi_j \phi^{*k} \phi^{*l} + \text{h.c.} \ .$$

$$\tag{5.12}$$

from Lagrangian (5.12), one can appreciate that the scalar potential $V(\phi, \phi^*)$ is automatically bounded from below and non-negative. Furthermore, it can be easily verified that fermions and scalars have the same squared-mass matrix with real non-negative eigenvalues, namely $(M^2)_i^j = M_{ik}^* M^{kj}$. This is in accordance with the imperative requirement of complex scalar and Weyl fermions to be coupled in mass-degenerate supermultiplets.

Together with the mass terms for fermions and scalars, Lagrangian (5.12) displays Yukawa interactions between fermions and scalars as well as trilinear and quadrilinear interactions among scalars, all governed by the M^{ij} and y^{ijk} parameters. We will see that, when gauge symmetry is introduced, strong bounds arises for the possible non-zero elements of the M^{ij} and y^{ijk} tensors.

We should now introduce vector supermultiplets in our discussion. Calling $F_{\mu\nu}^a$ the usual Yang–Mills filed strength tensor for gauge bosons and λ^a the gauginos (where a is the index of the adjoint representation of the gauge group), the vector Lagrangian is

$$\mathcal{L}_{\text{gauge}} = -\frac{1}{4} F_{\mu\nu}^a F^{\mu\nu a} + i\lambda^{\dagger a} \bar{\sigma}^\mu \nabla_\mu \lambda^a \ , \tag{5.13}$$

where the covariant derivative for the gaugino field reads

$$\nabla_\mu \lambda^a = \partial_\mu \lambda^a - g f^{abc} A_\mu^b \lambda^c \ . \tag{5.14}$$

Lagrangian (5.13) is easy to digest. Together with the familiar piece involving the field strength tensor $F_{\mu\nu}^a$, it only features the kinetic term for the gaugino field λ^a, with the only substitution of the ordinary derivative ∂^μ with a suitably defined covariant derivative ∇^μ. We can straightforwardly define such covariant derivative also for chiral supermultiplets,

$$\nabla_\mu \phi_i = \partial_\mu \phi_i - igA_\mu^a (T^a \phi)_i \ ,$$
$$\nabla_\mu \phi^{*i} = \partial_\mu \phi^{*i} + igA_\mu^a (\phi^* T^a)^i \ ,$$
$$\nabla_\mu \psi_i = \partial_\mu \psi_i - igA_\mu^a (T^a \psi)_i \ . \tag{5.15}$$

One would be tempted to conclude that the full supersymmetric Lagrangian involving both chiral and vector supermultiplets could be obtained summing $\mathcal{L}_{\text{chiral}}$ of Eq. (5.12) and $\mathcal{L}_{\text{gauge}}$ of Eq. (5.13), with the substitution in the former of ordinary derivatives with the covariant derivatives defined in Eqs. (5.15). Though appealing, this would not be completely correct and it turns out that additional terms are required in order to preserve supersymmetry invariance. Once taken such extra pieces into account, the full supersymmetric Lagrangian becomes

$$\mathcal{L} = \mathcal{L}_{\text{gauge}} + \mathcal{L}_{\text{chiral}}|_{\partial \to \nabla} - \sqrt{2} \, g_a \left((\phi^* T^a \psi) \lambda^a + \text{h.c.} \right) - \frac{1}{2} \sum_a g_a^2 (\phi^* T^a \phi)^2 \, , \quad (5.16)$$

where g_a are the gauge couplings of the distinct simple subgroups of the complete gauge group (for instance, the Standard Model gauge group $SU(3)_C \times SU(2)_L \times U(1)_Y$) has three different gauge couplings g_s, g and g').

Few comments are in order:

- The additional terms in Lagrangian (5.16) consist of interactions whose strength is fixed by the requirements of supersymmetry to be proportional to gauge couplings, even though they are not gauge interactions from the point of view of ordinary gauge field theories. The scalar-fermion-gaugino terms can be thought of as the "supersymmetrisation" of the usual gauge boson couplings to matter fields. The second term contributes instead to the scalar potential.

- The complete scalar potential now reads

$$V(\phi, \phi^*) = M_{ik}^* M^{kj} \phi^{*i} \phi_j + \left(\frac{1}{2} M^{in} y_{jkn}^* \phi_i \phi^{*j} \phi^{*k} + \text{h.c.} \right)$$
$$+ \frac{1}{4} y^{ijn} y_{kln}^* \phi_i \phi_j \phi^{*k} \phi^{*l} + \frac{1}{2} \sum_a g_a^2 (\phi^* T^a \phi)^2 \, . \quad (5.17)$$

It is an interesting and unique feature of supersymmetric theories that the scalar potential is completely determined by the other interactions of the theory: fermion mass terms (M^{ij}), Yukawa couplings (y^{ijk}) and gauge couplings (g_a).

- In a given theory, only a subset of the parameters M^{ij}, y^{ijk} are allowed to be non-zero. The mass matrix entries M^{ij} can only be non-vanishing for i and j such that ϕ_i and ϕ_j belongs to gauge group representations which are conjugate of each other. Likewise, the Yukawa couplings y^{ijk} can be non-zero only if ϕ_i, ϕ_j and ϕ_k belong to representations that can be combined to form a singlet.

We are now left with the discussion of the last irreducible ingredient of every realistic phenomenological supersymmetric model, namely the soft supersymmetry breaking interactions. From a theoretical perspective, we expect that supersymmetry, if it exists at all, should be an exact symmetry that is broken spontaneously. Many models of spontaneous symmetry breaking have indeed been proposed, involving new particles and interactions at very high mass scales, but there is no consensus on exactly how this should be done.

Nevertheless, from a practical point of view, we can completely disregard any theoretical detail on how to achieve spontaneous supersymmetry breaking and simply

parametrise our ignorance introducing in the effective supersymmetric Lagrangian extra terms that break supersymmetry explicitly.

Recalling, as argued in section 5.1.1, that supersymmetry-breaking couplings should be soft, i.e. of positive mass dimension, such possible soft terms[3] in the Lagrangian of a general theory are

$$\mathcal{L}_{\text{soft}} = -\frac{1}{2}\left(M_a\,\lambda^a\lambda^a + \frac{1}{3}a^{ijk}\phi_i\phi_j\phi_k + b^{ij}\phi_i\phi_j + \text{h.c.}\right) - (m^2)^i_j\,\phi^{j*}\phi_i\ . \qquad (5.18)$$

They consist of gaugino masses M_a for each gauge group, scalar squared-mass terms $(m^2)^j_i$ and b^{ij} and trilinear scalar couplings a^{ijk}. It has been shown rigorously that a softly broken supersymmetric theory with $\mathcal{L}_{\text{soft}}$ as given by Eq. (5.18) is indeed free of quadratic divergences in quantum corrections to scalar masses, to all orders in perturbation theory [104].

The terms in $\mathcal{L}_{\text{soft}}$ clearly do break supersymmetry, because they involve only scalars and gauginos and not their respective superpartners. In fact, the soft terms in $\mathcal{L}_{\text{soft}}$ are capable of giving masses to all of the scalars and gauginos in a theory, even if the gauge bosons and fermions in chiral supermultiplets are massless (or relatively light). Gaugino masses M_a are always allowed by gauge symmetry. The $(m^2)^i_j$ terms are allowed for i, j such that ϕ_i, ϕ^{j*} transform in complex conjugate representations of each other under all gauge symmetries; in particular this is true of course when $i = j$, so every scalar is eligible to get a mass in this way if supersymmetry is broken. The remaining soft terms may or may not be allowed by symmetries. The a^{ijk} and b^{ij} terms have the same form as the y^{ijk} and M^{ij} terms in the superpotential (5.11), so they will each be allowed by gauge invariance if and only if a corresponding superpotential term is allowed.

5.2 Minimal Supersymmetric Standard Model

Once discussed the general features of supersymmetric theories and Lagrangians, we turn now our attention to viable phenomenological supersymmetric models.

Clearly, the irreducible requirement for a realistic supersymmetric model [105,106] is to embrace all Standard Model particles. A crucial observation, already outlined above, is that only chiral supermultiplets can contain fermions whose left- and right-handed components have different quantum numbers under the gauge group. Therefore, all Standard Model fermions must be member of chiral supermultiplets. Each chiral Standard Model fermion thus has its complex scalar superpartner, whose name is constructed by prepending an 's' to the fermion's name (e.g. "selectron" and "stau" are the scalar superpartners of electron and tau, respectively, and both are of course "sleptons"). In addition, Standard Model vector bosons must clearly reside in vector supermultiplets, therefore they have fermionic superpartners called "winos", "bino", "zino" and "gluino" (superpartners of the Ws, Z, B and g bosons, respectively).

The Higgs sector deserves a separate discussion. It might be tempting to just advocate one extra chiral supermultiplet, the Higgs being the scalar component and

---

[3]More exotic terms as "tadpole" scalar interactions, non-holomorphic trilinear scalar interactions and fermion-gaugino mass mixing [100–103] are of no concern for the subsequent discussion and are therefore omitted.

Names	spin 0	spin 1/2	$SU(3)_C,\ SU(2)_L,\ U(1)_Y$
(s)quarks	$\tilde{Q} = (\tilde{u}_L\ \tilde{d}_L)$	$Q = (u_L\ d_L)$	$\left(\mathbf{3},\ \mathbf{2},\ \frac{1}{6}\right)$
	$\tilde{u}_R$	u_R	$\left(\mathbf{3},\ \mathbf{1},\ \frac{2}{3}\right)$
	$\tilde{d}_R$	d_R	$\left(\mathbf{3},\ \mathbf{1},\ -\frac{1}{3}\right)$
(s)leptons	$\tilde{L} = (\tilde{\nu}_L\ \tilde{e}_L)$	$L = (\nu_L\ e_L)$	$\left(\mathbf{1},\ \mathbf{2},\ -\frac{1}{2}\right)$
	$\tilde{e}_R$	e_R	$(\mathbf{1},\ \mathbf{1},\ 1)$
Higgs(inos)	$H_u = (H_u^+\ H_u^0)$	$\tilde{H}_u = (\tilde{H}_u^+\ \tilde{H}_u^0)$	$\left(\mathbf{1},\ \mathbf{2},\ \frac{1}{2}\right)$
	$H_d = (H_d^0\ H_d^-)$	$\tilde{H}_d = (\tilde{H}_d^0\ \tilde{H}_d^-)$	$\left(\mathbf{1},\ \mathbf{2},\ -\frac{1}{2}\right)$

Table 5.1: Chiral supermultiplets in the Minimal Supersymmetric Standard Model. There are three replicas (flavours) for each (s)fermion supermultiplet. The spin-0 fields are all complex scalars while spin-1/2 are all Weyl fermions.

Names	spin 1/2	spin 1	$SU(3)_C,\ SU(2)_L,\ U(1)_Y$
gluino, gluon	$\tilde{g}$	g	$(\mathbf{8},\ \mathbf{1},\ 0)$
winos, W	$\tilde{W}^\pm\ \tilde{W}^0$	$W^\pm\ W^0$	$(\mathbf{1},\ \mathbf{3},\ 0)$
bino, B	$\tilde{B}^0$	B^0	$(\mathbf{1},\ \mathbf{1},\ 0)$

Table 5.2: Vector supermultiplets in the Minimal Supersymmetric Standard Model.

the "Higgsino" its spin-1/2 superpartner. As a matter of fact, it can be easily shown (analysing the quantum numbers of the theory) that just one Higgs doublet cannot reproduce all Higgs Yukawa couplings of the Standard Model through an holomorphic superpotential W. Furthermore, such a single-Higgs supersymmetric theory can be proven to feature electroweak gauge anomalies. Therefore, at least two distinct Higgs chiral supermultiplets are needed to successfully reproduce the Standard Model Higgs sector. This means that there will be two different scalar Higgs doublets, together with their fermionic superpartners.

Tables 5.1, 5.2 summarise the particle content outlined above. These chiral and vector supermultiplets are the minimal ensemble needed to enclose the Standard Model within a supersymmetric theory and, for this reason, the model with such particle content is called Minimal Supersymmetric Standard Model (MSSM). In the remaining of this section, we will review the key features of the MSSM needed for the phenomenological discussion of chapter 6, starting from the MSSM Lagrangian. We refer the reader to the literature (see e.g. [97]) for more thorough reviews.

5.2.1 MSSM Lagrangian

From the general (though synthetic) review of section 5.1.2 we already know the generic structure of supersymmetric Lagrangians. Therefore, once owing the particle content of the MSSM (Tables 5.1 and 5.2) it is straightforward to construct its Lagrangian.

The supersymmetric-conserving piece of $\mathcal{L}_{\mathrm{MSSM}}$ can be read from Eq. (5.16) once specified the superpotential (see Eq. (5.11)) for the MSSM. It is easy to show that its most generic form is

$$W_{\mathrm{MSSM}} = \mu\,\tilde{H}_u\tilde{H}_d + \tilde{u}_R^* \, Y_u\, \tilde{Q}\tilde{H}_u - \tilde{d}_R^* \, Y_d\, \tilde{Q}\tilde{H}_d - \tilde{e}_R^* \, Y_e\, \tilde{L}\tilde{H}_d\ . \tag{5.19}$$

The four terms in W_{MSSM} are the only mass and Yukawa terms (i.e. non-vanishing M^{ij} and y^{ijk} coefficients) allowed by gauge symmetry, according to the quantum numbers of MSSM's supermultiplets (see section 5.1.2, in particular the discussion after Eq. (5.16)).

The first term in Eq. (5.19), $\mu\,\tilde{H}_u\tilde{H}_d$, is traditionally called "μ term". It is the supersymmetric version of the Higgs boson mass in the Standard Model. From the explicit expression for the scalar potential, Eq. (5.17), we can see that the μ term provides for Higgsino mass terms

$$\mathcal{L}_{\mathrm{Higgsino\ mass}} = -\mu\,(\tilde{H}_u^+ \tilde{H}_d^- - \tilde{H}_u^0 \tilde{H}_d^0) + \mathrm{h.c.}\ , \tag{5.20}$$

as well as Higgs squared-mass terms

$$\mathcal{L}_{\mathrm{supersymmetric\ Higgs\ mass}} = -|\mu|^2 \left(|H_u^0|^2 + |H_u^+|^2 + |H_d^0|^2 + |H_d^-|^2\right)\ . \tag{5.21}$$

Since Eq. (5.21) is non-negative with a minimum at $H_u^0 = H_d^0 = 0$, we cannot understand electroweak symmetry breaking before including supersymmetry-breaking terms for the Higgs scalars. This will be done later in this section.

The other three terms in Eq. (5.19) are the Yukawa couplings needed to phenomenologically reproduce the Standard Model. Given the impossibility of adding pieces proportional to $H_{u,d}^*$ due to supersymmetry requirements, it is now clear why two separate Higgs doublets with different quantum numbers are needed even in the most minimal supersymmetrisation of the Standard Model. Y_u, Y_d, Y_e are 3×3 matrices in flavour space, the supersymmetry version of the Standard Model Yukawa matrices; it is customary to assume their entries negligible but for their $(3,3)$ flavour component, matching the top, bottom and tau Yukawa couplings, respectively:

$$Y_u = \begin{pmatrix} 0 & 0 & 0 \\ 0 & 0 & 0 \\ 0 & 0 & y_t \end{pmatrix}\ , \quad Y_d = \begin{pmatrix} 0 & 0 & 0 \\ 0 & 0 & 0 \\ 0 & 0 & y_b \end{pmatrix}\ , \quad Y_e = \begin{pmatrix} 0 & 0 & 0 \\ 0 & 0 & 0 \\ 0 & 0 & y_\tau \end{pmatrix}\ . \tag{5.22}$$

Supersymmetric Lagrangian (5.16) and superpotential (5.19) are all is needed to define the supersymmetric part of MSSM Lagrangian. Remarkably, even if the particle content of the theory is more than doubled with respect to the Standard Model, we are actually left with less parameters than the Standard Model itself: gauge and Yukawa parameters are the same, we have traded the Higgs v.e.v. for μ and there is no room left for free parameters in the scalar potential (as λ). Of course, such a counting is misleading since, as observed, such supersymmetric Lagrangian is not even able to account for electroweak symmetry breakdown.

It is therefore advisable to introduce the soft supersymmetry-breaking Lagrangian of the MSSM before going any further in the discussion. Referring to the general form of $\mathcal{L}_{\mathrm{soft}}$, Eq. (5.18), it can be seen that the most generic one for the MSSM reads

$$\mathcal{L}_{\mathrm{soft}}^{\mathrm{MSSM}} = -\frac{1}{2}\left(M_1\tilde{B}\tilde{B} + M_2\tilde{W}\tilde{W} + M_3\tilde{g}\tilde{g} + \mathrm{h.c.}\right)$$

$$-\left(\tilde{u}_R^* A_u \tilde{Q} H_u - \tilde{d}_R^* A_d \tilde{Q} H_d - \tilde{e}_R^* A_e \tilde{L} H_d + \text{h.c.}\right)$$
$$-\tilde{Q}^\dagger M_{\tilde{Q}}^2 \tilde{Q} - \tilde{L}^\dagger M_{\tilde{L}}^2 \tilde{L} - \tilde{u}_R^* M_{\tilde{u}}^2 \tilde{u}_R - \tilde{d}_R^* M_{\tilde{d}}^2 \tilde{d}_R - \tilde{e}_R^* M_{\tilde{e}}^2 \tilde{e}_R$$
$$-m_{H_u}^2 H_u^* H_u - m_{H_d}^2 H_d^* H_d - (b\,H_u H_d + \text{h.c.}) \ . \tag{5.23}$$

This is the most general soft supersymmetry-breaking Lagrangian of the form (5.18) that is compatible with gauge invariance and matter parity conservation in the MSSM.

In the first line of Eq. (5.23), where gauge indices of gauginos have been suppressed, M_1, M_2 and M_3 are bino, wino and gluino mass terms, respectively. The second line contains the trilinear scalar couplings of the type a^{ijk} in Eq. (5.18), where A_u, A_d and A_e are all complex 3×3 matrices in flavour space with mass dimension 1. These terms resembles the ones in superpotential (5.19) since, as discussed in section 5.1.2, both terms shall exist under the same requirements. The third line consists of squark and slepton masses of the $(m^2)_i^j$ type in Eq. (5.18), where $M_{\tilde{Q}}^2$, $M_{\tilde{L}}^2$, $M_{\tilde{u}}^2$, $M_{\tilde{d}}^2$ and $M_{\tilde{e}}^2$ are all 3×3 hermitian matrices in flavour space with mass dimension 2. Finally, in the last line we have supersymmetry-breaking contributions to the Higgs potential: $m_{H_u}^2$ and $m_{H_d}^2$ are squared-mass terms of the $(m^2)_i^j$ type, while b is the only squared-mass term of the type b^{ij} inEq. (5.18) that can occur in the MSSM[4] (for the same reason why the μ term is the only supersymmetric mass term in the superpotential). As argued in section 5.1.1, we expect

$$M_1, M_2, M_3, A_u, A_d, A_e \sim m_{\text{soft}} \ ,$$
$$M_{\tilde{Q}}^2, M_{\tilde{L}}^2, M_{\tilde{u}}^2, M_{\tilde{d}}^2, M_{\tilde{e}}^2, m_{H_u}^2, m_{H_d}^2, b \sim m_{\text{soft}}^2 \ . \tag{5.24}$$

Unlike the supersymmetry-preserving part of the Lagrangian, the above $\mathcal{L}_{\text{soft}}^{\text{MSSM}}$ introduces many new parameters that were not present in the ordinary Standard Model. A careful count [107] reveals that there are 105 physical masses, phases and mixing angles in the MSSM Lagrangian that have no counterpart in the ordinary Standard Model. Thus, in principle, supersymmetry breaking (as opposed to supersymmetry itself) appears to introduce a tremendous arbitrariness in the Lagrangian.

5.2.2 Electroweak symmetry breaking

In the MSSM, the description of electroweak symmetry breaking is slightly complicated by the fact that there are two complex Higgs doublets $H_u = (H_u^+, H_u^0)$ and $H_d = (H_d^0, H_d^-)$ rather than just one as in the ordinary Standard Model. The classical scalar potential for the Higgs scalar fields in the MSSM is given by

$$V = (|\mu|^2 + m_{H_u}^2)(|H_u^0|^2 + |H_u^+|^2) + (|\mu|^2 + m_{H_d}^2)(|H_d^0|^2 + |H_d^-|^2)$$
$$+ [b(H_u^+ H_d^- - H_u^0 H_d^0) + \text{h.c.}]$$
$$+ \frac{1}{8}(g^2 + g'^2)(|H_u^0|^2 + |H_u^+|^2 - |H_d^0|^2 - |H_d^-|^2)^2 + \frac{1}{2}g^2|H_u^+ H_d^{0*} + H_u^0 H_d^{-*}|^2 \ . \tag{5.25}$$

---

[4]It is worth mentioning that b can be taken real and positive without loss of generality.

The terms proportional to $|\mu|^2$ come from Eq. (5.21). The terms proportional to g^2 and g'^2 come from the last term of supersymmetric Lagrangian (5.16). Finally, terms proportional to $m_{H_{u,d}}^2$, b come from the last line of Eq. (5.23).

We now want to investigate classical field configurations looking for the minimum of potential (5.25). First, one can see that, exploiting gauge invariance, it is possible to set

$$\langle H_u^+ \rangle = \langle H_d^- \rangle = 0 \tag{5.26}$$

and $\langle H_u^0 \rangle, \langle H_d^0 \rangle$, b real without loss of generality. This, among all, ensures the electromagnetic vacuum to be unbroken and CP to be preserved after electroweak symmetry breakdown. Exploiting Eq. (5.26), the scalar potential becomes

$$V = (|\mu|^2 + m_{H_u}^2)|H_u^0|^2 + (|\mu|^2 + m_{H_d}^2)|H_d^0|^2 - 2\,b\,H_u^0 H_d^0$$
$$+ \frac{1}{8}(g^2 + g'^2)(|H_u^0|^2 - |H_d^0|^2)^2 \ . \tag{5.27}$$

In order for scalar potential (5.27) to be viable, we must first make sure that such potential is bounded from below. In fact, the second line in Eq. (5.27) is a positive quartic interaction which stabilises the potential in all directions but the flat one, $\langle H_u^0 \rangle = \langle H_d^0 \rangle$. Along such flat direction, we must require the quadratic coupling to be positive, so that a first important requirement is

$$2|\mu|^2 + m_{H_u}^2 + m_{H_d}^2 > 2b \ . \tag{5.28}$$

Once assured the scalar potential to have a minimum for finite values of $H_{u,d}^0$, we should further require such minimum to break the electroweak symmetry. In other words, we should avoid the field configuration $\langle H_u^0 \rangle = \langle H_d^0 \rangle = 0$ to be a minimum of the theory. It is rather easy to prove that such requirement is fulfilled if and only if

$$(|\mu|^2 + m_{H_u}^2)(|\mu|^2 + m_{H_d}^2) < b^2 \ . \tag{5.29}$$

Condition (5.29) will play an important role in the analysis of chapter 6. For the time being, let us stress that this condition is needed for the scalar potential to realistically reproduce the spontaneous symmetry breakdown that the electroweak gauge group undergoes at the electroweak scale. In other words, Eq. (5.29) must be interpreted as a condition for the running parameters μ, b and $m_{H_{u,d}}^2$, to be required specifically at the electroweak scale.

A consequence of the above caveat is that, even in the case Eq. (5.29) is satisfied and the electroweak symmetry is spontaneously broken at low scales, the situation at m_{soft} or higher scales might be radically different. Namely, it is not difficult to design models where Eq. (5.29) is not satisfied at m_{soft} but then, through running effects, it is fulfilled at lower scales. In these models, electroweak symmetry breakdown is actually triggered by quantum corrections: this mechanism is therefore known as *Radiative Electroweak Symmetry Breakdown* (REWSB) [108, 109]. This is a very interesting possibility and great attention will be given to it in the next chapter.

Having established the conditions necessary for $\langle H_u^0 \rangle$ and $\langle H_d^0 \rangle$ to break the electroweak vacuum, we can now require that they are compatible with the observed phenomenology of electroweak symmetry breaking. Let us write

$$v_u = \langle H_u^0 \rangle \ , \qquad\qquad v_d = \langle H_d^0 \rangle \ . \tag{5.30}$$

These vacuum expectation values are related to the known mass of the Z^0 boson and the electroweak gauge couplings:

$$v_u^2 + v_d^2 = v^2 = \frac{2m_Z^2}{g^2 + g'^2} \approx (174 \, \text{GeV})^2 \ . \tag{5.31}$$

The $v_{u,d}$ ratio is traditionally written as

$$\tan\beta \equiv \frac{v_u}{v_d} \ . \tag{5.32}$$

The value of $\tan\beta$ is not fixed by present experiments, but it depends on the Lagrangian parameters of the MSSM in a calculable way. Since $v_u = v\sin\beta$ and $v_d = v\cos\beta$ were taken to be real and positive by convention, we have $0 < \beta < \pi/2$. Actually, it can be done much better than that and $\tan\beta \gtrsim 1.1$ can be shown to be a necessary requirement to avoid Landau poles in the running value of $y_t(Q)$.

Now we can write down the conditions under which the potential (5.27) has a minimum satisfying Eqs. (5.31) and (5.32):

$$\begin{cases} m_{H_u}^2 + |\mu|^2 - b\cot\beta - \frac{1}{2}\,m_Z^2\cos(2\beta) = 0 \\ m_{H_d}^2 + |\mu|^2 - b\tan\beta + \frac{1}{2}\,m_Z^2\cos(2\beta) = 0 \end{cases} \ . \tag{5.33}$$

It is easy to check that these equations also satisfy the necessary conditions (5.28), (5.29).

Once understood the vacuum of the theory, one can go back to the scalar potential (5.25) to work out the mass eigenstates after electroweak symmetry breakdown. Referring to the literature for a detailed analysis, let us just account here for the important results. In the unbroken phase, H_u and H_d doublets have a total of 8 degrees of freedom (two complex scalars each). Once the electroweak symmetry is spontaneously broken, 3 degrees of freedom are "eaten" to give mass to W and Z bosons and we are left with 5 real scalars: 2 CP-even neutrals (the old-fashioned Higgs, h, and a more massive H^0), 1 CP-odd neutral (A^0) and two charged Higgses ($H^\pm$). At tree level, their masses reads:

$$m_{A^0}^2 = 2|\mu|^2 + m_{H_u}^2 + m_{H_d}^2 \ , \tag{5.34}$$

$$m_{h,H^0}^2 = \frac{1}{2}\left(m_{A^0}^2 + m_Z^2 \mp \sqrt{(m_{A^0}^2 - m_Z^2)^2 + 4m_Z^2 m_{A^0}^2 \sin^2(2\beta)}\right) \ , \tag{5.35}$$

$$m_{H^\pm}^2 = m_{A^0}^2 + m_W^2 \ . \tag{5.36}$$

In principle, the masses of A^0, H^0 and $H^\pm$ can be arbitrarily large. In contrast, the mass of h is bounded from above. From Eq. (5.35), one finds at tree-level [110, 111]:

$$m_h < m_Z|\cos(2\beta)| \ . \tag{5.37}$$

Tree level bound (5.37) is spectacularly wrong. However, such formula is subjected to quantum corrections that are relatively drastic, the largest contributions typically coming from top quark and stop squark loops. As a matter of fact, such quantum

corrections are able to account for the tree-level defiance of Eq. (5.37) and for the experimentally measured Higgs mass of 125 GeV [24].

The most important information carried by Eq. (5.35) is actually that the Higgs mass itself can be in principle expressed as a function of the other parameters of the MSSM. Differently but equivalently said, conversely from the Standard Model the MSSM does not feature the quartic Higgs coupling λ as a free parameter of the scalar potential (as already observed in section 5.2.1); rather the opposite, λ is a prediction of the MSSM. One can therefore turn its attention to the matching condition of λ at the scale at which supersymmetry is broken, i.e. m_{soft}. At tree level, one finds:

$$\lambda(m_{\text{soft}}) = \frac{1}{4}\left[g^2(m_{\text{soft}}) + g'^2(m_{\text{soft}})\right]\cos^2 2\beta \ . \tag{5.38}$$

Once again, tree-level condition (5.38) receives sizeable loop corrections that must be taken into account in order to perform a meaningful phenomenological investigation. These will be discussed further in chapter 6, where the λ matching condition at m_{soft} will be a fundamental ingredient of our analysis.

5.2.3   Renormalisation group equations

Once analysed the features of MSSM at its low-energy frontier, we now turn our attention to the high energy behaviour of the most important MSSM parameters.

Renormalisation group (RG) equations are a fundamental tool to relate the physics at the electroweak scale with the values of MSSM parameters at higher scales, where supersymmetry holds and is eventually broken. A careful study of the high-energy running of MSSM parameters can indeed furnish interesting and important insights into supersymmetric theories. An example, sketched in section 5.2.2 and that will be further elaborated the next chapter, is REWSB, i.e. the fact that electroweak symmetry breakdown might be entirely triggered at low energy by running effects. Another celebrated example is the apparent unification of gauge couplings in the MSSM, as we will now discuss.

Let us adopt the canonical normalisation of gauge couplings according to grand unification theories,

$$g_1 = \sqrt{5/3}\, g' \ , \qquad g_2 = g \ , \qquad g_3 = g_s \ . \tag{5.39}$$

The one-loop RG equations for Standard Model and MSSM are

$$\frac{\mathrm{d}}{\mathrm{d}t}g_a = \frac{1}{16\pi^2}b_a g_a^3 \ , \quad (b_1, b_2, b_3) = \begin{cases} (41/10, -19/6, -7) & \text{Standard Model} \\ (33/5, 1, -3) & \text{MSSM} \end{cases} \tag{5.40}$$

where $t = \log(\mu/\mu_0)$ and μ is the RG scale. The MSSM coefficients are larger because of the extra positive contributions from MSSM particles. The quantities $\alpha_a = g_a^2/4\pi$ have the nice property that their reciprocals run linearly with RG scale at one-loop order:

$$\frac{\mathrm{d}}{\mathrm{d}t}\alpha_a^{-1} = -\frac{b_a}{2\pi} \ , \qquad (a = 1, 2, 3) \ . \tag{5.41}$$
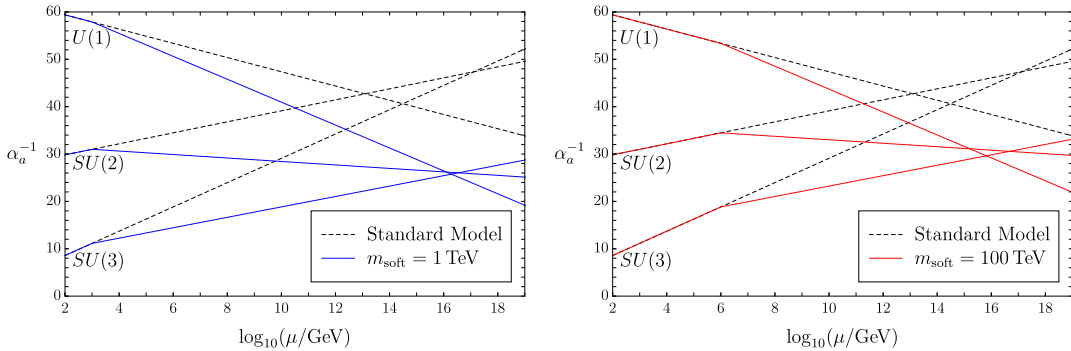
Figure 5.1: One-loop renormalisation group evolution of the inverse gauge couplings $\alpha_a^{-1}(\mu)$ in the Standard Model (dashed black lines) and in the MSSM for two different values of m_{soft}: 1 TeV (left plot, blue lines) and 100 TeV (right plot, red lines). In the MSSM, all sparticles masses are taken at the common threshold m_{soft}.

Figure 5.1 compares the RG evolution of the inverse of the gauge couplings, α_a^{-1}, in the Standard Model (dashed lines) and MSSM (solid lines) for two different values of m_{soft}. Unlike the Standard Model, the MSSM includes just the right particle content to ensure that the gauge couplings can unify [93–96], as predicted by grand unified theories (GUTs) [37,38], around a scale $m_G \sim 10^{16}$ GeV [36]. This unification is of course not perfect and there is a residual mismatch (at the percent level), which however can easily be ascribed to threshold corrections due to whatever new particles exist at the GUT scale. While such apparent unification might be just an accident, it may also be taken as a strong hint in favour of supersymmetry and grand unified theories.

Note that as m_{soft} raises, m_G decreases slightly and the merging of the gauge coupling is progressively ruined, as appreciable by comparison of left and right plot of Figure 5.1. It would be interesting to understand at which energy scale m_{soft} becomes too large to account for unification at all any more. Such question is clearly plagued by some subjectivity in the quantitative definition of satisfactory gauge coupling unification, since a certain amount of mismatch can be always accounted for advocating sufficiently large threshold corrections at m_G. Nevertheless, attempts to address this issue will be discussed further in the next chapter, see section 6.1.1.

If the hint furnished by RG analysis to gauge couplings are to be taken seriously, we can hope to extract other interesting features of supersymmetric theories if we push further our study of RG evolutions of MSSM parameters. This will be indeed the focus of chapter 6. Before moving to such investigation, although, we necessarily have to review the relevant one-loop RG equations of the MSSM parameters that will be used and the approximations under which such equations have been derived.

Having already discussed the RG equations for the gauge couplings $g_{1,2,3}$, we turn first our attention to the other supersymmetric parameters. A necessary RG equation is the one for the supersymmetric top Yukawa y_t, introduced in Eq. (5.22). It should be pointed out that y_t is related to the Standard Model top Yukawa g_t through the matching condition

$$g_t(m_{\mathrm{soft}}) = y_t(m_{\mathrm{soft}}) \sin\beta \ . \tag{5.42}$$

Such matching is clearly imposed at the scale m_{soft}, where the supersymmetric theory breaks into the ordinary Standard Model. The $\sin\beta$ factor comes from the fact that up-type quarks couple to H_u, whose v.e.v. obeys the relation $v_u = v\sin\beta$ (see Eq. (5.32) and discussion below).

The RG equation for y_t is

$$16\pi^2 \frac{\mathrm{d}}{\mathrm{d}t} y_t = y_t \left[6|y_t|^2 - \frac{13}{15}g_1^2 - 3g_2^2 - \frac{16}{3}g_3^2 \right] \ , \tag{5.43}$$

where additional contributions proportional to the other Yukawa couplings, in particular y_b and y_τ, have been omitted[5]. As a matter of fact, y_t will be the only relevant Yukawa coupling in our analysis and the only one that will be further considered for the rest of this section and for whole chapter 6.

The last supersymmetric parameter left is μ. It RG equation reads

$$16\pi^2 \frac{\mathrm{d}}{\mathrm{d}t} \mu = \mu \left(3y_t^2 - \frac{3}{5}g_1^2 - 3g_2^2 \right) \ . \tag{5.44}$$

One important property displayed both by Eqs. (5.43) and (5.44) is that the β-functions for each supersymmetric parameter are proportional to the parameter itself: this is actually a result of a very important theorem known as supersymmetric non-renormalisation theorem [112, 113].

Switching to supersymmetry-breaking parameters, the simplest RG equations to introduce next are the ones for the gaugino masses $M_{1,2,3}$, which read

$$16\pi^2 \frac{\mathrm{d}}{\mathrm{d}t} M_a = 2\, b_a g_a^2 M_a \ , \qquad (a = 1, 2, 3) \ , \tag{5.45}$$

with b_a given in Eq. (5.40). It follows that the three ratios M_a/g_a^2 are each constant (RG scale independent) up to small two-loop corrections. Since the gauge couplings are observed to unify at m_G, it is a popular assumption that gaugino masses also unify around that scale,

$$M_1(m_G) = M_2(m_G) = M_3(m_G) \ . \tag{5.46}$$

This is a common result for GUT models and we will rely on it in the next chapter. As a further assumption, $M_{1,2,3}$ will all be taken real-valued and positive.

Next we consider the holomorphic soft parameters A_u, A_d, A_e. A common simplifying assumption to deal with those complex matrices is to assume them proportional to the Yukawa couplings Y_u, Y_d and Y_e, respectively:

$$A_u \propto Y_u \ , \qquad A_d \propto Y_d \ , \qquad A_e \propto Y_e \ . \tag{5.47}$$

Such assumption can be traced back to the fact that Yukawa interactions in the superpotential, Eq. (5.19), and A terms in $\mathcal{L}_{\text{soft}}$, Eq. (5.23), have the same form and therefore they might have a common origin.

---

[5]This is justified only as long as $\tan\beta \ll m_t/m_b$, otherwise one would actually get $y_b \sim y_t$ and our approximation would be plainly wrong. Even though such large $\tan\beta$ models exist (see [97] and references therein), we will not consider them further in our discussion.

Given Eq. (5.22) and neglecting y_b and y_τ contributions, assumption (5.47) leaves us with

$$A_u = \begin{pmatrix} 0 & 0 & 0 \\ 0 & 0 & 0 \\ 0 & 0 & A_t\,y_t \end{pmatrix}, \qquad A_d \sim 0, \qquad A_e \sim 0, \qquad (5.48)$$

and the only parameter left to care about is A_t. Its RG equation reads

$$16\pi^2 \frac{\mathrm{d}}{\mathrm{d}t} A_t = 12\,A_t y_t^2 + \frac{26}{15}\,g_1^2 M_1 + 6\,g_2^2 M_2 + \frac{32}{3}\,g_3^2 M_3 . \qquad (5.49)$$

Differently from supersymmetric parameters, β-functions of soft parameters are not proportional to the parameter itself. So, even if A_t vanishes at the input scale, the RG corrections proportional to gaugino masses appearing in Eq. (5.49) ensure that it will not vanish at the electroweak scale. This is also the case for the b term, whose RG equation is

$$16\pi^2 \frac{\mathrm{d}}{\mathrm{d}t} b = b\left(3y_t^2 - \frac{3}{5}g_1^2 - 3g_2^2\right) + \mu\left(6A_t y_t^2 + \frac{6}{5}g_1^2 M_1 + 6g_2^2 M_2\right). \qquad (5.50)$$

The last RG equations still to be discuss are the one for the scalar squared masses of the MSSM, namely the Higgs scalar squared masses $m_{H_{u,d}}^2$ and the sfermion squared-mass matrices M_ζ^2. A common simplifying assumption for the latter is to assume them to be flavour blind at the input scale:

$$M_\zeta^2(m_G) = m_{\zeta 0}^2\,\mathbb{1}, \qquad \zeta = \{\tilde{Q}, \tilde{u}, \tilde{d}, \tilde{L}, \tilde{e}\}. \qquad (5.51)$$

Even assuming Eq. (5.51) to hold at m_G, third-generation squarks and sleptons receive extra contributions to their RG flow due to their large Yukawa couplings, determining at low energies a mass splitting between the first two and the third family of sfermions. Nevertheless, at least the flavour-diagonal form of M_ζ^2 can be assumed to hold at any scale up to negligible corrections.

Under assumption (5.51), the RG equations of $m_{H_{u,d}}^2$ read

$$16\pi^2 \frac{\mathrm{d}}{\mathrm{d}t} m_{H_u}^2 = -6\,g_2^2 M_2^2 - \frac{6}{5}\,g_1^2 M_1^2 + \frac{3}{5}\,g_1^2 S + 3X_t, \qquad (5.52)$$

$$16\pi^2 \frac{\mathrm{d}}{\mathrm{d}t} m_{H_d}^2 = -6\,g_2^2 M_2^2 - \frac{6}{5}\,g_1^2 M_1^2 - \frac{3}{5}\,g_1^2 S, \qquad (5.53)$$

where

$$X_t = 2|y_t|^2\left(m_{H_u}^2 + m_{Q3}^2 + m_{u3}^2 + |A_t|^2\right), \qquad (5.54)$$

$$S = \mathrm{Tr}[Y_\zeta M_\zeta^2] = m_{H_u}^2 - m_{H_d}^2 + \mathrm{Tr}[M_{\tilde{Q}}^2 - 2M_{\tilde{u}}^2 + M_{\tilde{d}}^2 - M_{\tilde{L}}^2 + M_{\tilde{e}}^2], \qquad (5.55)$$

where m_{Q3}^2 and m_{u3}^2 are the $(3,3)$ entries of the $M_{\tilde{Q}}^2$ and $M_{\tilde{u}}^2$ matrices, respectively.

A first important remark is that the X_t term in Eq. (5.52) is in standard configurations the dominant contribution to the RG flow of $m_{H_u}^2$. Being $X_t(t) > 0$, such term usually drives $m_{H_u}^2(t)$ negative in the infrared despite the opposite contribution of gaugino terms. In turns, negative (or positive but nevertheless very small) values

of $m_{H_u}^2(m_{\text{soft}})$ are crucial to trigger electroweak symmetry breakdown, Eq. (5.29), in viable MSSM scenarios. We will return to this issue next chapter.

A second point is that the S term, present in both Eqs. (5.52), (5.53) and defined in Eq. (5.55), let all squark and sfermion masses of all generations come into play when analysing the RG flow of $m_{H_{u,d}}^2$. This is particularly troublesome since it makes an exact analysis of one-loop supersymmetry RG flows considerably more complicated. Fortunately, the trace over sfermion squared-mass matrices in Eq. (5.55) can be seen to have a numerically negligible contribution to the MSSM RG flow. We can therefore safely approximate its expression to a more docile one: forgetting about the first two sfermion generations, in chapter 6 we will assume

$$S \approx m_{H_u}^2 - m_{H_d}^2 + m_{Q_3}^2 - 2\,m_{u_3}^2 \ . \tag{5.56}$$

Once made unnecessary to deal with the RG flow of the full squared-mass sfermion matrices, we are left with discussing RG equations for m_{Q_3,u_3}^2, since they enter in the expression of the crucial X_t term, Eq. (5.54). They obey the differential equation

$$16\pi^2 \frac{\mathrm{d}}{\mathrm{d}t} m_{Q_3}^2 = X_t - \frac{2}{15} g_1^2 M_1^2 - 6\,g_2^2 M_2^2 - \frac{32}{3}\,g_3^2 M_3^2 + \frac{1}{5} g_1^2 S \ , \tag{5.57}$$

$$16\pi^2 \frac{\mathrm{d}}{\mathrm{d}t} m_{u_3}^2 = 2\,X_t - \frac{32}{15} g_1^2 M_1^2 - \frac{32}{3}\,g_3^2 M_3^2 - \frac{4}{5} g_1^2 S \ . \tag{5.58}$$

Aspects of High-Scale Supersymmetry

6.1 Study motivations

The parameter space of the MSSM is poorly constrained by experimental data. Little (or nothing) we know about the mass spectrum of superpartners and, disregarding naturalness considerations concerning the Higgs mass, we do not even have a clear hint of what the supersymmetry scale[1] m_S (at which supersymmetry is broken) might be.

Despite such disorienting lack of direct experimental hints, very interesting insights can come from theoretical studies of the structure and behaviour of supersymmetric theories under renormalisation group (RG) flow, which intimately connects high- and low-energy aspects of such theories. These investigations, in turns, can furnish clues on the viable MSSM parameter space and possibly shed light on important issues like at what scale supersymmetry is broken and superpartners' masses are. This is the philosophy that motivates the approach adopted in the study of this last chapter.

6.1.1 Review of literature's previous results

Several important progresses have already been made along the direction outlined above. In order to frame this chapter's contributions in the right contest, we should therefore first review what has already been obtained in the literature.

As discussed in section 5.2.3, gauge coupling unification is a very promising feature of MSSM. Understanding to what extent and under which premises such unification can be achieved is a very interesting issue which has been addressed in past and recent literature [26, 93–96].

At first approximation, the running of gauge couplings is only influenced by the supersymmetry scale m_S. Such a rough analysis has been exemplified in Figure 5.1. A more refined treatment must of course take into account threshold corrections at m_S

---

[1]Along the present chapter, to reduce the notation clutter, we will use the shorter notation m_S for the supersymmetry-breaking scale m_{soft} of chapter 5, referring to it simply as the supersymmetry scale.
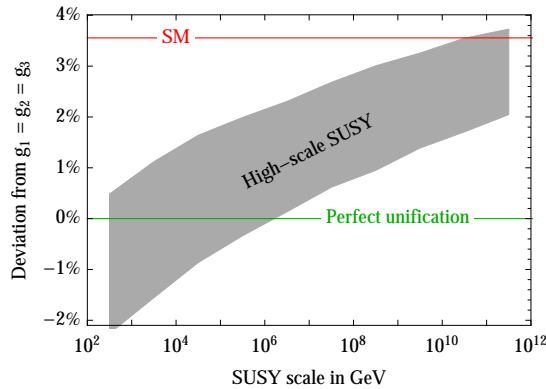
Figure 6.1: Minimum amount (in percent) by which gauge coupling unification is missed in High-Scale Supersymmetry. The gray band is obtained by scanning supersymmetric mass parameters within the range $[1/3, 3] \, m_S$, under the condition of reproducing observed Higgs mass (from Ref. [26]).

due to the new particle content, i.e. the corrections due to the fact that superpartner's masses are not all perfectly degenerate at m_S. In the absence of clear hints of how the superpartner's spectrum might look like, a reasonable approach could be to assume it limited to a "natural" window around m_S and scan over the parameter space.

In Figure 6.1 we show the result of such an analysis, performed in Ref. [26]. The sparticles spectrum has been assumed to lie in a natural range within $1/3$ and 3 times the supersymmetry scale m_S and a scan of the parameter space has been performed. A first conclusion is that perfect gauge coupling unification can be achieved within natural configuration of supersymmetric parameters for m_S up to $\sim 10^6$ GeV. Technically, even slightly higher scales for m_S can still be advocated considering additional (unknown) threshold corrections at the GUT scale, although for too high m_S the original improvement of gauge unification with respect to the Standard Model simply fades away.

The approach outlined above, i.e. overcoming our ignorance of parameter space by identifying a reasonable region to scan, is a prototype of the strategy that we will exploit in our study. This methodology is of course a double-edged sword. On the one hand, it undoubtedly increase the generality of whatever conclusion could be drawn from such analysis. On the other hand, without a careful choice of the region of parameter space to scan, such an investigation might be both extremely time-consuming and fruitless, since enlarging the freedom of a model always enlarge the range of possibilities and (almost) everything might be obtained under sufficiency loose assumptions. Particular attention should therefore always been paid to the choice made to perform the scan.

Another major feature of supersymmetric theories, suitable for these kind of analyses, is the celebrated prediction of the Higgs quartic coupling λ in terms of the other MSSM parameters. In section 5.2.2 we have already introduced the tree-level relation for $\lambda(m_S)$, Eq. (5.38), warning that one-loop corrections are extremely sizeable. In particular, corrections proportional to the top-Yukawa coupling g_t, arising when integrating out the stop scalars, should be considered de facto $\mathcal{O}(1)$.
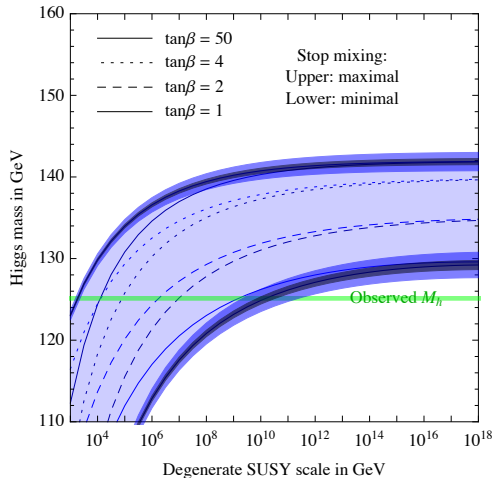
Figure 6.2: Higgs mass as a function of supersymmetry scale m_S, with degenerate sparticles spectrum. The stop-mixing parameter A_t has been scanned to maximise (upper lines) and minimise (lower lines) m_h for different $\tan\beta$ values (see Ref. [26] for details).

The full one-loop expression of $\lambda(m_S)$ is extremely lengthy and not particularly enlightening and we refer to the literature for the explicit formulas [25, 26]. The important point is that such expression provides a powerful matching condition of the Standard Model value of $\lambda(m_S)$ in terms of MSSM parameters at the same scale. Schematically:

$$\lambda_{\text{SM}}(m_S) = \lambda_{\text{MSSM}}(m_S) \; ,$$
$$\lambda_{\text{MSSM}}(m_S) = \frac{1}{4}\left[g^2(m_S) + g'^2(m_S)\right]\cos^2 2\beta + \Delta\lambda^{1loop} \; , \tag{6.1}$$

where $\Delta\lambda^{1loop}$ depends upon the sparticles spectrum and other MSSM parameters values at the supersymmetry scale m_S.

Before the Higgs discovery, relation (6.1) has been deployed as a predicting tool to guess the possible mass range for the Higgs. In Ref. [24] an upper limit for the Higgs mass of 141 ± 2 GeV was set through a detailed study of matching condition Eq. (6.1). A more recent example of such kind of analysis is taken from Ref. [26] and shown in Figure 6.2, where the upper limit $m_h \lesssim 141$ GeV can still be appreciated.

It might be thought that, after Higgs discovery and precise measurement of its mass, this approach is only of historical interest. On the contrary, the exact knowledge of the Higgs mass have eventually opened the possibility of a different interpretation of these analyses. Indeed, a conscientious study of the "space of possible Higgs masses" might reveal intriguing features of the particular Higgs mass chosen by nature among all viable vacua, as it will be discussed below.

6.1.2   Novelties of our approach

Our analysis will investigate some intriguing features of the MSSM, adopting a scanning approach similar to the ones exemplified in the previous section. Therefore, we will scan among the parameter space of MSSM (including different benchmark values

of the supersymmetry scale m_S itself), the basic reason for this being to enlarge the generality of our conclusions.

However, there will be a significant novelty in our handling of MSSM parameter space. As discussed above, the choice of the parameter region to be analysed is a delicate issue and, typically, a natural range for the parameters is chosen at the matching scale m_S. This might seems a reasonable choice but, as a matter of fact, is slightly inconsistent. Indeed, naturalness can be considered a legitimate requirement of a theory only at its input scale, i.e. before any running effect could spuriously ruin it. For this reason, we will impose our natural boundary conditions for the MSSM parameters not at m_S but at m_G, i.e. at the energy scale where MSSM might eventually encounter its GUT completion. A clear drawback of this choice is that such an analysis unavoidably becomes more convoluted and a whole computational machinery should be developed to run all parameters down to the matching scale m_S for each scanned configuration in a reasonable computational time.

Together with MSSM parameters, we will also scan over the quartic Higgs coupling λ. In other words, we will consider different MSSM scenarios with different values of the Higgs mass m_h, as already done in the literature [25, 26] and exemplified in the previous section. This choice is meant to study the landscape of possible Standard Model parameter configurations, in order to enlarge our perspective and to shed a different light on the physical m_h value, perhaps unrevealing hidden and surprising features of it. Furthermore, the study of the landscape of possible m_h values can acquire a physical meaning in the light of some cosmological arguments such as "multiverse" approaches and anthropic selection [114].

Another important novelty of our approach is to consider not only Higgs but also top-quark mass m_t (i.e. its Yukawa coupling g_t) as a scanned parameter, something that has never been done before in the context of supersymmetric theories. There are multiple reasons for taking such additional step. On the one hand, m_t can be considered a peculiar Standard Model value just as m_h, deserving a similar consideration and subject to analogous anthropic arguments. On the other hand, g_t has an $\mathcal{O}(1)$ influence on the λ matching condition, Eq. (6.1). It could be therefore seen as inconsistent to take into account possible variations of the input parameter λ_{SM}, neglecting potentially more important changes in g_t. Finally, y_t (the supersymmetric top-Yukawa coupling) has a strong influence on the RG flow of many soft parameters and changes in its values have deep consequences in other sectors of the theory and on the electroweak symmetry breakdown itself, as we will see. For these reasons, it is definitely interesting to study the m_t landscape and the effects of different g_t values on the MSSM features.

Our novel point of view just outlined, that is examining the (m_h, m_t) landscape[2] for High-Scale MSSM with natural parameter configurations at the GUT scale, gives us the opportunity to investigate another interesting feature of these theories: the Radiative Electroweak Symmetry Breakdown (REWSB). As sketched in section 5.2.2, REWSB is an interesting scenario in which the $SU(2)_L$ symmetry is preserved at the input scale (in our case, m_G) and its spontaneous breakdown (i.e. condition (5.29)) is triggered at lower energies purely by RG effects. Therefore within our approach, where configuration of parameters at m_G is given and all RG flows are handled,we

---

[2]Which is really the (λ, g_t) landscape.

are in the position of including the study of REWSB with little effort.

To summarise the key new features of the approach adopted in the following, we immerse the MSSM in the $\{m_h, m_t\}$ landscape, not limiting ourselves to vary only the quartic Higgs coupling λ but also the top-Yukawa g_t. With these premises, we will study the fulfilment of λ matching condition (6.1) imposing natural configuration of MSSM parameters at the GUT scale m_G, rather than at that supersymmetry scale m_S as usually done in the literature. Such a different point of view requires a difficult handling of RG flows to relate parameter's values at high and low scales. As a reward, we will be in position of studying with little effort the conditions under which REWSB can be achieved.

6.2   Methodology

In the previous section we have explained philosophy and motivations of our analysis. Furthermore, we have outlined the intriguing features that supersymmetric theories can display and that we want to investigate in detail for the MSSM. These are

- gauge coupling unification,

- prediction of the quartic Higgs coupling λ in terms of the other parameters of the model,

- naturalness of the theory at its input scale (the GUT scale for us) and

- electroweak symmetry breakdown triggered at low scales by RG flow (REWSB).

First of all, the above requirements should be formulated in a quantitative fashion. Next, we want to develop a strategy to study their simultaneous fulfilment, rather than analyse them one by one. Both these issues will be addressed in this section.

6.2.1   Quantitative definition of requirements

Before moving any further in our discussion, we should state precisely what we mean by imposing gauge coupling unification and λ matching, as well as provide a quantitative prescription for REWSB and naturalness of parameters.

As explained in sections 5.2.3 and 6.1.1, the issue of gauge coupling unification has already been extensively studied in the literature with many dedicated analyses. We will not try to reproduce literature's results here, but rather exploit them to take certain conclusions for granted. In particular, we will simply translate gauge coupling unification requirement into an upper limit for m_S of 10^6 GeV, according to Ref. [26] and similar studies. In other words, we will assume that the merging of gauge coupling at the GUT scale (which worsen as m_S increases) is satisfactory as long as $m_S \lesssim 10^6$ GeV.

Once taken for granted that gauge coupling unification is achieved, we should only care about a sensible definition of the GUT scale itself, m_G. Given that a small residual mismatch among gauge couplings always remain, it is reasonable to define

m_G in such a way to minimise it. For this reason, we will operatively define m_G as:

$$m_G = \min_\mu \left(\frac{\sqrt{(g_1(\mu) - g_2(\mu))^2 + (g_2(\mu) - g_3(\mu))^2 + (g_1(\mu) - g_3(\mu))^2}}{g_1(\mu) + g_2(\mu) + g_3(\mu)} \right) . \quad (6.2)$$

A different choice, common in the literature, could have been to simply set m_G as the energy at which $g_1(\mu) = g_2(\mu)$. It is worth noting that different definitions may lead to $\mathcal{O}(1)$ variations in the exact value of m_G. However, being the sensitivity of the RG flow to the input scale only logarithmic, it is intrinsically irrelevant for our purposes to define m_G with an accuracy better than $\mathcal{O}(1)$.

Another important requirement concerns the matching at m_S of the RG-improved value of the quartic Higgs coupling, $\lambda_{\mathrm{SM}}(m_S)$, with its prediction in terms of MSSM parameters, $\lambda_{\mathrm{MSSM}}(m_S)$, as sketched in Eq. (6.1). We will from now on refer to such condition simply as λ-matching. Since both the RG equations and the matching expression are derived in perturbation theory, higher-order corrections are unavoidably neglected and clearly an exact equality cannot be required. Therefore, the λ-matching condition takes the form

$$|\lambda_{\mathrm{SM}}(m_S) - \lambda_{\mathrm{MSSM}}(m_S)| < \lambda_{\mathrm{thr}} , \quad (6.3)$$

where λ_{thr} is the established threshold of a satisfactory matching. Such threshold has been chosen to be an absolute difference, rather than a ratio, since λ_{SM} renormalise in a non-multiplicative fashion and therefore the absolute magnitude of corrections is the physically meaningful value.

A suitable definition of λ_{thr} is clearly of crucial importance. A reasonable choice is to set λ_{thr} of the same size of the leading terms neglected in the expression for $\lambda_{\mathrm{MSSM}}(m_S)$. In our setup, we will use for $\lambda_{\mathrm{MSSM}}(m_S)$ the full one-loop result given in Ref. [26]. Therefore, it would be advisable to adjust

$$\lambda_{\mathrm{thr}} \sim \max \left(\Delta\lambda^{2\ell oop} \right) , \quad (6.4)$$

where $\Delta\lambda^{2\ell oop}$ are the leading two-loop contributions to $\lambda_{\mathrm{MSSM}}(m_S)$, which also are given in Ref. [26]. The maximal values of $\Delta\lambda^{2\ell oop}$ for different supersymmetry scales are plotted in Figure 6.3. According to this analysis, the chosen values of λ_{thr} for $m_S = \{5, 100, 1000\}$ TeV (i.e. the m_S values that will be used for the analysis of section 6.3) are summarised in Table 6.1.

The next issue to be discussed is a suitable definition of naturalness of soft MSSM parameters at the input scale m_G. Let us first summarise the dimensionful parameters we will be concerned with in our analysis:

$$M_1 , M_2 , M_3 , m_{H_u}^2 , m_{H_d}^2 , m_{Q_3}^2 , m_{u_3}^2 , A_t , |\mu|^2 , b . \quad (6.5)$$

Operatively, we will take $M_3(m_G)$ as the reference mass to quantitatively define a natural range for the above parameters at m_G. In other words, naturalness at m_G of all parameters listed in Eq. (6.5) will be judged through their quantitative comparison with $M_3(m_G)$ or $M_3^2(m_G)$. As a more conservative requirement, we will also assume that

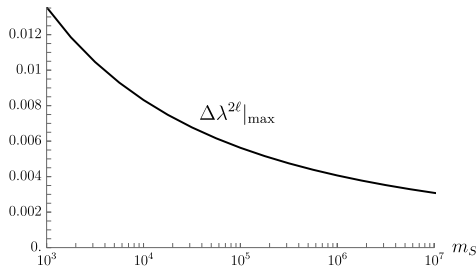$$M_1(m_G) = M_2(m_G) = M_3(m_G) , \quad (6.6)$$

Figure 6.3: Maximal value of $\Delta\lambda^{2loop}$ as a function of m_S.

m_S	λ_{thr}
5 TeV	0.01
100 TeV	0.006
1000 TeV	0.004

Table 6.1: Selected values of λ_{thr} for different m_S used in our analysis.

as it is usually the case in GUT models.

The last feature we are interested in is the REWSB, discussed in section 5.2.3. From the algorithmic point of view, requiring the electroweak symmetry to be broken the way it is at low scale means to impose Eqs. (5.29) and (5.33) at the scale m_S. If we want to superimpose the condition that electroweak symmetry is not broken at all at m_G, we should require Eq. (5.29) to be unfulfilled at high scales, that is:

$$\left(|\mu(m_G)|^2 + m_{H_u}^2(m_G)\right)\left(|\mu(m_G)|^2 + m_{H_d}^2(m_G)\right) > b^2(m_G) . \tag{6.7}$$

Eq. (6.7) will be our operative definition of REWSB.

6.2.2 Development of a global analysis

Given the individual definitions above for all the requirements we are interested in, we now want to perform an integrated analysis that takes all of them into account. Let us recall that we want to perform our study considering different input values of m_h and m_t. Such values are understood to be given at the electroweak scale, that will be precisely identified with the $\overline{\text{MS}}$ top-quark mass, $\bar{m}_t = 163$ GeV.

We therefore need to develop a machinery that, given (m_h, m_t) as input parameters (at the scale $\bar{m}_t$), performs a scan over $\tan\beta$ and over a natural range of parameters (6.5), determining whether a parameter configuration exists that displays all the features we want to impose.

Such a machinery is summarised in Table 6.2. It is a four-step procedure that can be summarised as follows.

- Step 1, in which the GUT scale m_G is determined.

  The one-loop running of the Standard Model coupling constants $g_{1,2,3}(\mu)$ is performed up to m_S using Standard Model RG equations and further up using supersymmetric RG equations. We are then able to determine the GUT scale m_G using Eq. (6.2). It is worth pointing out that this step is just needed once for each m_S value.

- Step 2, in which needed boundary conditions at m_S and m_G are determined.

  Starting from $m_h(\bar{m}_t)$ and $m_t(\bar{m}_t)$, we can determine the quartic Higgs coupling $\lambda_{\text{SM}} = m_h^2/2v^2$ and the Standard Model top-Yukawa coupling $g_t = m_t/v$ at the

Step	$\bar{m}_t$	m_S	m_G
1	$g_{1,2,3}(\bar{m}_t) \quad \longrightarrow$	$g_{1,2,3}(m_S) \quad \longrightarrow$	$g_{1,2,3}(\mu)$
			Eq. (6.2) $\to m_G$
2		$M_3(m_S) = m_S \quad \longrightarrow$	$M_3(m_G)$
	$g_t(\bar{m}_t) = \frac{m_t}{v} \quad \longrightarrow$	$y_t(m_S) = \frac{g_t(m_S)}{\sin\beta}$	
	$\lambda(\bar{m}_t) = \frac{m_h^2}{2v^2} \quad \longrightarrow$	$\lambda(m_S)$	
3	scan over different $\{\tan\beta, A_t, m_{Q_3,u_3}, m_{H_{u,d}}\}$ configurations at m_G:		
			Eqs. (6.6), (6.11):
	$\left\{\begin{array}{c} M_{1,2}(m_S) \\ A_t(m_S) \\ m_{Q_3,u_3}(m_S) \\ m_{H_{u,d}}(m_S) \end{array}\right\} \quad \longleftarrow$		$\left\{\begin{array}{c} M_{1,2}(m_G) \\ A_t(m_G) \\ m_{Q_3,u_3}(m_G) \\ m_{H_{u,d}}(m_G) \end{array}\right\}$
	$\downarrow$		
	Eq. (6.9):		
	$\left\{\begin{array}{c} \mu(m_S) \\ b(m_S) \end{array}\right\} \quad \longrightarrow$		$\left\{\begin{array}{c} \mu(m_G) \\ b(m_G) \end{array}\right\}$
	$\downarrow$		$\downarrow$
	• EWSB, Eq. (6.12) • Naturalness, Eq. (6.13)		
	• λ match, Eq. (6.3) • REWSB, Eq. (6.7)		
4	Is there a configuration of Step 3 that satisfies all conditions?		
	• Yes $\to \{m_h, m_t\}$ is a viable point.		
	• No $\to \{m_h, m_t\}$ is not a viable point.		

Table 6.2: Performed analysis on a specific (m_h, m_t) point.

electroweak scale and run them up to m_S. From $g_t(m_S)$ we are able to infer the supersymmetric top-Yukawa coupling $y_t = g_t/\sin\beta$, while $\lambda_{\text{SM}}(m_S)$ will be later compared with its MSSM prediction.

As an operative assumption, we identify the gluino pole mass with the supersymmetry scale itself, $M_3(m_S) = m_S$. Through the RG equations, $M_3(m_G)$ can thus be derived. As already discussed, such value will be used as a reference value for the natural range of all soft parameters (6.5) at the GUT scale.

• Step 3, in which the scan over different configurations of MSSM parameters is performed.

So far, the only MSSM parameters fixed are gaugino masses $M_{1,2,3}$ (M_3 has been determined in Step 2 and $M_{1,2}(m_G)$ follow from Eq. (6.6)) and the top-Yukawa coupling y_t. The parameters still unknown and relevant for our analysis are:

$$\tan\beta \ , \ A_t \ , \ m_{Q_3,u_3} \ , \ m_{H_{u,d}} \ , \ \mu \ , \ b \ . \tag{6.8}$$

Not all of them are independent, given the two conditions (5.33). To scan the viable parameter configurations, we will use the following strategy: to fix $\{\tan\beta, m_{Q_3,u_3}, A_t, m_{H_{u,d}}\}$ at m_G, to run them down to m_S, to invert Eq. (5.33) to find $|\mu(m_S)|, b(m_S)$,

$$\begin{cases} |\mu|^2 = -\frac{1}{2}\tan 2\beta\left(m_Z^2\cot 2\beta + m_{H_d}^2\cot\beta - m_{H_u}^2\tan\beta\right) \\ b = -\frac{1}{2}\tan 2\beta\left(m_Z^2\cos 2\beta + m_{H_d}^2 - m_{H_u}^2\right) \end{cases}, \qquad (6.9)$$

and finally to run μ and b up to m_G.

The definition of the scanned region is of critical importance. For $\tan\beta$, it is sufficient to fix a reasonable range; we will use[3]

$$\tan\beta \in [1.1, 10] . \qquad (6.10)$$

For the remaining parameters, a "natural" range around $M_3(m_G)$ is implemented:

$$\begin{cases} m_{H_{u,d}}^2(m_G) = r_{H_{u,d}}\, M_3^2(m_G) \\ m_{Q_3,u_3}^2(m_G) = r_{Q,U}\, M_3^2(m_G) \quad, \quad \{r_{t,Q,u,H_u,H_d}\} \in \left(\frac{1}{\bar{r}}, \bar{r}\right) , \\ A_t(m_G) = r_t\, M_3(m_G) \end{cases} \qquad (6.11)$$

where we will choose $\bar{r} = 3$. For each parameter configuration, we check:

– Electroweak symmetry breakdown achievement. In our setup, to require the EWSB to take place means to check $|\mu|^2$ of Eq. (6.9) to be positive:

$$-\frac{1}{2}\tan 2\beta\left(m_Z^2\cot 2\beta + m_{H_d}^2(m_S)\cot\beta - m_{H_u}^2(m_S)\tan\beta\right) > 0 . \quad (6.12)$$

– λ matching condition, Eq. (6.3).

– $\mu(m_G)$ and $b(m_G)$ naturalness. To be consistent with Eq. (6.11), naturalness requirement for μ and b at GUT scale clearly reads

$$r_{\mu,b} \in \left(\frac{1}{\bar{r}}, \bar{r}\right) , \quad \begin{cases} r_\mu \equiv \mu(m_G)^2/M_3(m_G)^2 \\ r_b \equiv b(m_G)/M_3(m_G)^2 \end{cases}, \qquad (6.13)$$

where the same $\bar{r}$ as in Eq. (6.11) should be used.

– REWSB, Eq. (6.7), as an optional condition.

• Step 4, in which the (m_h, m_t) point is judged.

The scan of Step 3 can have two outcomes: either no configuration that satisfies all requirements has been found, or at least one configuration has fulfilled all of them. In the former case the (m_h, m_t) point is considered not viable, in the latter is considered viable.

---

[3]We are not interested in large-$\tan\beta$ scenarios.

The whole (m_h, m_t) plane can be scanned using the four-steps procedure outlined above. The set of all (m_h, m_t) points which results viable according to this analysis will be referred to as the *viable region* for the MSSM in the (m_h, m_t) plane.

From the computational point of view, the most challenging task is to perform Step 3, i.e. the scan of a natural range of soft parameters A_t, $m^2_{Q_3, u_3}$, $m^2_{H_{u,d}}$, in a reasonable running time. As a matter of fact, for a sensible scan of such five-dimensional parameter space at least $\mathcal{O}\left(10^4\right)$ configurations should be probed. Clearly, a full numerical handling of such RG flow would be prohibitively time consuming and, to avoid it,, analytical solutions to the RG equations of the soft parameters have been developed and implemented. A brief discussion of them is provided in appendix C.

6.3   Analysis of the results

Exploiting the machinery developed in section 6.2, we are now ready to present the results of our analysis. We will investigate the shape and important features of the viable region for the MSSM in the (m_h, m_t) plane for different values of the supersymmetry scale m_S and for different setups of our requirements.

6.3.1   Low-energy MSSM

First, we analyse the results obtained in a low-energy MSSM scenario, setting $m_S = 5$ GeV. Figure 6.4 shows the viable regions according to two different approaches:

- In green is shown the viable region obtained through simple arguments concerning the λ-matching only. In such an analysis, only condition (6.3) is imposed, no RG flow is handled and the scanning of relevant MSSM parameters is performed directly at the matching scale m_S. In the following, we will refer to this approach as the *naive λ-matching* analysis and to its results as the *naive viable region*.

- In blue the result of our complete analysis is shown, without the REWSB requirement.

The naive viable region (in green) has two boundaries determined by two opposite situations. For points on the right of the lower green curve, the quartic Higgs coupling is too high to be properly matched even when threshold corrections are taken into account. For points above the upper green curve, instead, $\lambda(m_S)$ eventually becomes negative of an amount that cannot be accommodate through threshold corrections.

Our viable region (in blue) is obviously more restrictive that the naive one, since it is found through a more thorough study. It has a peculiar shape that can be divided in three different pieces: an up border (representing the highest allowed m_t value for a given m_h), a right border (that goes from the end of the up border down to a visible "shoulder") and a down border (that from the above mentioned shoulder goes down to $m_t = 0$). Each of these curves has a different origin and explanation.

- The blue up border, though a continuous line, can be better understood if split in two parts: a low-m_h part ($m_h \lesssim 100$ GeV, viable for low $\tan \beta$ values,
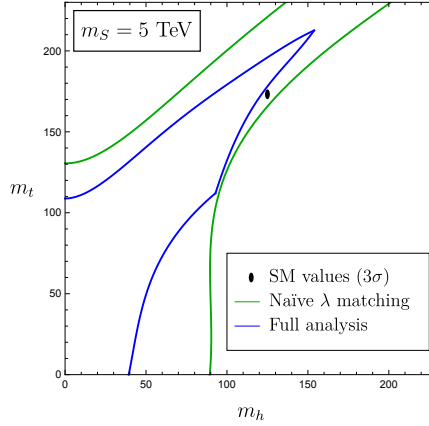
Figure 6.4: Viable region from naive arguments on λ-matching (green) and from the whole developed procedure without REWSB (blue). The physical Standard Model values for (m_h, m_t) are also shown for reference.

$\tan \beta \lesssim 3$) and a high-m_h part ($m_h \gtrsim 100$ GeV, viable for high $\tan \beta$ values, $\tan \beta \gtrsim 3$).

The low-m_h part has in principle the same origin as the green up border of Figure 6.4: it is a limit above which $\lambda(m_S)$ has become too negative to be addressed even considering threshold corrections. The reason for the blue curve to be lower than the green one is simple: the latter has been computed by tuning threshold corrections to their best-case value, regardless whether or not a scenario exists in which such value can be obtained. The blue border, retaining also information of this kind, is clearly more restrictive.

In the high-m_h part of the up border (i.e. the high-m_t part) an additional consideration plays a major role. Namely, the requirement that $y_t(\mu)$ does not develop a Landau pole before reaching the GUT scale m_G becomes a non-trivial constraint. This forces us to raise $\tan \beta$ as m_t increases (since this has the effect of lowering the input value $y_t(m_S)$), thus affecting the λ matching conditions.

- The blue right border has the same origin as the green right border: it is a limit over which $\lambda(m_S)$ becomes too high to be accommodated. Again, the shift between green and blue curves is not a surprise, since the latter is obtained through a more constrained analysis.

  Instead, a qualitative difference between the two right borders is their low end point: while the green one goes down to $m_t \sim 0$, the blue one stops at $m_t \sim 100$ GeV, where a shoulder appears. For m_t values below this edge, the origin of the blue border is qualitative different, as explained below.

- The blue down border not only presents a visible discontinuity that separates it from the blue right border, but it also has a completely different explanation. Namely, for m_t values below this curve, the smaller value of $\tan \beta$ required by λ-matching is too high to achieve electroweak symmetry breakdown (within our naturalness assumptions). Some comments are in order:
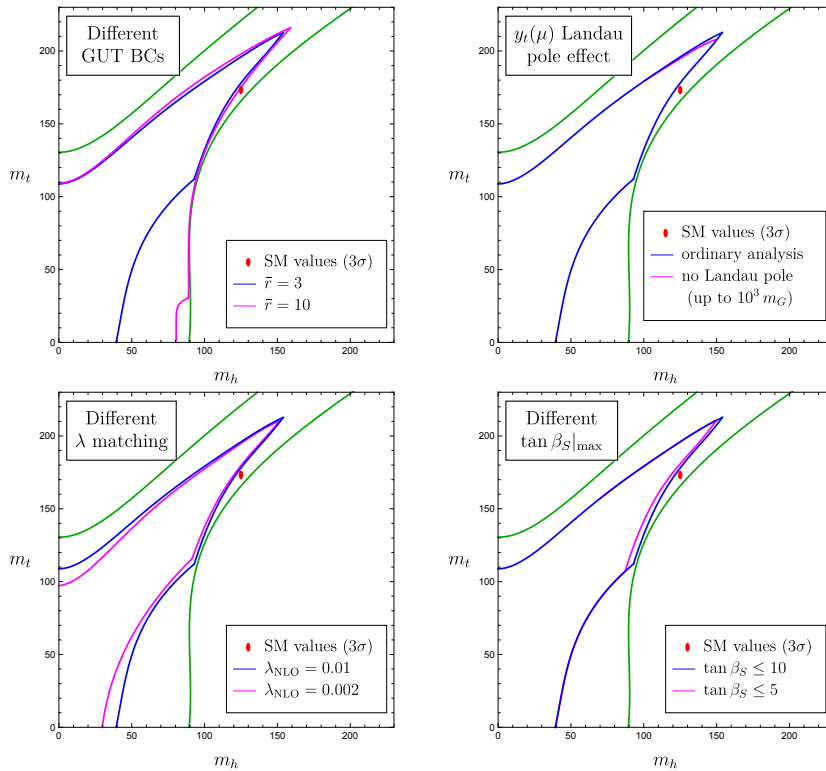
Figure 6.5: Comparison between the viable region for the chosen set of parameter (in blue) and the region resulting from the modification of one of these parameters (in magenta, see the discussion for details). The green curves of Figure 6.4 are also shown for reference.

- For low m_t, the tension between λ-matching and condition (6.12) is clear. The former prefers high values for $\tan\beta$, in order to increase λ_{MSSM}. The latter prefers low values for $\tan\beta$ to compensate the small m_t value, which reduces the y_t influence on RG flows (such influence being crucial to achieve electroweak symmetry breakdown).

- Once understood that this "shoulder" featured by the blue region originates from more involved considerations regarding the achievement at once of electroweak symmetry breakdown and λ-matching, it is rather clear why the green borders, based on a more naive analysis, are missing such feature completely.

- The achievement of electroweak symmetry breakdown in the absence of big RG flow effects) depends critically on the choice of boundary conditions imposed at m_G. In particular, if the $\bar{r}$ in Eq. (6.11) was enlarged, one would expect this excluded region to shrink.

In order to get a better understanding of the viable region's features discussed above, it is interesting to study how its shape changes as the analysis parameters are modified. These comparisons are proposed in Figure 6.5.

The top-left plot of Figure 6.5 shows (in magenta) how the viable region expands when the boundary conditions at m_G are scanned more widely (precisely, in Eq. (6.11)
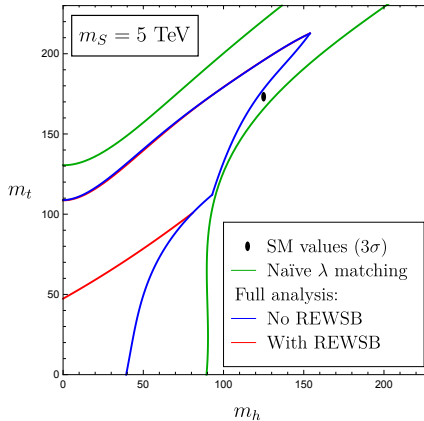
Figure 6.6: Naive viable region (green) and viable region with (red) and without (blue) the additional REWSB condition.

we switch from $\bar{r} = 3$ to $\bar{r} = 10$). For up and right borders a small shift toward the green curves can be seen, due to the larger parameter space scanned searching for a satisfactory λ-matching. In addition, there is a dramatic change in the down border. The reason for this has been already foreseen above: since now a bigger splitting between $m^2_{H_u}(m_G)$ and $m^2_{H_d}(m_G)$ is allowed, electroweak symmetry breakdown is achievable for higher $\tan\beta$, making the λ-matching easier.

The top-right plot of Figure 6.5 shows (in magenta) the slight change in the high-m_h part of the up border when the requirement of the absence of a Landau pole for $y_t(\mu)$ is made more stringent (precisely, that such a pole does not arise up to $\mu = 10^3 \, m_G$). This prove what claimed above, i.e. that such condition plays a major role in bounding from above this part of the border.

The bottom-left plot of Figure 6.5 shows (in magenta) how the viable region shrinks if the λ-matching condition is made tighter (precisely, in Eq. (6.3) we switch from $\lambda_{\text{thr}} = 0.01$ to $\lambda_{\text{thr}} = 0.002$). The shift between blue and magenta borders is higher wherever $\lambda(m_S)$ is harder to match: these "tougher" regions are the down border (as already exhaustively explained) and the low-m_h part of the up border, where (as already said) λ-matching is the main obstacle.

The bottom-right plot of Figure 6.5 is the last comparison we propose. In magenta is shown the shift in the right border due to a reduction of the maximal $\tan\beta$ value considered (precisely, from $\tan\beta \leq 10$ to $\tan\beta \leq 5$). One can appreciate how small is the contribution to the overall viable region from configurations with high $\tan\beta$.

6.3.2 The Radiative EWSB condition

Still considering a low-energy MSSM scenario (with $m_S = 5$ TeV), we can now examine how the viable region shrinks when the additional requirement of REWSB, Eq. (6.7), is imposed.

Before showing the results, it is useful to comment further on meaning and consequences of requiring REWSB. First, at zero order one can interpret Eq. (6.7) as a constraint to the boundary conditions at m_G for $m^2_{H_{u,d}}$. Since the main conse-

quence of reducing the range of initial conditions for $m_{H_{u,d}}^2(m_G)$ is to obstacle the λ-matching, we should expect the REWSB requirement to affect predominantly the regions where such matching is harder to reach. Second, REWSB is clearly easier to achieve when the RG flow effects are bigger, with particular emphasis on the radiative effects of $y_t(\mu)$ on $m_{H_u}^2(\mu)$. Thus, we should expect REWSB to be harder to achieve in the low-m_t region.

Keeping the above considerations in mind, Figure 6.6 compares the resulting viable regions with (red) and without (blue) requiring REWSB. One can see a slight difference in the low-m_h part of the up border and dramatic change of the down border behaviour. In fact, according to the discussion above, these were the regions where changes were expected, since the most sensible to the λ-matching condition (see Figure 6.4, top-right plot and respective discussion).

The down border (in red) appearing once REWSB is imposed deserves a more detailed discussion. Starting from its shoulder with the right border and going to lower m_h (i.e. lower m_t), the first part of this border just follows the former one (blue curve): m_t is still sufficiently high to trigger REWSB without difficulties. Around $m_t \approx 75$ GeV the red border detaches itself from the blue one, still allowing smaller values for m_t as m_h decreases but with a milder slope than the blue curve: REWSB is starting to be a non-trivial requirement.

Besides from small quantitative changes, the main outcome of the REWSB requirement is the existence of a critical m_t value (~ 50 GeV for $m_S = 5$ TeV) below which REWSB cannot be achieved whatsoever. This is rather clear once considered that a sufficiently large y_t value is crucial in order to trigger the essential RG flow effects involved.

6.3.3   Analysis for different supersymmetry scales

So far, we have discussed the behaviour of the allowed region only in a low-energy MSSM scenario ($m_S = 5$ GeV). It is interesting to see how these results change when adopting different supersymmetry scales: Figure 6.7 shows the viable regions (according to the different analyses) obtained for $m_S = 100$ TeV (left plot) and $m_S = 1000$ TeV (right plot). One can immediately recognise in both plots the general qualitative features already outlined for the $m_S = 5$ TeV scenario. In fact, the whole discussion above can be straightforwardly applied also to these cases. As explained in section 6.2.1, we will not consider supersymmetry scales higher than $m_S \sim 10^6$ GeV.

More can be said if we compare together the results from different supersymmetry scales. Before showing such comparisons, let us point out a few remarks about what we are expecting.

- As a consequence of raising the supersymmetry scale, we are lengthening the Standard Model RG flow of $\lambda(\mu)$. In particular, in the high-m_t region the negative contribution to such RG flow from g_t results in $\frac{\mathrm{d}}{\mathrm{d}\mu}\lambda(\mu) < 0$, thus $\lambda_{\mathrm{SM}}(m_S)$ is sensibly decreasing as m_S increases. In the low-m_t region, instead, $\frac{\mathrm{d}}{\mathrm{d}\mu}\lambda(\mu) > 0$ and $\lambda_{\mathrm{SM}}(m_S)$ is increasing with m_S. We can expect this to have major consequences.

- Another consequence of the amplified Standard Model RG flow effects is the different matching value of y_t at m_S, $y_t(m_S) = g_t(m_S)/\tan\beta$. More precisely,
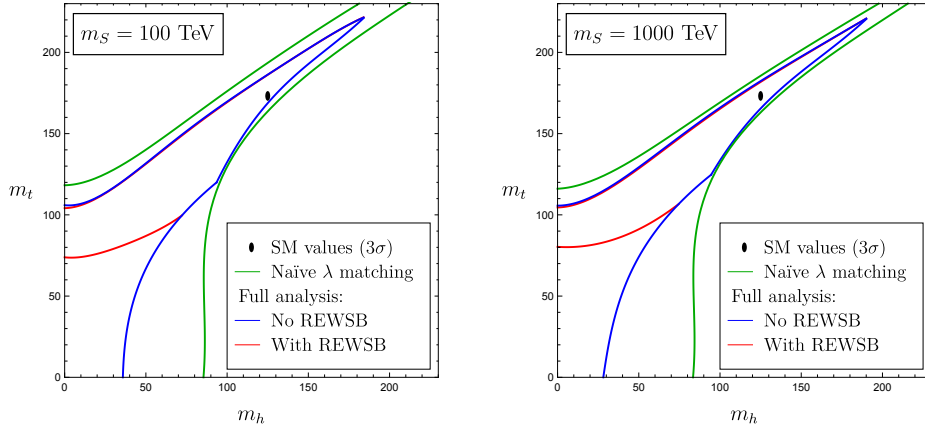
Figure 6.7: Naive viable region (green curves), viable region with (red curves) and without (blue curves) REWSB, for $m_S = 100$ TeV (left plot) and $m_S = 1000$ TeV (right plot).

since $\frac{\mathrm{d}}{\mathrm{d}\mu}g_t(\mu) < 0$, $g_t(m_S)$ (and thus $y_t(m_S)$) decreases as m_S increases. This has two major effects: it reduces the problem concerning a Landau pole for $y_t(\mu)$ and it reduces the influence of $y_t(\mu)$ in the MSSM RG flow.

- As m_S increases, the energy gap with the GUT scale reduces. However, one immediately notice that this is a small effect, since $m_S \approx 10^3 \div 10^6$ GeV while $m_G \approx 10^{16}$ GeV. Therefore, this effect is not expected to play any significant role.

Stated the above remarks, we are ready to compare the results for three different supersymmetry scales: $\{5, 100, 1000\}$ TeV. Such comparison is proposed in Figure 6.8. For reference, in all three plots a dot indicates the physical (m_h, mt) values, thus spotting the physical Standard Model point.

The left plot of Figure 6.8 shows the naive viable region for the three m_S values (solid line: $m_S = 5$ TeV, dashed line: $m_S = 100$ TeV, dotted line: $m_S = 1000$ TeV). The up border presents an overall shift to lower m_t values as m_S increases. The right border presents a similar shift (though milder) for high m_t values, whereas it has a shift to smaller m_h as m_S increases in the low-m_t region.

These features of the borders for of naive viable regions are well explained by the above remarks about $\lambda(\mu)$. The up border (being in the high-m_t region) faces negatives $\lambda(m_S)$ values for lower m_t as m_S increases, causing the overall down shift. The right border present a right (left) shift for high (low) m_t values: provided a longer negative (positive) running for $\lambda(\mu)$, a higher (lower) $\lambda(m_h)$ value can be matched for higher m_S scales.

From the left plot of Figure 6.8 one can infer the overall naive viable region allowed by λ-matching arguments only, for arbitrary supersymmetry scale. For the reasons just explained, the overall up border will correspond to the up border for the lowest m_S value. The overall right border, instead, will be a combination of the right borders for different m_S, the main contributions coming from the lowest m_S value for small m_t and from the highest m_S value for big m_t.

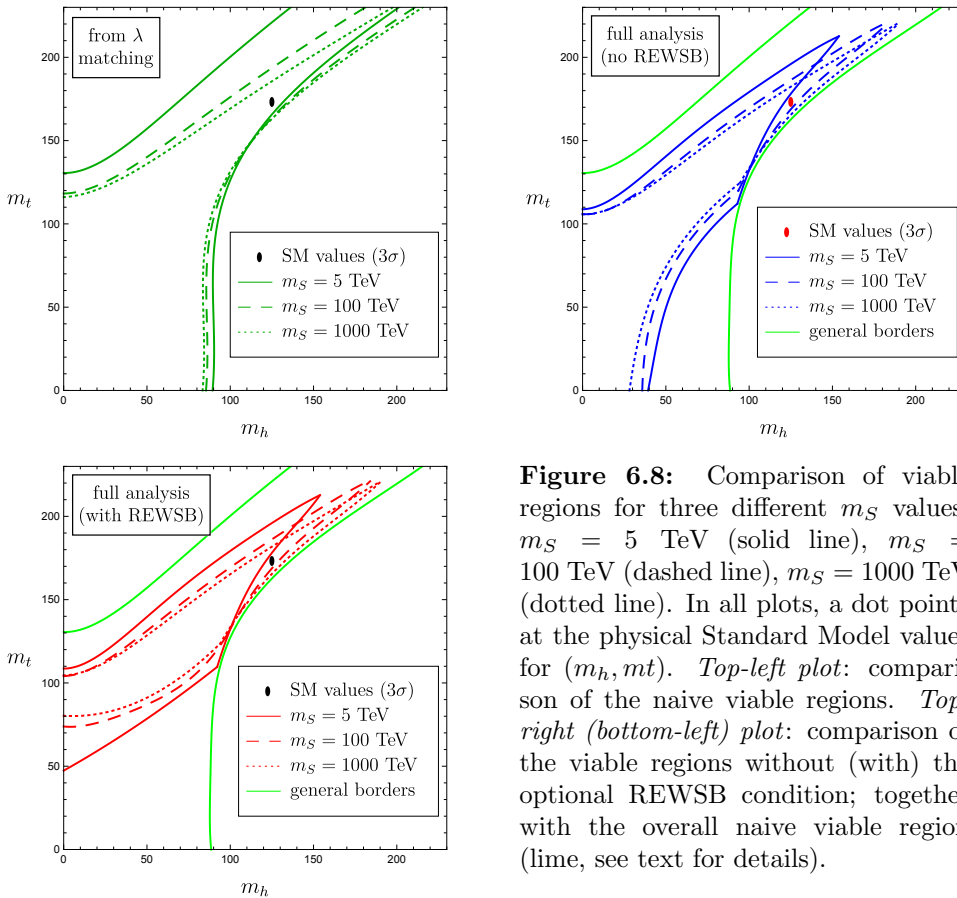In the central plot of Figure 6.8, the viable regions coming from the complete

Figure 6.8: Comparison of viable regions for three different m_S values: $m_S = 5$ TeV (solid line), $m_S = 100$ TeV (dashed line), $m_S = 1000$ TeV (dotted line). In all plots, a dot points at the physical Standard Model values for (m_h, mt). *Top-left plot*: comparison of the naive viable regions. *Top-right (bottom-left) plot*: comparison of the viable regions without (with) the optional REWSB condition; together with the overall naive viable region (lime, see text for details).

analysis (without REWSB condition) are compared. Together with the three blue regions, the overall naive viable region discussed above is superimposed in lime. The down shift of the up border, the right shift of the right border and the left shift of the down border as m_S increases are explained by the same arguments used for the left plot. As an additional remark, the tip of the blue regions not only shifts to higher m_h but also to higher m_t for higher m_S. This is a direct consequence of the remark made above about the $g_t(\mu)$ running: since $y_t(m_S)$ is smaller for higher m_S, the absence of a Landau pole is a less severe constraint and higher m_t values are allowed as m_S increases.

The right plot of Figure 6.8 shows the viable regions coming from the complete analysis including the REWSB condition, together with the overall naive viable region (lime). Together with the features already discussed for the central plot, one can notice a clear up shift of the lowest allowed m_t value as m_S increases. The reason is again to be ascribed to the different values of $y_t(m_S)$ for different m_S, that critically affects the running of $m_{H_u}^2(\mu)$: bigger m_S implies smaller $y_t(m_S)$ and thus smaller $y_t(\mu)$, resulting in a reduced pull-down effect of $y_t(\mu)$ on $m_{H_u}^2(\mu)$ in the infrared due to RG flow, which crucially challenges the REWSB achievement.

It is actually quite puzzling, and perhaps a bit annoying, that the physical Standard Model values for m_h, m_t lie in a spot which results viable for supersymmetry scales spanning from $m_S \gtrsim 5$ TeV up to energies much higher than the ones required
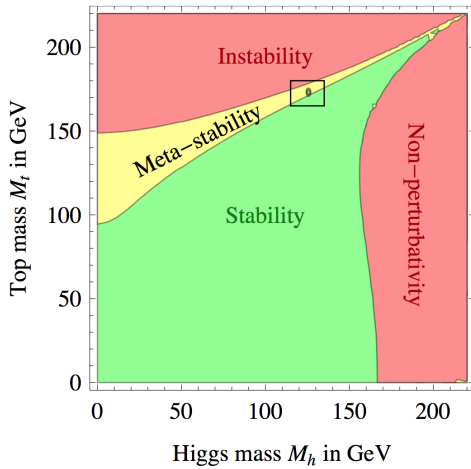
Figure 6.9: Regions of absolute stability, metastability and instability of Standard Model vacuum in the (m_h, m_t) plane (from [120]).
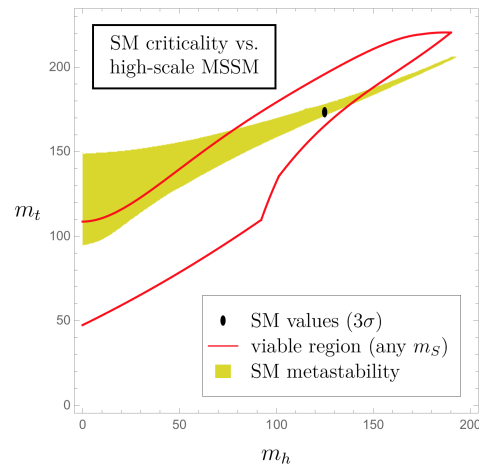
Figure 6.10: Comparison, in the (m_h, m_t) plane, between MSSM viable region (for any m_S) and Standard Model vacuum metastability region.

for gauge coupling unification (actually as high as 10^9 GeV and perhaps even higher).

6.3.4 A comparison with Standard Model vacuum metastability

The point of view we have adopted in this chapter, that is the (m_h, m_t) plane perspective, has been notably used in the literature for another scenario: the Standard Model itself.

Those studies have focused their attention on a fascinating Standard Model feature, that is the instability of the Higgs potential and therefore of the electroweak vacuum [24, 115–120]. An example of such vacuum stability analysis is shown in Figure 6.9 [120]. Intriguingly, we seem to be rather close to the boundary of stability [120–122] and this translates into a very long lifetime (many orders of magnitude larger than the age of the universe) against decay by quantum tunnelling. One therefore concludes that this metastability does not represent an inconsistency of the Standard Model and cannot be used to argue in favour of new physics. The potential instability has also very interesting cosmological implications and might have a deeper significance (see e.g. [123–125] for some attempts in those direction).

It is not in our purposes to give here a thorough review of those studies. The point we would like to stress is that such a peculiar feature of the Standard Model, namely that it has apparently chosen a narrow window of metastability among all the viable (m_h, m_t) choices available, has triggered a rising interest and lots of speculations in recent literature.

With the study we carried out in this chapter, we are now in the position to make a claim of similar philosophy for the MSSM (and somehow more loosely for supersymmetric theories in general). Combining the viable regions for different m_S values (and requiring REWSB), we can infer an overall MSSM viable region for any m_S. According to our analysis, such a region enclose all (m_h, m_t) points which admit an

MSSM parameter configuration satisfying all conditions we imposed: gauge coupling unification, λ-matching, naturalness at the input scale m_G and REWSB.

The resulting overall viable region is shown in Figure 6.10, compared with the Standard Model metastability region of Figure 6.9. As it can be appreciated, we again find an intriguing double criticality of both the m_h and m_t masses, which lie in the narrow window of the MSSM viable region. We claim that such result is not less surprising that the vacuum metastability of the Standard Model, suitable for the same kind of speculations which were proposed for the latter and arguably subjected to even more interesting conclusions.

Conclusion

Though its experimental triumph, the Standard Model of Particle Physics is theoretically unsatisfactory for many reasons. Therefore, since its formulation in the early 1970's a formidable theoretical effort has been undertaken to answer the many open issues left unsolved by such a theory.

Most, if not all, of Standard Model open questions resides in the Higgs sector. Yukawa interactions create a queer and inscrutable pattern of fermion masses and mixing angles, which within the Standard Model cannot but be assumed without explanations. The scalar potential is tuned and unjustified: the Higgs mass scale raises unsolved naturalness issues, the quartic Higgs coupling value results in a mysterious criticality of the electroweak vacuum, the cosmological constant problem itself can be associated with a tuning of the constant scalar potential term. Furthermore, the very Higgs nature (elementary or composite, $SU(2)_L$ doublet or non-linear representations, how many Higgses) is still largely unknown and the possible existence of non-standard Higgs interactions is nowadays widely discussed in the literature.

Undertaking the task of unveiling the mysteries of the Higgs sector, a possibility is to tackle the problem of studying Higgs features and interactions with high precision and minimum theoretical bias. The language of Pseudo Observables (POs) developed in the 1990's to deal with LEP precision measurements [58, 59], being based on the analytical characterisation of on-shell amplitudes, provides the optimal tool to achieve such goal.

For these reason, the Higgs PO (hPO) framework has been developed to fully characterise Higgs production and decays processes relevant for LHC physics [3, 4]. An important effect to be taken into account in collider experiments is the kinematic distortion of spectra due to QED and QCD initial- and final-state radiation (ISR and FSR). To embed such effects into the hPO language is therefore of the utmost importance for precise measurements of PO parameters [8].

In chapter 3, we have provided a clean and general discussion of electrodynamic ISR and FSR effects in the case of fermion currents, being them the most sizeable ones (due to the light fermion masses, especially of electrons). Exploiting theoretical results of the 1960's regarding the factorisation of QED radiative corrections [13–16],

we derived a completely general master formula for the radiator function of a fermion current. Such radiator universally describes ISR and FSR effects due to fermions in terms of its mathematical convolution with the spectrum of the hard process involved, regardless of what such process might be.

As a second step, we focused our attention to $h \to 2e\,2\mu$, a particularly clean and interesting decay channel. In such specific case study, we showed the effectiveness and precision of our formalism. First we reproduced at the percent level, through our radiator function, the up-to-date Standard Model results available in the literature for $h \to 4\ell$ radiative corrections [73]. Second, we applied such formalism within the hPO framework, as an example of its flexibility. As a matter of fact, we could have applied it to a generic new physics scenario, without relying on the hPO formalism which, in this respect, is just a complementary tool.

For scattering processes at energies sufficiently higher than the electroweak scale, W and Z bosons produces kinematic distortion analogous to ISR and FSR in cromo- and electrodynamics. A detailed discussion of such effects within the Standard Model was already present in the literature [23], however a suitable generalisation to new physics scenarios was missing. Furthermore, the above mentioned analysis was relying on a perturbative expansion at leading order in v/E (v being the Higgs v.e.v. and E the energy scale of the process), which was to be push at next-to-leading order to describe the processes we were interested in (Higgsstrahlung).

In chapter 4, we provided a solution to the above shortcomings. In the explicit case of associated Higgs production and focusing on double-logarithmic mass singularities, we first extended at the next-to-leading order in v/E the Standard Model analysis of Ref. [23]. Such a result provides a relevant step forward in the direction of a full next-to-leading order result for electroweak radiative corrections within the Standard Model.

Next, we identified all necessary precautions needed to extend our results to the more general hPO framework, which were summarised in a simple set of rules. Through such rules, we derived completely general expressions for electroweak double-logarithmic mass singularities in associated Higgs production processes. We also characterised the underlying structure of next-to-leading order mixing among different POs, due to their non-trivial relations under $SU(2)_L$ rotation of initial and final states. Once again, the hPO framework should be seen as a complementary tool and our discussion and results for electroweak double-logarithmic mass singularities can as well be adapted to different new physics descriptions.

Another possible direction to investigate the Higgs sector is to adopt a top-down perspective, trying to understand if the Standard Model parameters can be derived from theoretical speculations on well-motivated new physics scenarios. On this regard, supersymmetry unquestionably represents an appealing Beyond Standard Model proposal. It possesses many mathematical properties which furnish flourishing premises for fascinating theoretical speculations such as supergravity and string theory. It also displays intriguing features such as gauge coupling unification, which opens the possibility of Grand Unified Theories.

Most of all, supersymmetry could shed light on the structure of the Higgs scalar potential, since supersymmetric theories predict it in terms of the other Lagrangian

parameters. In these contexts, the quartic Higgs coupling (λ) should therefore be seen as fixed from other theory features, instead of an input parameter (with mysterious features within the Standard Model). Furthermore, if the supersymmetry-breaking scale is taken sufficiently near the electroweak scale, such theories provides a clear-cut solution to the hierarchy problem, a feature which has made the fortune of supersymmetry in the past decades.

Even disregarding naturalness considerations, to impose the quartic Higgs coupling to match its supersymmetry prediction (a procedure we called λ-matching) is actually a non-trivial condition. By analysing the feasibility of such requirement for different values of λ (and therefore of the Higgs mass), intriguing considerations can be made regarding the peculiarities of its physical value chosen by nature. Several investigations in this direction were already present in the literature (see e.g. [24–26]).

In chapter 6, the above and other considerations were gathered together to perform an investigation of the feasibility of the Minimal Supersymmetric Standard Model (MSSM) for different values of both λ and the top-Yukawa coupling (g_t). The reason to include the top Yukawa among the interesting parameters to be scanned were several: it has a major influence on the renormalisation group flow of the MSSM parameters, it give sizeable contributions to the one-loop λ-matching conditions and its physical value makes the top-quark mass (m_t) arguably as peculiar as the Higgs mass (m_h) itself.

Adopting such original (m_h, m_t) plane perspective, the MSSM parameter space was explored, searching for "natural" parameter configurations at the input scale (that we assumed to be the GUT scale) which allow for concomitant gauge coupling unification, electroweak symmetry breakdown and satisfactory λ-matching. The imposition of a suitably defined "natural" spectrum for the soft breaking terms at high scales, rather than at the low supersymmetry breaking scale, was technically more involved but definitely more legitimate and was another major novelties of our approach.

We found out that the above requirements highly constrain the viable MSSM region in the (m_h, m_t) plane. Interestingly enough, the physical Standard Model values put themselves almost at the upper border of such region, revealing the peculiarity not only of the Higgs mass (as already pointed out in the literature) but also of the top-quark mass. Furthermore, it is intriguing (though unfortunate) to notice that the physical m_h, m_t values do not allow to put sensible constraints to the supersymmetry scale itself.

Our novel approach also allowed us to investigate another fascinating feature of supersymmetric theories, the possibility of Radiative Electroweak Symmetry Breakdown (REWSB) [108, 109]. In such scenarios, the electroweak symmetry is unbroken at the input scale and its breakdown at lower energies is triggered by radiative effects. As was reasonable to presume, such additional requirement sets a lower limit on m_t, below which the influence of the top Yukawa on the renormalisation group flow of the soft breaking terms is insufficient to trigger the necessary radiative effects needed for REWSB achievement.

Gathering together the obtained results, we were finally able to derive the general viable MSSM region in the (m_h, m_t) plane. We observed that such a region is not much bigger than the Standard Model electroweak vacuum metastability region,

which has triggered so much theoretical attention over the past years [24, 115–125]. As a final remark, we advocated that our results are not less intriguing than the above mentioned ones regarding Standard Model cosmological metastability, suitable for the same kind of speculations and arguably subjected to even more interesting conclusions.

Acknowledgements

Scientific acknowledgements

I would like to express my gratitude to the colleagues who contributed in different ways to the research projects this dissertation consists of, in primis to my supervisor G. Isidori. I am also thankful to A. Greljo and D. Marzocca for many clarifications of the original articles dealing with Higgs pseudo observables parametrisation. I should acknowledge M. Bordone, with whom part of the work exposed in chapter 3 was performed. I am deeply grateful to S. Pozzorini, with whom I had countless discussions regarding electroweak mass singularities, without which I would never had been able to achieve the results exposed in chapter 4. I would also like to thank D. Guadagnoli for his very useful comments on chapter 3 and R. Zwicky for his interest and feedbacks on the results exposed in appendix A.

My research activity has been broader than just the arguments exposed in this dissertation. On this regard, it would be profoundly unfair not to thank F. Feruglio and P. Paradisi for our numerous and fruitful scientific collaborations. I am quite regretful not to have discussed here any of our works, but a topic was to be chosen and some articles unavoidably to be excluded. I beg their pardon for such injustice.

Personal acknowledgements

My gratitude toward Ferruccio, Gino and Paride (listed, as everybody else, in strict alphabetical order) extends far beyond the boundaries of our scientific collaborations. My years as a Ph.D. candidate have been formative as I would have never imagined them to be and I am deeply grateful to enjoy their esteem, which I wholeheartedly return. My poor command of English is the only thing that stops me from more lengthy and appropriate thanksgivings.

I must thank all members of Gino's theory group but in particular Admir and David, with whom I shared the office for three years and had innumerable discussions virtually about everything, from US presidential elections to the math of the perfect juggle. Talking about discussions I must thank also Dario, with whom I shared the questionable delight of contradicting each other almost on purpose on any possible occasion.

Coming to the unavoidable sentimentalisms, I must express how important for me have been the unconditional support of my parents, Gabriella and Marco, and the affection of my sister, Silvia. I probably owe them more than what I think. Last but absolutely not least, I would like to thank Marta to an extent hard to achieve within an acknowledgement paragraph and with an intimacy definitely too personal for an acknowledgement paragraph. I hope she already knows how important she has been and still is to me.

Complements to Chapter 3

A.1 Non-interference of fermion current bremsstrahlung

In this appendix we explicitly prove the non-interference of the bremsstrahlung from a neutral fermion current with other amplitudes with same final state, as claimed in chapter 3, section 3.2.1. More precisely, we want to show that the interference between the two real emission diagrams in Figure A.1 vanishes in leading logarithmic approximation (LLA). This will be proved rigorously for soft divergences (single- and double-logarithmic), while as far as single-logarithmic collinear singularities are concerned we will limit ourselves to few important remarks.

First of all, we exploit the Kinoshita–Lee–Nauenberg (KLN) theorem [10, 11] to relate such real emission interference terms with a one-loop diagram. We can indeed exploit such theorem to state that:

$$2\,\mathrm{Re}\left(\ \cdot\ +\ \cdot\ \right)_{\mathrm{LLA}} = 0\ . \quad \text{(A.1)}$$

If we show that the virtual contribution is infrared-safe on its own, we can end our proof concluding that both addends on the left-hand side of Eq. (A.1) individually vanish in LLA.

The virtual contribution in Eq. (A.1) is given by the two diagrams depicted in Figure A.2. There, $\mathcal{G}_{\mu\alpha}$ is the Green function describing the hard process plus an additional photon leg. Details on the expression for such correlation function will be later derived. For the moment it is sufficient to observe that it is generally a function of a set of (irrelevant) kinematic variables $\{b_i\}$, of photon's outgoing momentum k and fermion current momentum q: $\mathcal{G}_{\mu\alpha}(\{b_i\}, k, q)$.

Calling $\mathcal{M}_a$ and $\mathcal{M}_b$ the amplitudes corresponding to diagrams in Figure A.2.a and A.2.b respectively, their explicit expressions read:

$$\begin{bmatrix} \mathcal{M}_a \\ \mathcal{M}_b \end{bmatrix} = \int \frac{\mathrm{d}^4 k}{(2\pi)^4}\, \mathcal{G}_{\mu\alpha}(\{b_i\}, k, q)\, D^{\alpha\beta}(k) \cdot \bar{u}_f(p_1) \begin{bmatrix} \gamma_\beta\, \frac{\slashed{p}_1 - \slashed{k} + m}{(p_1 - k)^2 - m^2}\, \Gamma^\mu \\ \Gamma^\mu\, \frac{-\slashed{p}_2 + \slashed{k} + m}{(p_2 - k)^2 - m^2}\, \gamma_\beta \end{bmatrix} v_f(p_2)\ ,$$
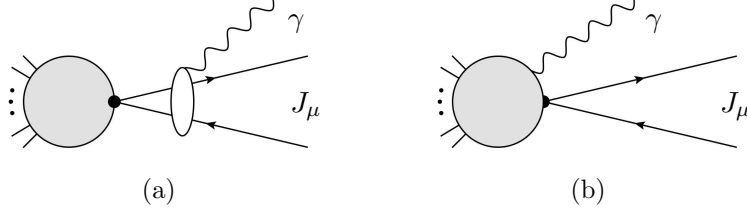
$$\text{(A.2)}$$

Figure A.1: The two classes of photon emission diagrams which are shown not to interfere in LLA. Diagram (a) depicts bremsstrahlung from the neutral current J_μ. Diagram (b) depicts a photon emission from a different part of the process, regardless whether from another external leg or not.
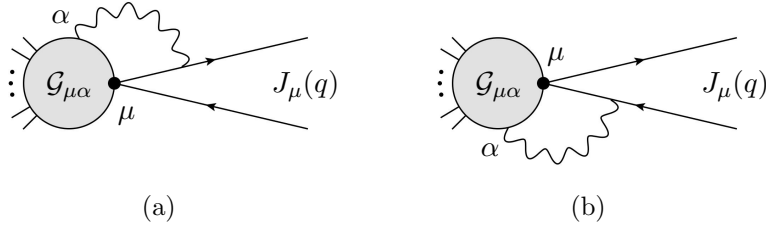

Figure A.2: The two loop diagrams contributing to the virtual term on the left-hand side of Eq. (A.1). One photon propagator's end is attached to either of the two fermions of J_μ and the other to the rest of the hard process. In $\mathcal{G}_{\mu\alpha}$ a sum over all possible ways with which the virtual photon can be connected to the hard process is understood, further details are irrelevant for the validity of the argument.

where $\Gamma^\mu = \gamma_\mu(v + a\,\gamma_5)$ generalises the notation used in chapter 3, where J^μ is either a left- ($v = -a = 1/2$) or right-handed ($v = a = 1/2$) vector current. $D^{\alpha\beta}(k)$ is the photon propagator, whose momentum has been chosen for convenience to be equal to the loop momentum. The (anti)fermion f, $(\bar f)$ has spinor u_f (v_f), momentum p_1 (p_2) and mass m.

The amplitudes $\mathcal{M}_{a,b}$ in Eq. (A.2) give rise to soft divergences in the soft-k region, where both the $\not k$ term in the numerator and the k^2 term in the denominator can be neglected. In such (eikonal) approximation, our one-loop amplitudes read:

$$\left[\begin{array}{c} \mathcal{M}_a \\ \mathcal{M}_b \end{array}\right]_{\text{eik}} = \int \frac{\mathrm{d}^4 k}{(2\pi)^4}\, \mathcal{G}_{\mu\alpha}(\{b_i\}, k, q)\, D^\alpha_{\ \beta}(k) \left[\begin{array}{c} -\frac{p_1^\beta}{p_1 \cdot k} \\ \frac{p_2^\beta}{p_2 \cdot k} \end{array}\right] \bar u_f(p_1)\Gamma^\mu v_f(p_2)\,, \qquad (A.3)$$

once the equations of motion $(\not p - m)u(p) = (\not p + m)v(p) = 0$ are exploited.

The $\mathcal{O}(\alpha)$ virtual contribution to $|\mathcal{M}|^2$ is found by interference of $\mathcal{M}_a + \mathcal{M}_b$ with the tree-level amplitude,

$$\mathcal{M}_{\text{tree}} = \tilde{\mathcal{G}}_\mu(\{b_i\}, q) \cdot \bar u_f(p_1)\, \Gamma^\mu\, v_f(p_2)\,, \qquad (A.4)$$

where there is no need to further specify $\tilde{\mathcal{G}}_\mu$ and, from now on, the explicit dependence of $\mathcal{G}_{\mu\alpha}$, $\tilde{\mathcal{G}}_\mu$ upon $\{b_i\}$ will be omitted to reduce the notation clutter. In the soft-k limit an summing over fermion polarisations, such interference term reads

$$(\mathcal{M}_a + \mathcal{M}_b)\mathcal{M}_{\text{tree}}^* = \int \frac{\mathrm{d}^4 k}{(2\pi)^4}\, \mathcal{G}_{\mu\alpha}(k, q)\, \tilde{\mathcal{G}}_\nu^*(q)\, D^\alpha_{\ \beta}(k) \left(\frac{p_2^\beta}{p_2 \cdot k} - \frac{p_1^\beta}{p_1 \cdot k}\right) T^{\mu\nu}\,, \qquad (A.5)$$

with

$$T^{\mu\nu} = \text{Tr}\left[(\slashed{p}_1 + m)\Gamma^{\mu}(\slashed{p}_2 - m)\Gamma^{\nu}\right]$$
$$= 4\left((v^2+a^2)(p_1^{\mu}p_2^{\nu} + p_1^{\nu}p_2^{\mu} - p_1{\cdot}p_2\,g_{\mu\nu}) - m^2(v^2-a^2)g_{\mu\nu} + 2\,i\,a\,v\,\epsilon^{\mu\nu\rho\sigma}p_{1\rho}p_{2\sigma}\right)\,. \tag{A.6}$$

Integrating Eq. (A.5) over the phase space $\mathrm{d}\Phi\left(\{b_i\}, p_1, p_2\right)$, which is obviously symmetric in the $p_1 \leftrightarrow p_2$ exchange, it is clear that only the piece of $T^{\mu\nu}$ antisymmetric in $p_1 \leftrightarrow p_2$ survives. Therefore:

$$\int \mathrm{d}\Phi\,(\mathcal{M}_a + \mathcal{M}_b)\mathcal{M}_{\text{tree}}^* = \int \mathrm{d}\Phi \int \frac{\mathrm{d}^4 k}{(2\pi)^4}\,\mathcal{G}_{\mu\alpha}(k,q)\,\tilde{\mathcal{G}}_{\nu}^*(q)\,D^{\alpha}{}_{\beta}(k) \times$$
$$\times \left(\frac{p_2^{\beta}}{p_2 \cdot k} - \frac{p_1^{\beta}}{p_1 \cdot k}\right) 8\,i\,a\,v\,\epsilon^{\mu\nu\rho\sigma}p_{1\rho}p_{2\sigma}\,. \tag{A.7}$$

The integral above lead to soft divergences only for the $\mathcal{G}_{\mu\alpha}(k,q)$ contributions with asymptotic $\mathcal{G}_{\mu\alpha}(k,q) \sim 1/\sqrt{k^2}$ behaviour. As a direct consequence of the KLN and the Low theorem[1] [13–16], such contributions are necessarily proportional to the tree level amplitude itself,

$$\mathcal{G}_{\mu\alpha}(k,q) = S_{\alpha}(q,k)\,\tilde{\mathcal{G}}_{\mu}(q) + \mathcal{O}\left((k^2)^0\right)\,, \qquad S_{\alpha} \sim \frac{1}{\sqrt{k^2}}\,, \tag{A.8}$$

and S_{α} real. Now, it is easy to realise that the real part of the soft-divergent interference term (A.7) is zero, being the contraction of a piece symmetric in (μ, ν) with the Levi–Civita tensor $\epsilon^{\mu\nu\rho\sigma}$.

Our proof that soft-divergent contributions of amplitudes (A.2) vanish has relied heavily on the soft photon approximation, which provided us with identity (A.8) and therefore (loosely speaking) with the evenness in (μ, ν) of $\mathcal{G}_{\mu\alpha}\tilde{\mathcal{G}}_{\nu}$. If we repeat our previous argument in the collinear limit, $k^{\mu} = x\,p_{1,2}^{\mu} + \epsilon^{\mu}$ and $p_{1,2}^2 = 0$, we eventually get

$$\int \mathrm{d}\Phi\,(\mathcal{M}_a + \mathcal{M}_b)\mathcal{M}_{\text{tree}}^* = \int \mathrm{d}\Phi \int \frac{\mathrm{d}^4 k}{(2\pi)^4}\,\mathcal{G}_{\mu\alpha}(k,q)\,\tilde{\mathcal{G}}_{\nu}^*(q)\,D^{\alpha}{}_{\beta}(k)\,(x-1) \times$$
$$\times \left(\frac{2\,p_2^{\beta}}{k^2 - p_2 \cdot k} - \frac{2\,p_1^{\beta}}{k^2 - p_2 \cdot k}\right) 8\,i\,a\,v\,\epsilon^{\mu\nu\rho\sigma}p_{1\rho}p_{2\sigma}\,. \tag{A.9}$$

Though the above expression resembles Eq. (A.7), we are not anymore able to argue a general cancellation of IR divergences. Nevertheless, one can appreciate the highly constrained structure that the possibly surviving collinear singularities must assume according to our general argument.

---

[1] To be politically correct, the Low–Burnett–Kroll–Goldberger–Gell-Mann soft theorem.

B.1 Standard Model trilinear Feynman rules

From discussion of section 4.2 clearly emerges that only trilinear Standard Model Feynman rules are needed to evaluate DL mass singularities. In this appendix, we introduce and explain the compact notation (involving the I^V and Υ^Φ matrices) used in chapter 4 to parametrise those trilinear vertices.

The Standard Model Feynman rules will be stated here without derivation. The consistency of our conventions can be easily checked by comparison with the existing literature (see e.g. [126]).

B.1.1 Gauge interactions and the $I^V_{\varphi_i \varphi_j}$ matrices

Through chapter 4 we have used matrices I^V to parametrise the trilinear gauge interactions, i.e. those interactions which arises from the Standard Model gauge sector (and thus do not feature a dependency upon the v.e.v. v), following the notation in Ref. [23].
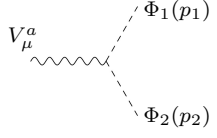
In fact, matrices I^V are just the generators of the $SU(2) \times U(1)$ gauge group, which can be expressed in terms of the electric charge Q and the weak isospin T^a as

$$I^A = -Q \ , \qquad I^Z = \frac{T^3 - s_W^2 Q}{s_W c_W} \ , \qquad I^\pm = \frac{T^1 \pm T^2}{\sqrt{2}\, s_W} \ , \tag{B.1}$$
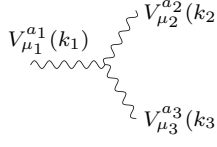
where s_W and c_W are the sine and cosine of the Weinberg angle θ_W, respectively.

Due to above definitions and normalisations, $ieI^V_{\varphi_1 \varphi_2}$ always corresponds to the coupling of the gauge vertex $V\bar{\varphi}_1\varphi_2$, where all fields are incoming. The exact expressions for the relevant Feynman rules are:

$$= i\, e\, I^{V^a}_{f_2 f_1} \, \gamma_\mu \ , \tag{B.2}$$

$$\text{(diagram)} = i\,e\,I^{V^a}_{\Phi_1\Phi_2}(p_2 - p_1)_\mu \ , \tag{B.3}$$

$$\text{(diagram)} = -i\,e\,I^{V^{a_1}}_{V^{a_2}V^{a_3}}\left[\eta_{\mu_1\mu_2}(k_1 - k_2)_{\mu_3} + \eta_{\mu_2\mu_3}(k_2 - k_3)_{\mu_1}\right. \tag{B.4}$$
$$\left. +\eta_{\mu_3\mu_1}(k_3 - k_1)_{\mu_2}\right] \ ,$$

where all particle and momenta are incoming.

For reference, we report below also the explicit values for the I^V matrices.

- Fermions.

$$I^A_{f_1 f_1} = -Q_{f_1} \ ,$$
$$I^Z_{f_1 f_1} = \frac{1}{s_W c_W}(T^3 - s_W^2 Q)_{f_1} \ ,$$
$$I^{W^\pm}_{f_1 f_2} = \begin{cases} \frac{1}{\sqrt{2}\,s_W} & \text{if } Q_{f_1} - Q_{f_2} = \pm 1 \ \text{and } f_{1,2} \text{ left handed} \\ 0 & \text{otherwise} \end{cases} \ . \tag{B.5}$$

For matrix elements involving antifermions $\bar{f}$, one should exploit the relation

$$I^V_{\bar{f}_1 \bar{f}_2} = -I^{\bar{V}}_{f_1 f_2} \ . \tag{B.6}$$

- Scalars. Defining our basis as $\{h, \phi_Z, \phi_+, \phi_-\}$, matrices $I^V_{\phi_1\phi_2}$ reads:

$$I^A = \begin{bmatrix} 0 & & & \\ & 0 & & \\ & & -1 & \\ & & & 1 \end{bmatrix} \ , \qquad I^{W^+} = \frac{1}{2s_W}\begin{bmatrix} 0 & 0 & 0 & -1 \\ 0 & 0 & 0 & -i \\ 1 & i & 0 & 0 \\ 0 & 0 & 0 & 0 \end{bmatrix} \ ,$$
$$\tag{B.7}$$
$$I^Z = \frac{1}{2s_W c_W}\begin{bmatrix} 0 & -i & & \\ i & 0 & & \\ & & \omega & \\ & & & -\omega \end{bmatrix} \ , \quad I^{W^-} = \left(I^{W^+}\right)^\dagger \ ,$$

where $\omega = c_W^2 - s_W^2$.

- Vectors.

$$I^{V^a}_{\bar{V}^c V^b} = \begin{cases} (-)^{p+1} & \text{if } V^a V^b V^c = \pi(AW^+W^-) \\ (-)^p \frac{c_W}{s_W} & \text{if } V^a V^b V^c = \pi(ZW^+W^-) \\ 0 & \text{otherwise} \end{cases} \ , \tag{B.8}$$

where $(-)^p$ is the sign of the permutation π and care must be taken for the first lower index $\bar{V}^c$ which is charged conjugate.

B.1.2 $VV\Phi$ vertices and the $\Upsilon^{\Phi}_{V_i V_j}$ matrices

The $VV\Phi$ trilinear interactions, arising from the EWSB of the theory and thus featuring a v dependence in their Feynman rules, have been parametrised using the $\Upsilon^{\Phi}_{V_i V_j}$ matrices. These matrices are formally defined through the I^V matrices as

$$\Upsilon^{\Phi}_{V_i V_j} \equiv \left\{ I^{\bar{V}_i}, I^{V_j} \right\}_{h\Phi} . \tag{B.9}$$

From the above definition follows that $ie^2 v \Upsilon^{\Phi}_{V_1 V_2} \eta_{\mu\nu}$ is the Feynman rule associated to the vertex $\Phi \bar{V}_1 V_2$, where all fields are incoming. Explicitly:

$$\Phi \cdots \begin{Bmatrix} V_1^\mu \\ V_2^\nu \end{Bmatrix} = i\, e^2\, v\, \Upsilon^{\Phi}_{V_1 V_2}\, \eta_{\mu\nu} . \tag{B.10}$$

The explicit values of the non-vanishing $\Upsilon^{\Phi}_{V_1 V_2}$ matrix elements, derivable from Eq. (B.9), read:

$$\Upsilon^{\phi^\pm}_{W^\pm Z} = \left\{ I^{W^\mp}, I^Z \right\}_{h\phi^\pm} = -\frac{1}{2\,c_W} , \quad \Upsilon^h_{W^\pm W^\pm} = \left\{ I^{W^\mp}, I^{W^\pm} \right\}_{hh} = \frac{1}{2\,s_W^2} ,$$

$$\Upsilon^{\phi^\pm}_{W^\pm A} = \left\{ I^{W^\mp}, I^A \right\}_{h\phi^\pm} = -\frac{1}{2\,s_W} , \qquad \Upsilon^h_{ZZ} = \left\{ I^Z, I^Z \right\}_{hh} = \frac{1}{2\,c_W^2 s_W^2} . \tag{B.11}$$

Of course we have $\Upsilon^{\phi}_{\bar{V}_1 V_2} = \Upsilon^{\phi}_{\bar{V}_2 V_1}$. Finally, it is immediate to verify that

$$M^2_{V^a} = \frac{1}{2} e^2\, v^2\, \Upsilon^h_{V^a V^a} . \tag{B.12}$$

B.2 Explicit results for DL mass singularities in Vh production

We list here the explicit results for the double-logarithmic (DL) electroweak mixing of POs. These are expressed in terms of the linear mixing matrices Λ^L, Λ^T, Λ^{CP}, Λ^f and of the non-linear mixing terms N^L, N^T, N^f. In addition, the expressions for the form factors Δ_T and $\tilde{\Delta}_T$, genuinely arising at next-to-leading order in v/E_{tot}, are also given.

As explained in chapter 4, the explicit expressions for the Λ and N elements are different for each of the six processes $f_1 \bar{f}_2 \to Vh$ in Eq. (4.16). Nevertheless, a common expression for them can be found leaving the f_1, f_2 couplings with the A and Z bosons (i.e. I^A and I^Z) implicit. In order to do so, we should introduce a short-cut notation for the $f_1 \bar{f}_2 \to Vh$ process: $q = f_1$, r its $SU(2)_L$ partner (for f_1 left-handed), $(-)^q$ the charge sign of q and $\delta_{qL} = 1$ for f_1 left-handed, $\delta_{qL} = 0$ otherwise. Such rather cumbersome (but necessary) notation is summarised in Table B.1.

Furthermore, we define the following invariants encoding the double logarithms:

$$\xi^S_q = I^{Z\,2}_{qq} \log^2\left(\frac{S}{m_V^2}\right) + I^{A\,2}_{qq} \left(\log^2\left(\frac{S}{\lambda^2}\right) - \log^2\left(\frac{m_q^2}{\lambda^2}\right)\right) , \tag{B.13}$$

	$u_L \bar{u}_L$	$u_R \bar{u}_R$	$d_L \bar{d}_L$	$d_R \bar{d}_R$	$d_L \bar{u}_L$	$u_L \bar{d}_L$
$f_1 \bar{f}_2$						
q	u_L	u_R	d_L	d_R	d_L	u_L
r	d_L		u_L		u_L	d_L
$(-)^q$	$+$	$+$	$-$	$-$	$-$	$+$
δ_{qL}	1	0	1	0		

Table B.1: Summary, for the six different processes $f_1 \bar{f}_2 \to Vh$, of the values for the q, r indices and the $(-)^q$, δ_{qL} invariants appearing in the expressions of appendix B.2.

$$\xi_W^S = \frac{1}{2s_W^2} \log^2 \left(\frac{S}{m_V^2} \right) \ , \tag{B.14}$$

$$\xi_{qr}^{TU} = I_{rr}^Z \log^2 \left(\frac{T}{m_V^2} \right) - I_{qq}^Z \log^2 \left(\frac{U}{m_V^2} \right) \ , \tag{B.15}$$

$$\xi_{\pm}^{TU} = \log^2 \left(\frac{T}{m_V^2} \right) \pm \log^2 \left(\frac{U}{m_V^2} \right) \ , \tag{B.16}$$

$$\xi_{qr}^{STU} = -\frac{2}{9} \mathrm{DL}(S, A, q, r) + (-)^q \left(I_{rr}^A \mathrm{DL}(U, A, q, W) - I_{qq}^A \mathrm{DL}(T, A, r, W) \right) \ , \tag{B.17}$$

with $\mathrm{DL}(\ldots)$ defined in Eq. (4.14).

Exploiting the notation discussed above, the entries of the Λ^L, Λ^T, Λ^{CP} matrices read:

$$\Lambda_{ZZ}^L = \Lambda_{ZZ}^T = \Lambda_{ZZ}^{CP} = - \left[\xi_q^S + \delta_{qL} \frac{I_{rr}^Z}{I_{qq}^Z} \xi_W^S \right] \ , \tag{B.18}$$

$$\Lambda_{ZW}^L = \frac{1}{c_W^2} \Lambda_{ZW}^T - \frac{1}{I_{qq}^Z} \left(\frac{s_W}{c_W} I_{qq}^A + (-)^q \delta_{qL} \frac{s_W^2 - c_W^2}{2 s_W c_W} \right) \xi_W^S \ , \tag{B.19}$$

$$\Lambda_{ZW}^T = \Lambda_{ZW}^{CP} = -(-)^q \delta_{qL} \frac{c_W^3}{2 s_W^3} \frac{1}{I_{qq}^Z} \xi_+^{TU} \ , \tag{B.20}$$

$$\Lambda_{Z\gamma}^T = -\Lambda_{Z\gamma}^{CP} = \frac{I_{qq}^A}{I_{qq}^Z} \xi_q^S + \delta_{qL} \frac{I_{rr}^A}{I_{qq}^Z} \xi_W^S \ , \tag{B.21}$$

$$\Lambda_{WW}^L = \Lambda_{WW}^T + \frac{1}{2} \xi_W^S - (-)^q \frac{1}{6 c_W^2} \xi_-^{TU} \ , \tag{B.22}$$

$$\Lambda_{WW}^T = \Lambda_{WW}^{CP} = -(-)^q \frac{c_W}{s_W} \xi_{rq}^{TU} - 2 s_W^2 I_{qq}^Z I_{rr}^Z \xi_W^S - \xi_{,}^{STU} \tag{B.23}$$

$$\Lambda_{WZ}^L = (-)^q \frac{1}{c_W s_W} \xi_{qr}^{TU} - \frac{s_W^2 - c_W^2}{2 c_W^2} \xi_W^S \ , \tag{B.24}$$

$$\Lambda_{WZ}^T = \Lambda_{WW}^{CP} = (-)^q \frac{1}{c_W s_W} \xi_{qr}^{TU} \ . \tag{B.25}$$

The entries of the Λ^f matrix read instead:

$$\Lambda_{[qq],[qq]}^f = -\xi_q^S \ , \tag{B.26}$$

$$\Lambda^f_{[qq],[rr]} = -\delta_{qL}\,\xi^S_W \;, \tag{B.27}$$

$$\Lambda^f_{[qq],[qr]} = -\frac{1}{2\sqrt{2}c_W s^2_W}\,(-)^q\,\delta_{qL}\,\xi^{TU}_+ \;, \tag{B.28}$$

$$\Lambda^f_{[qr],[uu]} = \frac{c_W}{4\sqrt{2}s^2_W}((-)^q\xi^{TU}_- - \xi^{TU}_+) \;, \qquad \Lambda^f_{[qr],[dd]} = \frac{c_W}{4\sqrt{2}s^2_W}((-)^q\xi^{TU}_- + \xi^{TU}_+) \;, \tag{B.29}$$

$$\Lambda^f_{[qr],[qr]} = -\xi^{STU}_{qr} + (-)^q\,\frac{s^2_W - c^2_W}{2s_W c_W}\xi^{TU}_{rq} - 2s^2_W I^Z_{qq}I^Z_{rr}\,\xi^S_W \;. \tag{B.30}$$

Finally, the entries of the non-linear mixing terms N are:

$$N^L_Z = N^f_Z = -\frac{1}{2c^2_W}\,\xi^S_W \;, \qquad\qquad N^L_W = N^f_W = -\frac{1}{2}\,\xi^S_W \;, \tag{B.31}$$

$$N^T_{Z,[f_1 f_1]} = -\delta_{f_1 q}\,\frac{1}{e\,c^2_W I^Z_{qq}}\,\xi^S_W \;, \qquad\qquad N^T_{W,[f_1 f_2]} = -\delta_{f_1 q}\,\frac{\sqrt{2}s_W}{e}\,\xi^S_W \;. \tag{B.32}$$

Regarding the additional form factors Δ_T and $\tilde{\Delta}_T$, their expression for neutral current processes read:

$$\Delta_T\big|_{q\bar{q}\to Zh} = \frac{\alpha}{4\pi}\,(-)^q\,\delta_{qL}\,\frac{s^2_W - c^2_W}{2\sqrt{2}c_W s^2_W}\left(\frac{1}{T}\log^2\left(\frac{T}{m^2_V}\right) + \frac{1}{U}\log^2\left(\frac{U}{m^2_V}\right)\right)\epsilon^{u_L d_L}_W \;, \tag{B.33}$$

$$\tilde{\Delta}_T\big|_{q\bar{q}\to Zh} = \frac{\alpha}{4\pi}\,(-)^q\,\delta_{qL}\,\frac{s^2_W - c^2_W}{2\sqrt{2}c_W s^2_W}\left(\frac{1}{T}\log^2\left(\frac{T}{m^2_V}\right) - \frac{1}{U}\log^2\left(\frac{U}{m^2_V}\right)\right)\epsilon^{u_L d_L}_W \;, \tag{B.34}$$

and one can indeed verify that $\lim_{U\to T}\tilde{\Delta}_T = 0$, as discussed in chapter 4 (see section 4.3.2, footnote 9). The expressions for charged current processes read instead:

$$\Delta_T\big|_{q\bar{r}\to Wh} = \frac{\alpha}{4\pi}\,(-)^q\left[\frac{c_W}{2\sqrt{2}s^2_W}\left(\frac{\epsilon^{rr}_Z}{T}\log^2\left(\frac{T}{m^2_V}\right) - \frac{\epsilon^{qq}_Z}{U}\log^2\left(\frac{U}{m^2_V}\right)\right)\right.$$
$$\left. - \frac{\epsilon^{qr}_W}{s_W c_W}\left(\frac{I^Z_{qq}}{T}\log^2\left(\frac{T}{m^2_V}\right) - \frac{I^Z_{rr}}{U}\log^2\left(\frac{U}{m^2_V}\right)\right)\right] \;, \tag{B.35}$$

$$\tilde{\Delta}_T\big|_{q\bar{r}\to Wh} = \frac{\alpha}{4\pi}\,(-)^q\left[\frac{c_W}{2\sqrt{2}s^2_W}\left(\frac{\epsilon^{rr}_Z}{T}\log^2\left(\frac{T}{m^2_V}\right) + \frac{\epsilon^{qq}_Z}{U}\log^2\left(\frac{U}{m^2_V}\right)\right)\right.$$
$$\left. - \frac{\epsilon^{qr}_W}{s_W c_W}\left(\frac{I^Z_{qq}}{T}\log^2\left(\frac{T}{m^2_V}\right) + \frac{I^Z_{rr}}{U}\log^2\left(\frac{U}{m^2_V}\right)\right)\right] \;. \tag{B.36}$$

C.1   Analytic solutions of the one-loop MSSM RG flow

In this appendix, we describe some analytical solutions of the renormalisation group (RG) equations, which turned out to be extremely useful to drastically reduce the running time of the scan described in chapter 6, section 6.2.2.

We first present some useful results that can be obtained by simple integrations of the RG equations for gauge couplings ($g_{1,2,3}$), supersymmetric top-Yukawa coupling (y_t) and gauginos' masses ($M_{1,2,3}$). Exploiting those results, analytical solutions for the RG flow of the soft parameters A_t, $m^2_{Q_3,u_3}$, $m^2_{H_{u,d}}$, μ, b are proved and its effectiveness for our scan is explained.

Along this appendix, we will express the RG equations in terms of the logarithmic parameter $t = \log(\mu/\mu_0)$, with μ the RG scale. Furthermore, we will use κ to denote the omnipresent loop factor

$$\kappa = \frac{1}{16\pi^2} \ . \tag{C.1}$$

C.1.1   Useful preliminary results

The RG equations for the gauge couplings were given in Eq. (5.40):

$$\frac{\mathrm{d}}{\mathrm{d}t}g_a = \kappa \, b_a \, g_a^3 \ , \qquad (b_1, b_2, b_3) = \left(\frac{33}{5}, 1, -3\right) \ , \tag{C.2}$$

which can be generalised in

$$\frac{\mathrm{d}}{\mathrm{d}t}g_a^\gamma = \kappa \, \gamma \, b_a \, g_a^{\gamma+2} \tag{C.3}$$

for $\gamma \neq 0$. Translating Eqs. (C.2), (C.3) into integral equations, one gets:

$$\int_{t_0}^{t} \mathrm{d}s \, g_a^2(s) = \frac{1}{k \, b_a} \log \frac{g_a^2(t)}{g_a^2(t_0)} \ , \tag{C.4}$$

$$\int_{t_0}^{t} \mathrm{d}s \, g_a^{\gamma}(s) = \frac{1}{k \, b_a(\gamma - 2)} \left(g_a^{\gamma-2}(t) - g_a^{\gamma-2}(t_0) \right) \, , \qquad \gamma \neq 2 \, . \tag{C.5}$$

The RG equation for y_t was given in Eq. (5.43):

$$\frac{\mathrm{d}}{\mathrm{d}t} y_t = \kappa \, y_t \left[6|y_t|^2 - \frac{13}{15} g_1^2 - 3g_2^2 - \frac{16}{3} g_3^2 \right] \, . \tag{C.6}$$

Translating it to an integral equation for future convenience,

$$\int_{t_0}^{t} \mathrm{d}s \, |y_t|^2(s) = \frac{1}{\kappa} \left(\frac{1}{6} \log \frac{y_t(t)}{y_t(t_0)} + \frac{13}{1188} \log \frac{g_1^2(t)}{g_1^2(t_0)} + \frac{1}{4} \log \frac{g_2^2(t)}{g_2^2(t_0)} - \frac{4}{27} \log \frac{g_3^2(t)}{g_3^2(t_0)} \right) \, , \tag{C.7}$$

where we have made used of Eq. (C.4).

The RG equation for gauginos' masses $M_{1,2,3}$ were given in Eq. (5.45):

$$\frac{\mathrm{d}}{\mathrm{d}t} M_a = 2 \, \kappa \, b_a \, g_a^2 \, M_a \, . \tag{C.8}$$

with b_a given in Eq. (C.4). Translating Eqs. (C.2), (C.8) into a general integral (which will turn our useful in the following):

$$\int_{t_0}^{t} \mathrm{d}s \, g_a^{\gamma}(s) M_a^{\delta}(s) = \frac{1}{\kappa \, b_a(\gamma + 2\delta - 2)} \left(g_a^{\gamma-2}(t) M_a^{\delta}(t) - g_a^{\gamma-2}(t_0) M_a^{\delta}(t_0) \right) \, . \tag{C.9}$$

The last useful integral is the one from the RG equation for A_t, Eq. (5.49),

$$\frac{\mathrm{d}}{\mathrm{d}t} A_t = \kappa \left[12 \, A_t \, y_t^2 + \frac{26}{15} g_1^2 \, M_1 + 6 \, g_2^2 \, M_2 + \frac{32}{3} g_3^2 \, M_3 \right] \, , \tag{C.10}$$

from which we find, using Eq. (C.9),

$$\int_{t_0}^{t} \mathrm{d}s \, A_t y_t^2 = \frac{1}{12\kappa} \Bigg(\left(A_t(t) - A_t(t_0) \right) - \frac{13}{99} \left(M_1(t) - M_1(t_0) \right)$$
$$- 3 \left(M_2(t) - M_2(t_0) \right) + \frac{16}{9} \left(M_3(t) - M_3(t_0) \right) \Bigg) \, . \tag{C.11}$$

C.1.2   Soft parameters' RG flow

The best way to handle the scan over the different A_t, m_{Q_3,u_3}^2, $m_{H_{u,d}}^2$ configurations would have been to own an analytical solution to their initial value problem. Unfortunately, such a general integral was out of our reach. Instead, we developed analytical formulas that furnish the general solution to the initial value problem once owing the numerical solution in a single case.

In other words, once found one numerical integration for a certain initial condition, the solution corresponding to a different initial condition have been derived analytically as a function of the given numerical solution and of the two sets of initial conditions. This was done for the RG equations of A_t, and for the coupled RG equations of m_{Q_3,u_3}^2, $m_{H_{u,d}}^2$.

In the following we report such analytical formulas. It is crucial to realise that, as far as the RG equations for A_t, $m^2_{Q_3,u_3}$ and $m^2_{H_{u,d}}$ are concerned, y_t, $g_{1,2,3}$, $M_{1,2,3}$ can all be seen as fixed functions (to be computed numerically) for each different (m_h, m_t) point.

According to the above observation, the RG equation for A_t, Eq. (C.10), can be regarded as a first-order linear inhomogeneous differential equation with non-constant coefficients,

$$\frac{\mathrm{d}}{\mathrm{d}t} A_t = d(t)\, A_t + f(t) \,, \tag{C.12}$$

with

$$d(t) = 12\, \kappa\, y_t^2 \,, \tag{C.13}$$

$$f(t) = \kappa \left[\frac{26}{15}\, g_1^2\, M_1 + 6\, g_2^2\, M_2 + \frac{32}{3} g_3^2\, M_3 \right] \,. \tag{C.14}$$

The general integral of the initial value problem $A_t(t_0) = A'_t$ therefore reads:

$$A_t(t) = e^{\Delta(t)} \left(A'_t + \int_{t_0}^{t} \mathrm{d}s\, f(s)\, e^{-\Delta(s)} \right) \,, \tag{C.15}$$

$$\Delta(t) = \int_{t_0}^{t} \mathrm{d}s\, d(s) = 2\log\frac{y_t(t)}{y_t(t_0)} + \frac{13}{99}\log\frac{g_1^2(t)}{g_1^2(t_0)} + 3\log\frac{g_2^2(t)}{g_2^2(t_0)} - \frac{16}{9}\log\frac{g_3^2(t)}{g_3^2(t_0)} \,, \tag{C.16}$$

where the expression for $\Delta(t)$ comes straightforwardly from Eq. (C.7). Though the explicit evaluation of the integral in Eq. (C.15) is prohibitive, we can notice that such term cancels when evaluating the difference between solutions. Therefore, assuming a numerical solution $A'_t(t)$ to the initial value problem $A'_t(t_0) = A'_t$ is given, the solution $A''_t(t)$ to the initial value problem $A''_t(t_0) = A''_t$ can be easily extrapolated:

$$A''_t(t) = A'_t(t) + (A''_t - A'_t) \left(\frac{y_t(t)}{y_t(t_0)} \right)^2 \left(\frac{g_1(t)}{g_1(t_0)} \right)^{\frac{26}{99}} \left(\frac{g_2(t)}{g_2(t_0)} \right)^6 \left(\frac{g_3(t)}{g_3(t_0)} \right)^{-\frac{32}{9}} \,. \tag{C.17}$$

A completely analogous procedure can be adopted for the coupled RG equations of $m^2_{Q_3,u_3}$, $m^2_{H_{u,d}}$. Considering y_t, $g_{1,2,3}$, $M_{1,2,3}$ as well as A_t as fixed functions and further assuming the approximate expression (5.56) for the S term appearing in the RG equations, those differential equations can again be seen to be first-order and linear:

$$\frac{\mathrm{d}}{\mathrm{d}t} \vec{v}_m = D\, \vec{v}_m + \vec{c} \,, \tag{C.18}$$

where

$$\vec{v}_m = \begin{bmatrix} m_{Q_3} \\ m_{u_3} \\ m_{H_u} \\ m_{H_d} \end{bmatrix} \,, \tag{C.19}$$

$$\frac{1}{\kappa}D = \begin{bmatrix} 1 & 1 & 1 & 0 \\ 2 & 2 & 2 & 0 \\ 3 & 3 & 3 & 0 \\ 0 & 0 & 0 & 0 \end{bmatrix} \cdot 2y_t^2 + \begin{bmatrix} 1 & -2 & 1 & -1 \\ -4 & 8 & -4 & 4 \\ 3 & -6 & 3 & -3 \\ -3 & 6 & -3 & 3 \end{bmatrix} \cdot \frac{1}{5}\, g_1^2 \;, \tag{C.20}$$

$$\frac{1}{\kappa}\vec{c} = \begin{bmatrix} 2 \\ 4 \\ 6 \\ 0 \end{bmatrix} A_t^2\, y_t^2 - \frac{1}{15} \begin{bmatrix} 2 \\ 32 \\ 18 \\ 18 \end{bmatrix} g_1^2\, M_1^2 - 6 \begin{bmatrix} 1 \\ 0 \\ 1 \\ 1 \end{bmatrix} g_2^2\, M_2^2 - \frac{32}{3} \begin{bmatrix} 1 \\ 1 \\ 0 \\ 0 \end{bmatrix} g_3^2\, M_3^2 \;. \tag{C.21}$$

The matrix $D(t)$ has the fortuitous and extremely convenient property to be diagonalisable by a t-independent matrix R,

$$R = \frac{1}{3} \begin{bmatrix} -1 & 1 & 1 & -3 \\ 4 & 2 & -1 & 0 \\ -3 & 3 & 0 & 3 \\ 3 & 0 & 3 & 0 \end{bmatrix} \;, \quad \hat{D} = R^{-1}\, D\, R = \kappa \begin{bmatrix} 3g_1^2 & & & \\ & 12y_t^2 & & \\ & & 0 & \\ & & & 0 \end{bmatrix} \;. \tag{C.22}$$

Exploiting the rotation matrix R, it is easy to decouple the linear system (C.18) into four independent equations and solve them with the same philosophy used for A_t.

Given the numerical solution $\vec{v}\,'_m(t)$ to the initial value problem $\vec{v}\,'_m(t_0) = \vec{v}\,'_m$, the solution $\vec{v}\,''_m(t)$ to the initial value problem $\vec{v}\,''_m(t_0) = \vec{v}\,''_m$ reads:

$$\vec{v}\,''_m(t) = \vec{v}\,'_m(t) + (\vec{v}\,''_m - \vec{v}\,'_m)R\, e^{\hat{\Delta}(t)}\, R^{-1} \;, \tag{C.23}$$

$$\hat{\Delta}(t) = \int_{t_0}^{t} \mathrm{d}s\; \hat{D}(s) \;. \tag{C.24}$$

Integral (C.24) can be performed using Eqs. (C.4), (C.7). One finds:

$$e^{\hat{\Delta}(t)} = \begin{bmatrix} \left(\frac{g_1(t)}{g_1(t_0)}\right)^{\frac{10}{22}} & & & \\ & \left(\frac{y_t(t)}{y_t(t_0)}\right)^2 \left(\frac{g_1(t)}{g_1(t_0)}\right)^{\frac{26}{99}} \left(\frac{g_2(t)}{g_2(t_0)}\right)^6 \left(\frac{g_3(t)}{g_3(t_0)}\right)^{-\frac{32}{9}} & & \\ & & 1 & \\ & & & 1 \end{bmatrix} \;. \tag{C.25}$$

We are left to discuss the RG equations for μ and b, given in Eqs. (5.44), (5.50),

$$\begin{cases} \dfrac{\mathrm{d}}{\mathrm{d}t}\mu = \kappa\, \mu \left(3\, y_t^2 - \dfrac{3}{5}\, g_1^2 - 3\, g_2^2\right) \\[3mm] \dfrac{\mathrm{d}}{\mathrm{d}t}b = \kappa \left[b \left(3\, y_t^2 - \dfrac{3}{5}\, g_1^2 - 3\, g_2^2\right) + \mu \left(6A_t\, y_t^2 + \dfrac{6}{5}\, g_1^2\, M_1 + 6g_2^2\, M_2\right)\right] \end{cases} \;. \tag{C.26}$$

Those equations can be conveniently recast into two homogeneous linear equations as follow:

$$\begin{cases} \dfrac{\mathrm{d}}{\mathrm{d}t}\mu = \kappa\, \mu \left(3y_t^2 - \dfrac{3}{5}\, g_1^2 - 3\, g_2^2\right) \\[3mm] \dfrac{\mathrm{d}}{\mathrm{d}t}\dfrac{b}{\mu} = \kappa \left[6\, A_t\, y_t^2 + \dfrac{6}{5}\, g_1^2\, M_1 + 6\, g_2^2\, M_2\right] \end{cases} \;. \tag{C.27}$$

Exploiting Eqs. (C.4), (C.7), (C.9), (C.11) we can analytically integrate the system (C.27) and find:

$$\log \frac{\mu(t)}{\mu(t_0)} = \frac{1}{2} \log \frac{y_t(t)}{y_t(t_0)} - \frac{5}{396} \log \frac{g_1^2(t)}{g_1^2(t_0)} - \frac{3}{4} \log \frac{g_2^2(t)}{g_2^2(t_0)} - \frac{4}{9} \log \frac{g_3^2(t)}{g_3^2(t_0)} , \qquad \text{(C.28)}$$

$$b(t) = \left(\frac{b(t_0)}{\mu(t_0)} + \frac{1}{2} \left(A_t(t) - A_t(t_0) \right) + \frac{5}{198} \left(M_1(t) - M_1(t_0) \right) \right.$$
$$\left. + \frac{3}{2} \left(M_2(t) - M_2(t_0) \right) + \frac{8}{9} \left(M_3(t) - M_3(t_0) \right) \right) \mu(t) . \qquad \text{(C.29)}$$

Published articles

- M. Bordone, A. Greljo, G. Isidori, D. Marzocca and **A. Pattori**, "Higgs Pseudo Observables and Radiative Corrections," Eur. Phys. J. C **75** (2015) no.8, 385 [arXiv:1507.02555 [hep-ph]].

- F. Feruglio, P. Paradisi and **A. Pattori**, "Lepton Flavour Violation in Composite Higgs Models," Eur. Phys. J. C **75** (2015) no.12, 579 [arXiv:1509.03241 [hep-ph]].

- R. Barbieri, G. Isidori, **A. Pattori** and F. Senia, "Anomalies in B-decays and $U(2)$ flavour symmetry," Eur. Phys. J. C **76** (2016) no.2, 67 [arXiv:1512.01560 [hep-ph]].

- M. Bordone, G. Isidori and **A. Pattori**, "On the Standard Model predictions for R_K and R_{K^*}," Eur. Phys. J. C **76** (2016) no.8, 440 [arXiv:1605.07633 [hep-ph]].

- F. Feruglio, P. Paradisi and **A. Pattori**, "Revisiting Lepton Flavor Universality in B Decays,'" Phys. Rev. Lett. **118** (2017) no.1, 011801 [arXiv:1606.00524 [hep-ph]].

- F. Feruglio, P. Paradisi and **A. Pattori**, "On the Importance of Electroweak Corrections for B Anomalies," JHEP **1709** (2017) 061 [arXiv:1705.00929 [hep-ph]].

Articles yet to be published

- G. Isidori and **A. Pattori**, "On the tuning in the (m_t, m_h) plane: Standard Model criticality vs. High-scale SUSY."

- G. Isidori and **A. Pattori**, "Double-logarithmic mass singularities in Vh production in the Higgs Pseudo Observables framework."

Bibliography

[1] G. Aad *et al.* [ATLAS Collaboration], Phys. Lett. B **716**, 1 (2012) [arXiv:1207.7214 [hep-ex]].

[2] S. Chatrchyan *et al.* [CMS Collaboration], Phys. Lett. B **716**, 30 (2012) [arXiv:1207.7235 [hep-ex]].

[3] M. Gonzalez-Alonso, A. Greljo, G. Isidori and D. Marzocca, Eur. Phys. J. C **75**, 128 (2015) [arXiv:1412.6038 [hep-ph]].

[4] A. Greljo, G. Isidori, J. M. Lindert and D. Marzocca, Eur. Phys. J. C **76**, no. 3, 158 (2016) [arXiv:1512.06135 [hep-ph]].

[5] A. David *et al.* [LHC Higgs Cross Section Working Group], arXiv:1209.0040 [hep-ph].

[6] [ATLAS Collaboration], ATLAS-CONF-2013-034.

[7] [CMS Collaboration], CMS-PAS-HIG-13-005.

[8] M. Bordone, A. Greljo, G. Isidori, D. Marzocca and A. Pattori, Eur. Phys. J. C **75**, no. 8, 385 (2015) [arXiv:1507.02555 [hep-ph]].

[9] D. R. Yennie, S. C. Frautschi and H. Suura, Annals Phys. **13**, 379 (1961).

[10] T. Kinoshita, J. Math. Phys. **3**, 650 (1962).

[11] T. D. Lee and M. Nauenberg, Phys. Rev. **133**, B1549 (1964).

[12] S. Weinberg, Phys. Rev. **140**, B516 (1965).

[13] F. E. Low, Phys. Rev. **96**, 1428 (1954).

[14] M. Gell-Mann and M. L. Goldberger, Phys. Rev. **96**, 1433 (1954).

[15] F. E. Low, Phys. Rev. **110**, 974 (1958).

[16] T. H. Burnett and N. M. Kroll, Phys. Rev. Lett. **20**, 86 (1968).

[17] M. Bordone, G. Isidori and A. Pattori, Eur. Phys. J. C **76**, no. 8, 440 (2016) [arXiv:1605.07633 [hep-ph]].

[18] M. Kuroda, G. Moultaka and D. Schildknecht, Nucl. Phys. B **350**, 25 (1991).

[19] G. Degrassi and A. Sirlin, Phys. Rev. D **46**, 3104 (1992).

[20] W. Beenakker, A. Denner, S. Dittmaier and R. Mertig, Phys. Lett. B **317**, 622 (1993).

[21] A. Denner and S. Pozzorini, Eur. Phys. J. C **18**, 461 (2001) [hep-ph/0010201].

[22] A. Denner and S. Pozzorini, Eur. Phys. J. C **21**, 63 (2001) [hep-ph/0104127].

[23] S. Pozzorini, hep-ph/0201077.

[24] L. J. Hall and Y. Nomura, JHEP **1003**, 076 (2010) [arXiv:0910.2235 [hep-ph]].

[25] G. F. Giudice and A. Strumia, Nucl. Phys. B **858**, 63 (2012) [arXiv:1108.6077 [hep-ph]].

[26] E. Bagnaschi, G. F. Giudice, P. Slavich and A. Strumia, JHEP **1409**, 092 (2014) [arXiv:1407.4081 [hep-ph]].

[27] P. A. R. Ade *et al.* [Planck Collaboration], Astron. Astrophys. **571**, A16 (2014) [arXiv:1303.5076 [astro-ph.CO]].

[28] M. B. Gavela, P. Hernandez, J. Orloff and O. Pene, Mod. Phys. Lett. A **9**, 795 (1994) [hep-ph/9312215].

[29] A. H. Guth, Phys. Rev. D **23**, 347 (1981).

[30] M. C. Gonzalez-Garcia and M. Maltoni, Phys. Rept. **460**, 1 (2008) [arXiv:0704.1800 [hep-ph]].

[31] A. Strumia and F. Vissani, hep-ph/0606054.

[32] M. C. Gonzalez-Garcia and Y. Nir, Rev. Mod. Phys. **75**, 345 (2003) [hep-ph/0202058].

[33] T. Schwetz, M. A. Tortola and J. W. F. Valle, New J. Phys. **10**, 113011 (2008) [arXiv:0808.2016 [hep-ph]].

[34] M. B. Green, J. H. Schwarz and E. Witten, Cambridge, Uk: Univ. Pr. (1987) 469 P. (Cambridge Monographs On Mathematical Physics)

[35] M. B. Green, J. H. Schwarz and E. Witten, Cambridge, Uk: Univ. Pr. (1987) 596 P. (Cambridge Monographs On Mathematical Physics)

[36] P. Langacker and N. Polonsky, Phys. Rev. D **47**, 4028 (1993) [hep-ph/9210235].

[37] H. Georgi and S. L. Glashow, Phys. Rev. Lett. **32**, 438 (1974).

[38] J. C. Pati and A. Salam, Phys. Rev. D **8**, 1240 (1973).

[39] W. Buchmuller and D. Wyler, Nucl. Phys. B **268**, 621 (1986).

[40] A. Goobar, S. Hannestad, E. Mortsell and H. Tu, JCAP **0606**, 019 (2006) [astro-ph/0602155].

[41] C. Patrignani *et al.* [Particle Data Group], Chin. Phys. C **40**, no. 10, 100001 (2016).

[42] G. 't Hooft, C. Itzykson, A. Jaffe, H. Lehmann, P. K. Mitter, I. M. Singer and R. Stora, NATO Sci. Ser. B **59**, pp.1 (1980).

[43] S. Raby, hep-ph/0608183.

[44] S. Weinberg, Phys. Rev. Lett. **40**, 223 (1978).

[45] F. Wilczek, Phys. Rev. Lett. **40**, 279 (1978).

[46] B. Grzadkowski, M. Iskrzynski, M. Misiak and J. Rosiek, JHEP **1010**, 085 (2010) [arXiv:1008.4884 [hep-ph]].

[47] A. V. Manohar and M. B. Wise, Phys. Lett. B **636**, 107 (2006) [hep-ph/0601212].

[48] G. F. Giudice, C. Grojean, A. Pomarol and R. Rattazzi, JHEP **0706**, 045 (2007) [hep-ph/0703164].

[49] T. Appelquist and C. W. Bernard, Phys. Rev. D **22**, 200 (1980).

[50] A. C. Longhitano, Nucl. Phys. B **188**, 118 (1981).

[51] B. Grinstein and M. Trott, Phys. Rev. D **76**, 073002 (2007) [arXiv:0704.1505 [hep-ph]].

[52] I. Brivio, T. Corbett, O. J. P. Éboli, M. B. Gavela, J. Gonzalez-Fraile, M. C. Gonzalez-Garcia, L. Merlo and S. Rigolin, JHEP **1403**, 024 (2014) [arXiv:1311.1823 [hep-ph]].

[53] G. Buchalla, O. Catá and C. Krause, Phys. Lett. B **731**, 80 (2014) [arXiv:1312.5624 [hep-ph]].

[54] G. Panico and A. Wulzer, Lect. Notes Phys. **913**, pp.1 (2016) [arXiv:1506.01961 [hep-ph]].

[55] J. R. Ellis and R. Peccei, CERN-86-02-V-1, CERN-YELLOW-86-02-V-1, CERN-86-02.

[56] J. R. Ellis and R. Peccei, CERN-86-02-V-2, CERN-YELLOW-86-02-V-2, CERN-86-02.

[57] G. Altarelli, R. Kleiss and C. Verzegnassi, CERN-89-08, CERN-89-08-V-1, CERN-YELLOW-89-08-V-1.

[58] D. Y. Bardin, M. Grunewald and G. Passarino, hep-ph/9902452.

[59] S. Schael *et al.* [ALEPH and DELPHI and L3 and OPAL and SLD Collaborations and LEP Electroweak Working Group and SLD Electroweak Group and SLD Heavy Flavour Group], Phys. Rept. **427**, 257 (2006) [hep-ex/0509008].

[60] D. de Florian *et al.* [LHC Higgs Cross Section Working Group], arXiv:1610.07922 [hep-ph].

[61] G. Isidori, A. V. Manohar and M. Trott, Phys. Lett. B **728**, 131 (2014) [arXiv:1305.0663 [hep-ph]].

[62] G. Isidori and M. Trott, JHEP **1402**, 082 (2014) [arXiv:1307.4051 [hep-ph]].

[63] L. Bergstrom and G. Hulth, Nucl. Phys. B **259**, 137 (1985) Erratum: [Nucl. Phys. B **276**, 744 (1986)].

[64] A. Djouadi, Phys. Rept. **457**, 1 (2008) [hep-ph/0503172].

[65] Y. Chen, R. Harnik and R. Vega-Morales, Phys. Rev. Lett. **113**, no. 19, 191801 (2014) [arXiv:1404.1336 [hep-ph]].

[66] A. Pomarol, arXiv:1412.4410 [hep-ph].

[67] J. C. Romao and S. Andringa, Eur. Phys. J. C **7**, 631 (1999) [hep-ph/9807536].

[68] A. De Rujula, J. Lykken, M. Pierini, C. Rogan and M. Spiropulu, Phys. Rev. D **82**, 013003 (2010) [arXiv:1001.5300 [hep-ph]].

[69] Y. Chen, N. Tran and R. Vega-Morales, JHEP **1301**, 182 (2013) [arXiv:1211.1959 [hep-ph]].

[70] G. Buchalla, O. Cata and G. D'Ambrosio, Eur. Phys. J. C **74**, no. 3, 2798 (2014) [arXiv:1310.2574 [hep-ph]].

[71] V. Khachatryan *et al.* [CMS Collaboration], Phys. Rev. D **92**, no. 1, 012004 (2015) [arXiv:1411.3441 [hep-ex]].

[72] A. Bredenstein, A. Denner, S. Dittmaier and M. M. Weber, Phys. Rev. D **74**, 013004 (2006) [hep-ph/0604011].

[73] A. Bredenstein, A. Denner, S. Dittmaier and M. M. Weber, Nucl. Phys. Proc. Suppl. **160**, 131 (2006) [hep-ph/0607060].

[74] S. Heinemeyer *et al.* [LHC Higgs Cross Section Working Group], arXiv:1307.1347 [hep-ph].

[75] T. Han, G. Valencia and S. Willenbrock, Phys. Rev. Lett. **69**, 3274 (1992) [hep-ph/9206246].

[76] T. Figy, C. Oleari and D. Zeppenfeld, Phys. Rev. D **68**, 073005 (2003) [hep-ph/0306109].

[77] S. Dittmaier *et al.*, arXiv:1201.3084 [hep-ph].

[78] P. Bolzoni, F. Maltoni, S. O. Moch and M. Zaro, Phys. Rev. D **85**, 035002 (2012) [arXiv:1109.3717 [hep-ph]].

[79] M. Cacciari, F. A. Dreyer, A. Karlberg, G. P. Salam and G. Zanderighi, Phys. Rev. Lett. **115**, no. 8, 082002 (2015) [arXiv:1506.02660 [hep-ph]].

[80] M. Ciccolini, A. Denner and S. Dittmaier, Phys. Rev. D **77**, 013002 (2008) [arXiv:0710.4749 [hep-ph]].

[81] V. V. Sudakov, Sov. Phys. JETP **3**, 65 (1956) [Zh. Eksp. Teor. Fiz. **30**, 87 (1956)].

[82] J. M. Cornwall, D. N. Levin and G. Tiktopoulos, Phys. Rev. D **10**, 1145 (1974) Erratum: [Phys. Rev. D **11**, 972 (1975)].

[83] G. J. Gounaris, R. Kogerler and H. Neufeld, Phys. Rev. D **34**, 3257 (1986).

[84] T. Hahn, Comput. Phys. Commun. **140**, 418 (2001) [hep-ph/0012260].

[85] C. Groß, T. Hahn, S. Heinemeyer, F. von der Pahlen, H. Rzehak and C. Schappacher, PoS LL **2014**, 035 (2014) [arXiv:1407.0235 [hep-ph]].

[86] G. Passarino and M. J. G. Veltman, Nucl. Phys. B **160**, 151 (1979).

[87] A. Denner, Fortsch. Phys. **41**, 307 (1993) [arXiv:0709.1075 [hep-ph]].

[88] A. Manohar, B. Shotwell, C. Bauer and S. Turczyk, Phys. Lett. B **740**, 179 (2015) [arXiv:1409.1918 [hep-ph]].

[89] S. R. Coleman and J. Mandula, Phys. Rev. **159**, 1251 (1967).

[90] R. Haag, J. T. Lopuszanski and M. Sohnius, Nucl. Phys. B **88**, 257 (1975).

[91] R. K. Kaul and P. Majumdar, Nucl. Phys. B **199**, 36 (1982).

[92] S. Dimopoulos and H. Georgi, Nucl. Phys. B **193**, 150 (1981).

[93] J. R. Ellis, S. Kelley and D. V. Nanopoulos, Phys. Lett. B **260**, 131 (1991).

[94] U. Amaldi, W. de Boer and H. Furstenau, Phys. Lett. B **260**, 447 (1991).

[95] P. Langacker and M. x. Luo, Phys. Rev. D **44**, 817 (1991).

[96] C. Giunti, C. W. Kim and U. W. Lee, Mod. Phys. Lett. A **6**, 1745 (1991).

[97] S. P. Martin, Adv. Ser. Direct. High Energy Phys. **21**, 1 (2010) [Adv. Ser. Direct. High Energy Phys. **18**, 1 (1998)] [hep-ph/9709356].

[98] J. Wess and B. Zumino, Phys. Lett. **49B**, 52 (1974).

[99] J. Wess and B. Zumino, Nucl. Phys. B **70**, 39 (1974).

[100] J. Polchinski and L. Susskind, Phys. Rev. D **26**, 3661 (1982).

[101] M. Dine and D. MacIntire, Phys. Rev. D **46**, 2594 (1992) [hep-ph/9205227].

[102] P. J. Fox, A. E. Nelson and N. Weiner, JHEP **0208**, 035 (2002) [hep-ph/0206096].

[103] Z. Chacko, P. J. Fox and H. Murayama, Nucl. Phys. B **706**, 53 (2005) [hep-ph/0406142].

[104] L. Girardello and M. T. Grisaru, Nucl. Phys. B **194**, 65 (1982).

[105] P. Fayet, Phys. Lett. **64B**, 159 (1976).

[106] P. Fayet, Phys. Lett. **69B**, 489 (1977).

[107] S. Dimopoulos and D. W. Sutter, Nucl. Phys. B **452**, 496 (1995) [hep-ph/9504415].

[108] L. E. Ibanez and G. G. Ross, Phys. Lett. **110B**, 215 (1982).

[109] J. R. Ellis, D. V. Nanopoulos and K. Tamvakis, Phys. Lett. **121B**, 123 (1983).

[110] K. Inoue, A. Kakuto, H. Komatsu and S. Takeshita, Prog. Theor. Phys. **67**, 1889 (1982).

[111] R. A. Flores and M. Sher, Annals Phys. **148**, 95 (1983).

[112] A. Salam and J. A. Strathdee, Phys. Rev. D **11**, 1521 (1975).

[113] M. T. Grisaru, W. Siegel and M. Rocek, Nucl. Phys. B **159**, 429 (1979).

[114] M. M. Cirkovic and N. Bostrom, Astrophys. Space Sci. **274**, 675 (2000) [gr-qc/9906042].

[115] J. A. Casas, J. R. Espinosa and M. Quiros, Phys. Lett. B **342**, 171 (1995) [hep-ph/9409458].

[116] G. Isidori, G. Ridolfi and A. Strumia, Nucl. Phys. B **609**, 387 (2001) [hep-ph/0104016].

[117] N. Arkani-Hamed, S. Dubovsky, L. Senatore and G. Villadoro, JHEP **0803**, 075 (2008) [arXiv:0801.2399 [hep-ph]].

[118] F. Bezrukov and M. Shaposhnikov, JHEP **0907**, 089 (2009) [arXiv:0904.1537 [hep-ph]].

[119] J. Ellis, J. R. Espinosa, G. F. Giudice, A. Hoecker and A. Riotto, Phys. Lett. B **679**, 369 (2009) [arXiv:0906.0954 [hep-ph]].

[120] G. Degrassi, S. Di Vita, J. Elias-Miro, J. R. Espinosa, G. F. Giudice, G. Isidori and A. Strumia, JHEP **1208**, 098 (2012) [arXiv:1205.6497 [hep-ph]].

[121] D. Buttazzo, G. Degrassi, P. P. Giardino, G. F. Giudice, F. Sala, A. Salvio and A. Strumia, JHEP **1312**, 089 (2013) [arXiv:1307.3536 [hep-ph]].

[122] F. Bezrukov, M. Y. Kalmykov, B. A. Kniehl and M. Shaposhnikov, JHEP **1210**, 140 (2012) [arXiv:1205.2893 [hep-ph]].

[123] J. R. Espinosa, M. Garny, T. Konstandin and A. Riotto, Phys. Rev. D **95**, no. 5, 056004 (2017) [arXiv:1608.06765 [hep-ph]].

[124] K. Enqvist, M. Karciauskas, O. Lebedev, S. Rusak and M. Zatta, JCAP **1611**, 025 (2016) [arXiv:1608.08848 [hep-ph]].

[125] D. Canko, I. Gialamas, G. Jelic-Cizmek, A. Riotto and N. Tetradis, arXiv:1706.01364 [hep-th].

[126] M. Böhm, A. Denner and H. Joos, "Gauge Theories" (Teubner, Stuttgart, 2001).